NASA Contractor Report 3366

Statistical Analysis of Atmospheric Turbulence About a Simulated Block Building

Sidney L. Steely, Jr., and Walter Frost

CONTRACT NAS8-32692
JANUARY 1981

NASA

NASA Contractor Report 3366

Statistical Analysis of Atmospheric Turbulence About a Simulated Block Building

Sidney L. Steely, Jr., and Walter Frost
The University of Tennessee Space Institute
Tullahoma, Tennessee

Prepared for
Marshall Space Flight Center
under Contract NAS8-32692

NASA
National Aeronautics
and Space Administration

Scientific and Technical
Information Branch

1980

ACKNOWLEDGMENTS

This research was supported under NASA Contract No. NAS8-32692. The authors are grateful for the support of A. Richard Tobiason of the Office of Aeronautical and Space Technology, NASA Headquarters, Washington, D.C. Special thanks go to Dennis W. Camp of the Space Sciences Laboratory, Atmospheric Sciences Division, NASA/George C. Marshall Space Flight Center, Alabama, who monitored the research program.

ABSTRACT

An array of towers instrumented to measure the three components of wind speed was used to study atmospheric flow about a simulated block building. Two-point space-time correlations of the longitudinal velocity component were computed along with two-point spatial correlations. These correlations are in good agreement with fundamental concepts of fluid mechanics.

The two-point spatial correlations computed directly were compared with correlations predicted by Taylor's hypothesis, and excellent agreement was obtained at the higher levels which were out of the building influence. The correlations fall off significantly in the building wake but recover beyond the wake to essentially the same values in the undisturbed, higher regions.

TABLE OF CONTENTS

LIST OF TABLES

LIST OF FIGURES

LIST OF SYMBOLS

f	Frequency
f_c	Nyquist frequency
f_k	Discrete frequency component
f_ℓ	Lowest recognizable frequency component
h	Record sampling interval
m	meter
t	time (seconds)
t_n	Discrete time corresponding to u_n
$u(t)$	Horizontal wind velocity (continuous record)
u_n	Discrete horizontal wind velocity
$v(t)$	Lateral wind velocity (continuous record)
v_n	Discrete lateral wind velocity
$w(t)$	Vertical wind velocity (continuous record)
w_n	Discrete vertical wind velocity
$x(t)$	Transformed record such that $\bar{x} = 0$
$\hat{B}_{xy}$	Cross-correlation coefficient
$\tilde{G}_k$	Discrete power spectral estimate
$\tilde{G}(f)$	Power spectral estimate
H	Height of building (3.2 meters)
L	Distance constant
N	Number of datum points
$\hat{R}_r$	Autocorrelation function estimate
$\hat{R}_x{}^c(rh)$	"Circular" correlation function
$\hat{R}_{xy}$	Cross-correlation function estimate
S	Sample standard deviation (unbiased)

S^2	Sample variance (unbiased)
$X(f)$	Infinite range Fourier transform
$X(f,T)$	Finite range Fourier transform
X_k	Discrete Fourier transform
X_k^*	Complex conjugate of X_k
δ	Elevation of the ground relative to the base of Tower 3
θ	Angular direction of mean wind speed relative to tower array
σ_x	Standard deviation of total population
σ_x^2	Variance of total population
τ	Lag time of correlation functions
Δt	Data sampling interval

SECTION I

INTRODUCTION

Studies of atmospheric flow have been conducted for many years, and much knowledge has been gained from research in this area. Statistical analysis has helped provide a better understanding of many phenomena and the knowledge necessary to predict certain yearly, seasonal and diurnal variations experienced in atmospheric flow about the earth.

These studies, being of large-scale flow, provide the knowledge to predict geostrophic and synoptic flow patterns for various locations on the surface of the earth and throughout the upper layers of the atmosphere. In comparison, little research has been devoted to atmospheric flow about surface protuberances or man-made structures which alter the local flow characteristics.

Understanding the flow of air past a surface obstacle has become very important in developing and enhancing new technologies needed in the present-day physical sciences and in future endeavors. Any protuberance or man-made obstruction existing on the surface of the earth will alter the flow pattern and change the path any fluid particles might have taken. Studying the flow phenomena about surface obstacles will help to better understand the predominant characteristics and provide valuable information relative to many design problems encountered by practicing engineers.

Many disciplines require specific knowledge of atmospheric flows and the changes which will be encountered by introducing into them surface changes or man-made obstructions. Architects and design engineers need pertinent knowledge of atmospheric flow when constructing high-rise buildings and tall towers which will be subjected to adverse wind conditions. The effects of large buildings (airport hangars, terminals, etc.) on the flow of air is very critical. If aircraft are landing and taking off in the vicinity of wakes, vortices, and/or regions of intense turbulence generated by surface obstructions upstream, then some knowledge of their effects on the control of aircraft in flight or when taxying must be gained. Some particular flow characteristics (wakes, vortices, severe wind shear, separated flow, intense turbulence, gust gradients, relative maximum wind speed, etc.) are of great concern when locating and operating conventional wind energy conversion systems. There is no end to the list of disciplines needing knowledge of atmospheric flows to advance the state of the art in their various technologies.

In general, the flow of air (atmospheric) is a very chaotic and unpredictable phenomenon. The motion of a particle or a "fluid point" in the atmosphere is sometimes described as a random process, but not in the strictest sense. Even if one of the velocity components (assuming

the wind velocity can be divided into three non-coplanar or orthogonal components) is random, the others are restricted in their range simply due to the conservations laws of fluid mechanics. Regardless, the motion is not deterministic and must be analyzed from a statistical point of view. For a more complete understanding of atmospheric turbulent flow about a three-dimensional surface obstruction, it is necessary to carry out an extensive experimental data collection and reduction routine in order to properly analyze the flow phenomena.

This study describes an experiment designed to investigate the structure and magnitude of the wind fields about a simulated building. A more thorough fundamental understanding of the mean wind and turbulence structure about a bluff obstacle is the final expected outgrowth of this study. This study addresses the following segments of the total research effort: nature and documentation of the data source; data reduction procedures; statistical analysis, which includes correlations; comparison of different computational procedures; and evaluation of Taylor's hypothesis.

Experimental studies [1,2,3]* have been attempted, with much success, to define regions of flow having characteristic differences such as recirculation,

---

*Numbers in brackets refer to similarly numbered references in the List of References.

vorticity, etc. A similar study, sponsored by the National Aeronautics and Space Administration (NASA), was conducted and carried out in the Colorado State University (CSU) boundary layer wind tunnel. The CSU study [4] concentrated on measuring mean velocities, velocity defects, turbulence intensities, and wake geometries measured at the same scaled locations as the wind towers located at the Marshall Space Flight Center (MSFC) Atmospheric Boundary Layer Facility (ABLF). The present tower arrangement was not modeled by CSU, however, several other tower arrangements in the past have been modeled and the wind tunnel results compared with the full-scale measurements at MSFC.

These studies have shown that the flow geometry behind and around a three-dimensional obstruction is a complex phenomenum to model, and most results have come from experiments similar to the CSU study. Even though the flow field is random, there is a definite pattern which can be determined statistically. In a similar manner, Plate [5] has attempted to describe the flow field about a wedge-shaped obstacle. In Figure 1-1 no less than seven flow zones of different aerodynamic behavior have been distinguished, evidencing the complexity of the flow. It should be remembered that each zone blends into the other in a continuous manner and that in this respect it is rather difficult to draw discrete regions where each is defined independently of the other. Rather, the attempt

1. Undisturbed boundary layer (outer layer)
2. Region of hill influence (middle layer)
3. Region of reestablished boundary layer (inner layer)
4. Blending region between middle and outer layer
5. Blending region between inner and middle layer
6. Standing eddy zone
7. Potential outer flow

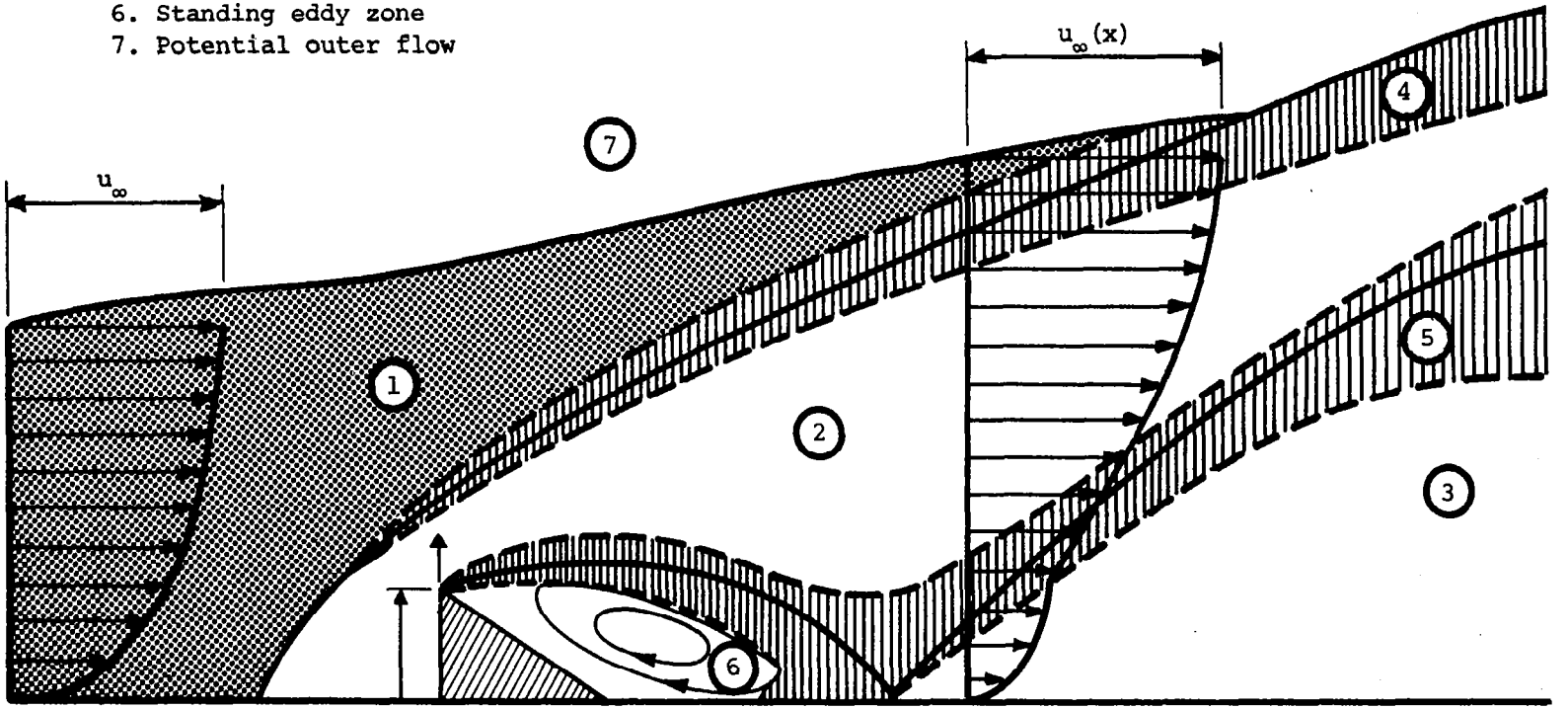

Figure 1-1 The flow zones of a boundary layer disturbed by a solid wedge [4].

is made to define a buffer zone where the separate regions blend together.

Since many questions regarding atmospheric flows about three-dimensional objects remain unanswered, this particular study has been extended, and this study describes the experiment designed to investigate the structure and magnitude of wind fields about a simulated block building. The present study describes the experimental arrangement, the type and expected accuracy of the data, the data reduction and documentation methods, and the extent to which data has been collected at the time of this writing. The results of an initial analysis of selected data is given along with the methods of analysis.

Most wind tunnel experiments, although very important, leave some doubt as to the validity of their results since the turbulence length scales, gustiness, etc. of the natural wind are difficult to simulate. To provide results comparable to wind tunnel studies, a field study (full-scale) of the wind over a simulated block building has been undertaken. Some of the results obtained from the full-scale experimental study are presented. (Comparison with wind tunnel studies [4,6,7] is planned at a future time.) The results presented consist of: autocorrelations computed by the direct method and by the Fast Fourier Transform (FFT) method; two-point spatial correlations

(with and without lag times); and autocorrelations of the horizontal velocity components computed by direct and FFT methods for comparison purposes only. Taylor's hypothesis is tested against directly measured and computed autocorrelations and is found to give good results at upper levels. At lower levels, however, the hypothesis is found to be invalid due to the disturbance of the building. These results are presented along with a discussion of the influence of the simulated block building.

The following sections have been arranged to facilitate an understanding of the experiment; data formatting, reduction and analysis techniques; and analysis of selected data sets. Section II provides an explanation of the experiment, including location, terrain, tower facilities, instrumentation and associated operating characteristics. Section III introduces some general considerations relative to data reduction and analysis techniques and describes the specific techniques used herein. Section IV describes the specific data formatting procedures used, along with necessary subroutines to extract data from magnetic tapes in a logical manner. Also given is a brief description of the computer systems used to generate the users' data tapes. Examples of plotted data available to researchers are included and briefly explained. Section V is devoted to presenting a few of the results obtained and to illustrating the validity of Taylor's

hypothesis for computing autocorrelations. Conclusions are given at the end of Section V.

The experiment described in Section II is one part of a three-phase study. Validation of analytical and numerical models of turbulent flow field and justification for using scale models in wind tunnels is needed. The experimental study described herein has been undertaken to satisfy this needed verification. Full-scale empirical data are needed to analyze the turbulent structure of the atmosphere. This study will supply the information needed to justify the use of and the improvement of numerical models, as well as justifying the usefulness of scale models tested in wind tunnels. Also, some of the information gained from this study will simply be applied to improve the state-of-the-art technology and for the sake of research in general.

Hopefully, the explanations and results presented herein will be helpful to individuals continuing this particular study and will inspire others to pursue a more thorough investigation of turbulent flow fields and related phenomena.

SECTION II

EXPERIMENTAL DESCRIPTION

A. TOWER FACILITY

The experiments were conducted at the MSFC, Atmospheric Sciences Division, Atmospheric Boundary Layer Facility (ABLF), located near Huntsville, Alabama. Figure 2-1 illustrates an aerial perspective of the block building and tower arrangement. The tower facility was originally arranged with eight in-line 20 meter towers instrumented at four levels. For the present experimental setup, schematically illustrated in Figure 2-2, the tower arrangement consists of five in-line 20 meter (65 ft) towers (indicated by T1 through T5) and four short towers (indicated by S1 through S4).

The tall towers are instrumented at the 3 m, 6 m, 12 m, and 20 m levels, with the exception of T3 on which the instruments from the 20 m level were lowered to the 9 m level and recorded as level 4. (This point is important in the data reduction format.) The short towers are instrumented at the 2 m, 3 m, and 6 m levels, with S1 and S2 stationed behind the block building laterally from T3, while S3 and S4 are stationed in line with the tall towers between T3 and T4.

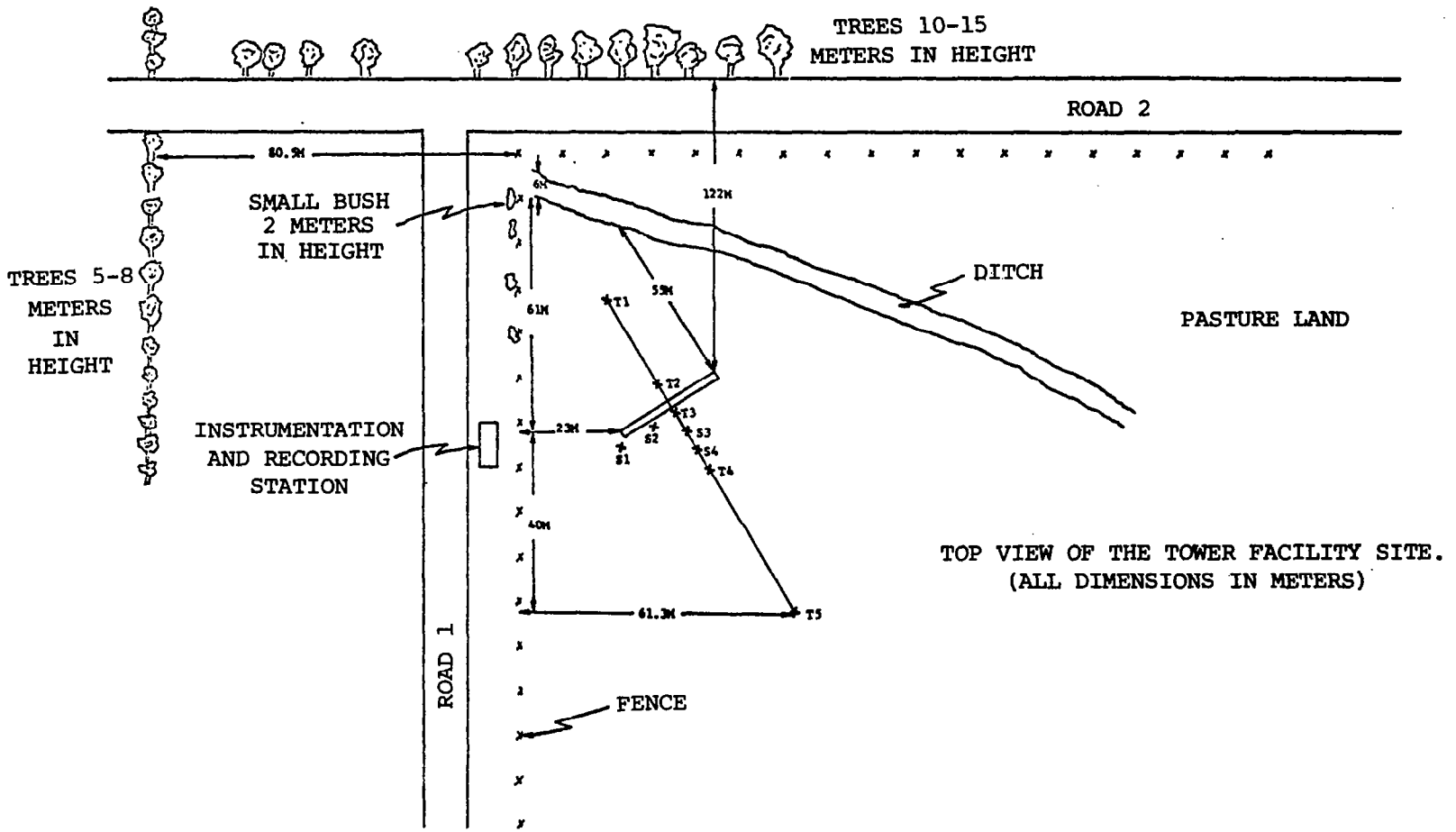

Figure 2-1 Aerial perspective of the tower array at NASA/George C. Marshall Space Flight Center, Boundary Layer Facility, in its present configuration. (All dimensions are given in meters.)

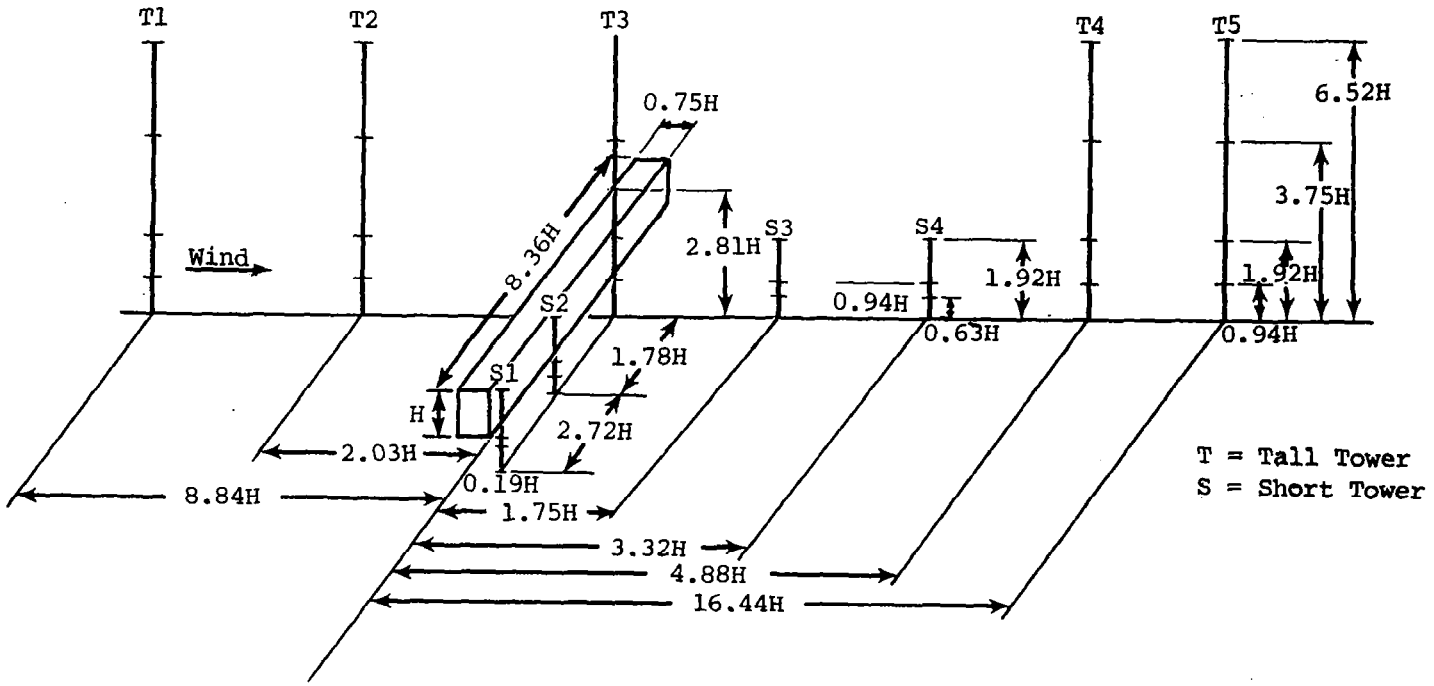

Figure 2-2 Schematic of the current configuration of the NASA/George C. Marshall Space Flight Center, Boundary Layer Facility. (Not to scale, H = 3.2 meters.)

B. DESCRIPTION OF AVAILABLE DATA

Several tower arrangements have been constructed and much data collected at the MSFC tower facility since its inception (1971). A description of the tower arrangements and data measurements prior to the present arrangement is given by Frost and Shahabi [2].

There are approximately 100 runs (40-minute recording periods) which have been carried out with the present tower arrangement. Half of the runs were conducted with a simulated block building included and half without. Run numbers 8600-8650 represent tower data which includes the building and run numbers 8700-8750 are no building cases. Only one building size was used for testing. The building dimensions are given in Tables 2-1 and 2-2.

C. FIELD SITE CONTOUR

The tower facility is located in an open field which is not exactly level and which has slight undulations along the line of towers. The elevation of the ground with respect to the profile of the tower array is shown in Figure 2-3. Measurements of elevation are relative to the base of T3. T3 serves as the zero elevation datum plane; the other tower elevations are given in Table 2-1. From this table it can be determined that the building is located on an approximate 6.3 : 1 grade. The study of wind data reported herein neglects these small variations in terrain elevation.

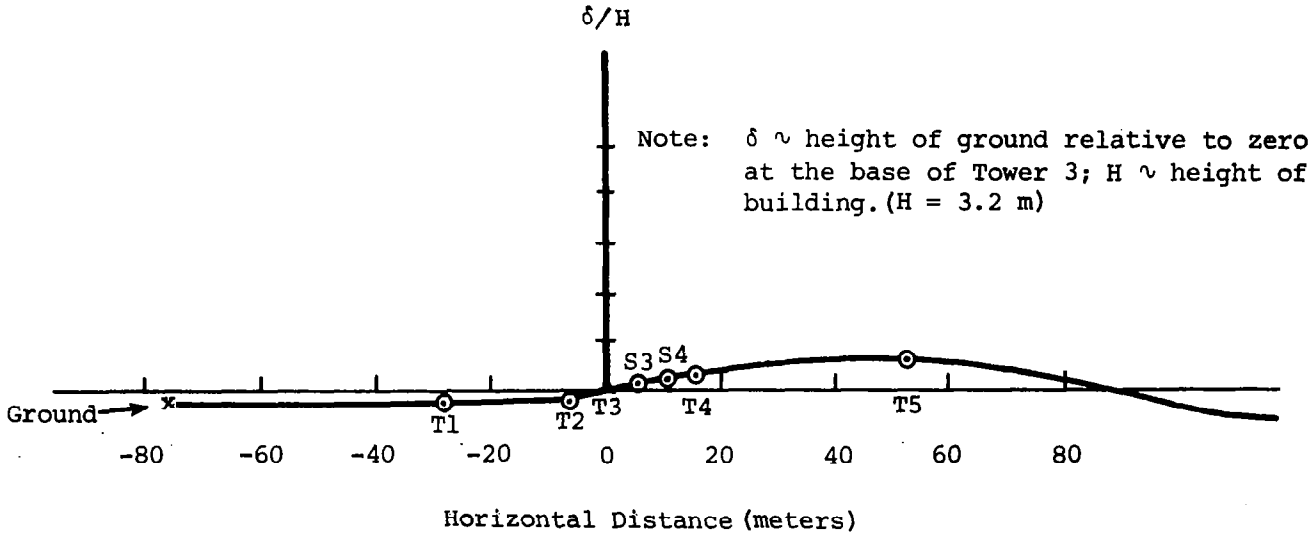

Figure 2-3 Cross-sectional contour of eight-tower array. (⊙ indicates the base of each tower. x indicates ground level.)

TABLE 2-1

TOWER LOCATION AND ELEVATION

	Horizontal		Elevation	
	Building Heights	Meters	Building Heights	Meters
Ground	-24.12	-77.18	-0.045	-0.144
Tower #1	-9.04	-28.93	-0.039	-0.125
Tower #2	-2.22	-7.10	-0.008	-0.026
Building*	-0.19	-0.61	-0.002	-0.006
Tower #3	0	0	0	0
Tower #S3	1.56	4.99	0.012	0.038
Tower #S4	3.13	10.02	0.031	0.099
Tower #4	4.69	15.01	0.043	0.138
Tower #5	16.25	52.00	0.103	0.330

*Building Dimensions:

Height (H) = 3.2 m.
Width = 2.4 m.
Length = 26.8 m.

D. INSTRUMENTATION

The instrumentation at each level on each tower consists of a Climet Model 011-1 three-cup anemometer (horizontal wind speed sensor), a Climet Model 012-1 vane (horizontal wind direction sensor), and a Gill Model 27100 propeller anemometer (vertical wind speed sensor). The four levels on T1 also contain Climet Model 016-5 thermistors.

Horizontal Wind Speed Sensor

Horizontal wind speed is measured with a Climet 011-1 three-cup anemometer assembly and a precision light beam. The beam is chopped to produce an amplified pulsed electrical output with a frequency proportional to wind speed. Table 2-2 lists the operational characteristics of the Model 011-1 sensor [2].

Table 2-3 gives the calibration of the Climet wind speed transmitter. A 12 volt supply to the anemometer results in the creation of a 0-12 volt square wave which is proportioned to the frequency of rotation [8]. The sensor output can be filtered through a translator and recorded as a 0-1 volt continuous output, or it can be processed through a capacitor and recorded as a spike without regard for the amplitude of the signal.

In the present study, the manufacturer's calibration is accepted, and only the tape recorder is calibrated

TABLE 2-2

SPECIFICATIONS OF CLIMET 011-1 WIND SPEED TRANSMITTER [8]

Model 4 Description	Climet Model 011-1
Power requirements	10.6 to 12.6 V at 15 ma
Operating range	0 to 110 mph
Calibrated range	0.6 to 90 mph
Signal output	Approximately 10 V p-p* square wave
Output	Less than 50 ohms
Accuracy	±1% or 0.15 mph, whichever is greater
Threshold	0.6 mph
Distance constant+	< 5 ft
Operating temperature	-50 °F to 155 °F
Weight	14 oz
Height	18.5 in
Housing dimensions	3.5 x 2.25 in (height x width)
Connector	Climet 49-2004

*p-p is peak-to-peak.

+The distance constant is the length of a column of air which passes an anemometer after it has been distributed by a sharp gust until it reaches 63 percent (1 - 1/e) of the new equilibrium value [8].

TABLE 2-3

MANUFACTURER'S CALIBRATION OF CLIMET WIND SPEED TRANSMITTER [8]

Velocity (m/s)	Frequency (Hz)	Velocity (mph)	Frequency (Hz)	Velocity (Knots)	Frequency (Hz)
0.000	-16.57	0.000	-16.57	0.000	-16.57
0.232	0.00	0.519	0.00	0.561	0.00
0.250	1.25	5.000	142.80	5.000	166.70
1.000	54.73	10.000	302.10	10.000	350.40
2.000	126.00	15.000	461.50	15.000	533.90
3.000	197.30	20.000	620.80	20.000	717.40
4.000	268.60	22.500	700.50	25.000	900.90
5.000	339.90	25.000	780.20	30.000	1084.40
7.000	482.50	30.000	939.50	35.000	1267.90
10.000	696.40	35.000	1098.90	40.000	1451.40
15.000	1052.90	40.000	1258.20	45.000	1634.90
20.000	1409.40	45.000	1417.60	50.000	1818.40
25.000	1765.90	50.000	1576.90	60.000	2185.40
30.000	2120.40	62.000	1895.60	70.000	2552.40
35.000	2478.90	70.000	2214.30	80.000	2919.40
40.000	2835.40	80.000	2533.00	90.000	3286.40
60.000	4261.00	90.000	2851.70	100.000	3653.40

before each run. This calibration consists of first shorting out the oscillator plug to give zero voltage and then employing a Hewlett Packard oscillator to give a 1409 cps record on each channel. In Table 2-3 this corresponds to a 44.74 mph (20 m/sec) reading which is taken as full-scale in the data reduction. Each calibration is run one minute, and a microphone is employed to inform the computer laboratory of the beginning of each calibration input. This microphone is also used to communicate with the computer laboratory as to the point on each tape where simultaneous reduction of test data is to begin. There is additionally an IRIG "B" timing unit for synchronizing events occurring on different tapes.

Wind Direction Transmitter

The Climet Model 021-1 vane type wind direction transmitter which delivers a 0-4.8 volt DC signal proportional to horizontal wind direction is employed to measure wind direction. The sensing potentiometer which proportions the voltage signal is sealed within the transmitter housing, thereby receiving maximum protection from contamination. Table 2-4 depicts the characteristics of this sensor.

The voltage amplitude output of the direction transmitter is proportional to the wind direction. The Climet wind direction sensor is a 10 kilohms continuous turn.potentiometer. A 4 volt input is porportioned according to the wind vane position. The instrument is calibrated [9]:

TABLE 2-4

SPECIFICATIONS OF CLIMET 021-4 WIND DIRECTION TRANSMITTER [9]

Model 4 Description	Climet Model 012-1
Power requirements	4.8 volts DC
Mechanical range	0 to 360° continuous
Horizontal range	354° ± 2°
Signal output	0 to 4.0 v corresponding to 0-360°
Output impedance	Potentiometric output, impedance varies from approximately zero to maximum of 10 kilohms
Linearity	±1/2%
Threshold	0.75 mph
Damping ratio	0.4 with Climet 014-6 vane
Distant constant	Less than 3.3 ft
Operating temperature	-50° to 155 °F
Weight	14 oz
Height	18.5 in
Housing dimensions	3.5 x 2.25 in (height x diameter)
Connector	Climet 49-2001

a. 1 volt -- 90 degrees

b. 2 volts -- 180 degrees

c. 3 volts -- 270 degrees

d. 4 volts -- 360 degrees

The 180 degree position has been aligned straight down the tower array in the present installation, i.e., from T1 to T6. A rifle scope is used to align the alignment collar on each tower. The towers were initially aligned with a surveyor's transit. The alignment procedure was conducted prior to each major measurement program (i.e., prior to the 8600 and 8700 runs). Calibrations of the recording tapes are performed with a precision power supply.

Vertical Wind Speed Anemometer

Vertical wind speed was measured with a Gill Model 27100 vertical axis propeller anemometer. This instrument is a sensitive precision air speed measuring instrument employing a framed polystyrene propeller molded in the form of a true generated helicoid. The horizontally positioned propeller (vertical axis) is designed to provide a given arc of revolution for each foot of vertically passing air. Extensive wind tunnel tests have shown that the propeller actually rotates 0.96 revolutions per foot of air for all wind speeds above 2.7 mph (4 ft/sec) [10]. Increasing slippage occurs down to the threshold speed of 0.5 mph (0.8 ft/sec). In the standard instrument the propeller drives a miniature

DC tachometer generator providing an analog voltage output which is directly proportional to wind speed.

The propeller anemometer will measure both forward and reverse air flow. When the propeller rotation reverses, the generator signal polarity reverses. Thus the meter or recorder can be calibrated to read both positively and negatively from a central zero position.

Calibration of the instrument is as follows: The positive or negative DC voltage amplitude is directly proportional to the vertical velocity. At 1800 rpm (0.96 actual propeller revolutions per foot of air) the velocity equals 69.9 mph (31.25 ft/sec). Figures 2-4 and 2-5 are used to find the vertical velocity, w(t), when the revolutions per minute are known [10]. The output voltage signal for an updraft is recorded as a positive voltage, and a negative voltage corresponds to a downdraft. Also, the output signal is calibrated to 26.6 mph at 1800 rpm. Propeller response follows the cosine law within ±3 percent in the range of 60 to 120 degrees (±60 degrees each side of stall). The propeller responds when the component of the wind is parallel to its axis of rotation. Four-blade polystyrene propellers provide slightly better symmetry of response to various wind angles, especially near the stall region. Figures 2-6 and 2-7 show the variation of wind angle with propeller and percentage of response. The Model 27100 was designed for optimum dynamic response in wind ranging from threshold to 50 mph.

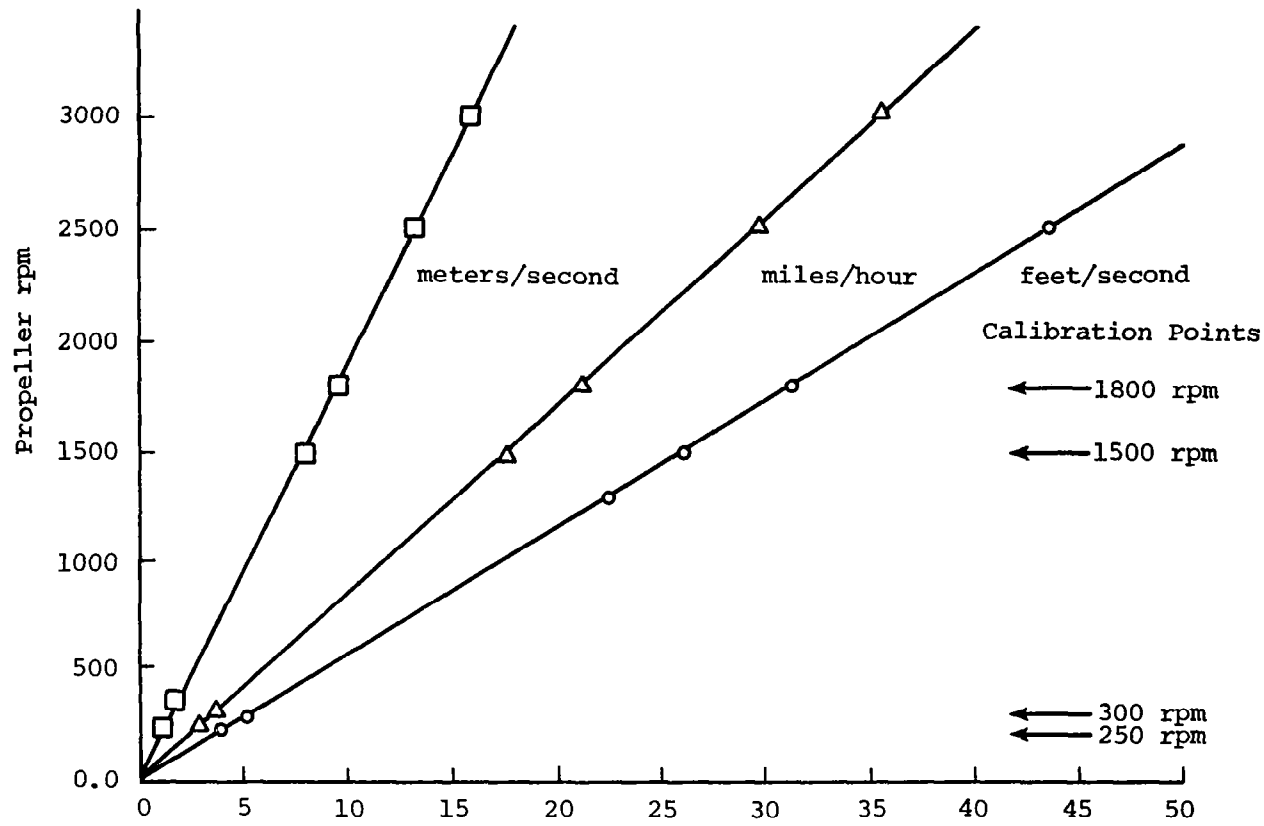

Figure 2-4 Propeller calibration (wind speed versus propeller rpm) [10].

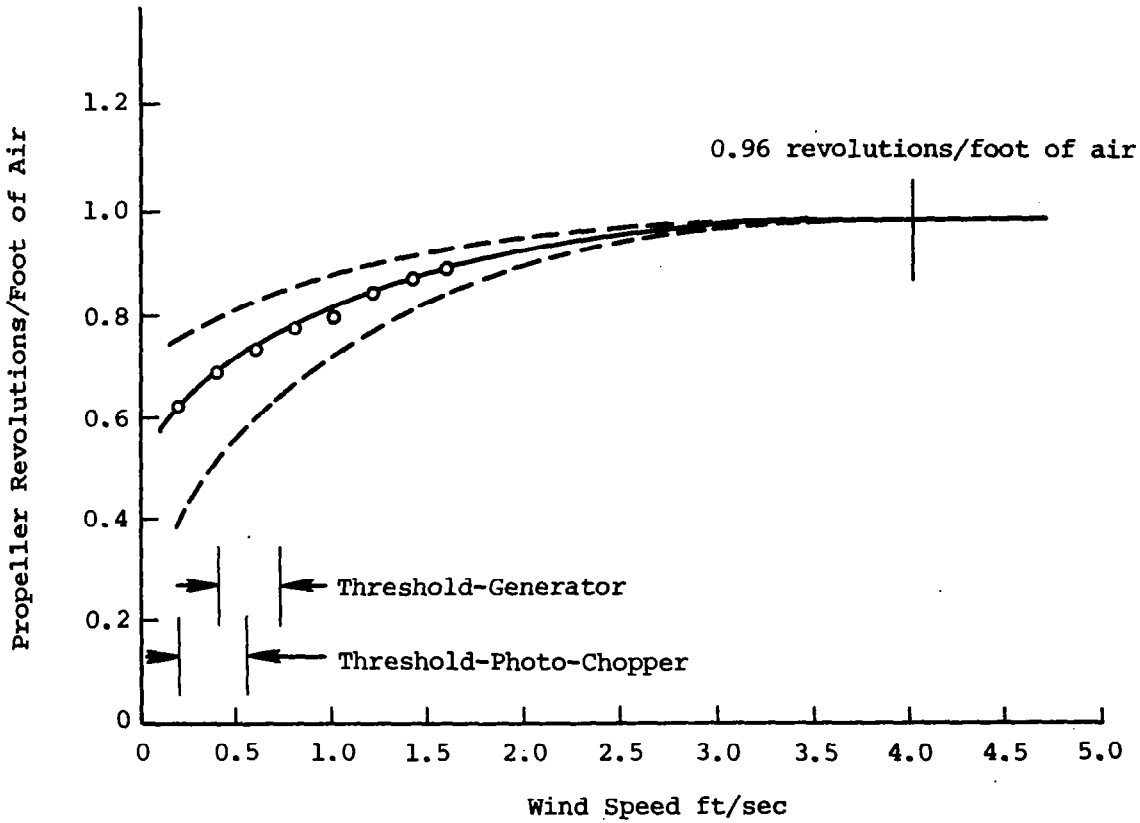

Figure 2-5 Response of four-blade propeller to wind speeds from threshold to 5 ft/sec [10].

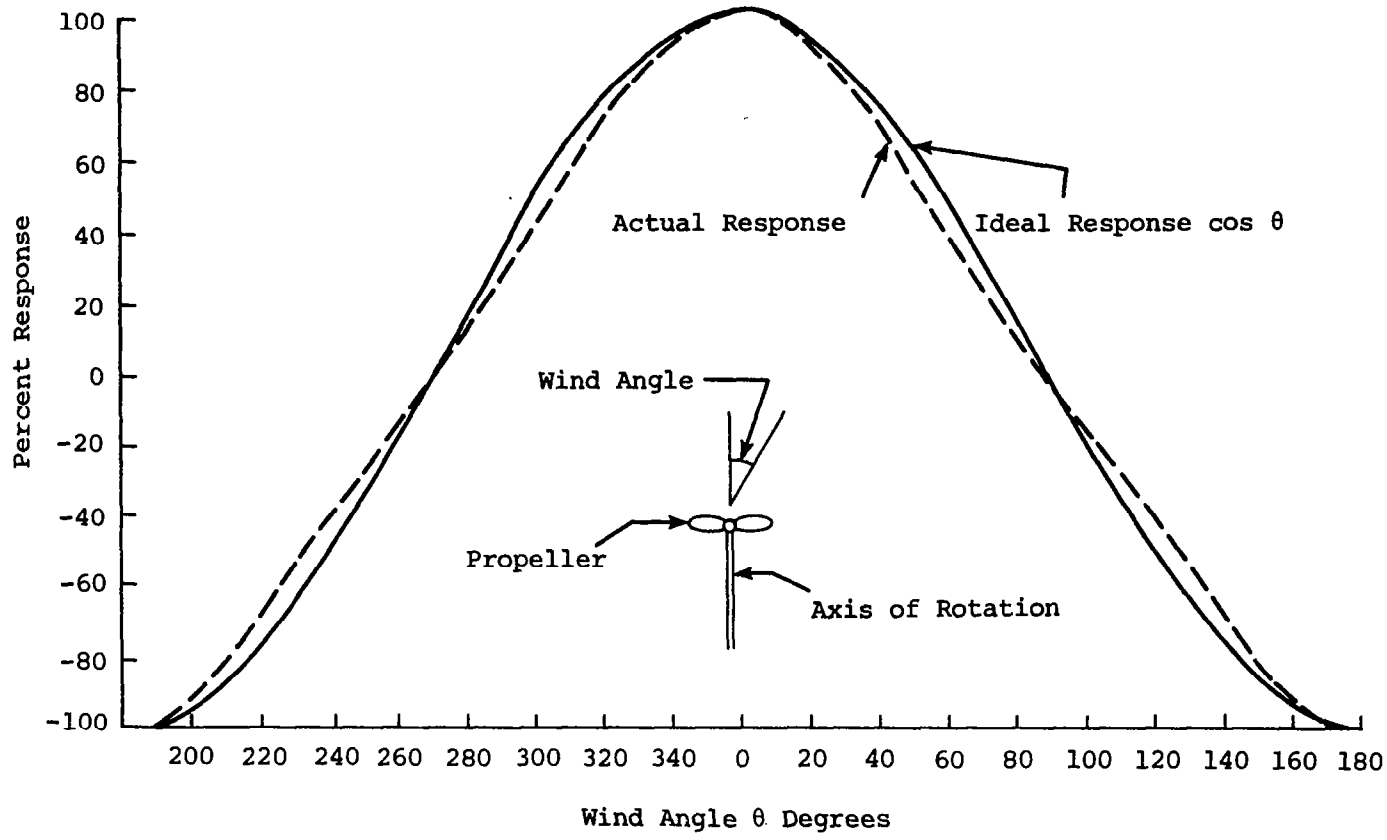

Figure 2-6 Propeller response versus wind angle (four-blade polystyrene propeller) [10].

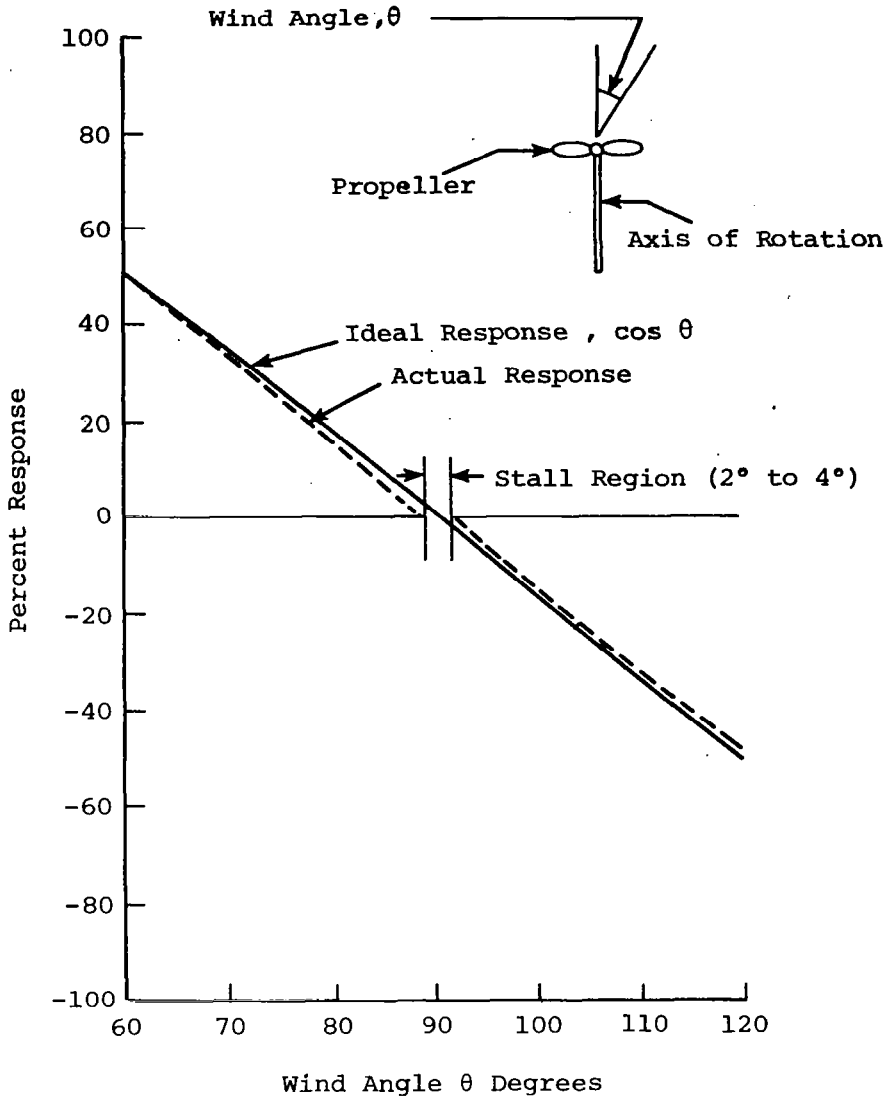

Figure 2-7 Propeller response versus wind angle between 60 and 120 degrees (four-blade polystyrene propeller) [10].

As angle of attack approaches 90 degrees, the distance constant, L, equals Tu', where T is the time constant and u' is the wind tunnel calibration equilibrium speed. The percentage of response is given by u_i/u', where u_i is the indicated speed. Also, the ratio is the cosine of the angle of attack $\cos \alpha = u_i/u'$.

The tape recorders are calibrated prior to each run by recording on each tape -0.2 volts for one minute and +0.2 volts for one minute supplied by a precision power source. The computer laboratory, when reducing the data, then assigns 0.0 to the -0.2 volt reading and 1000 to the +0.2 volt reading, thus dividing a range of -10.64 to 10.64 mph into 1/1000 increments.

SECTION III

DATA REDUCTION AND ANALYSIS

GENERAL CONSIDERATIONS

Data reduction and analysis is a process in which mathematical and statistical operations are performed with the assistance of probability theory to infer a logical conclusion from data which may otherwise seem practically impossible. In being called a process, these two steps (reduction and analysis) are necessary and inseparable when meaningful results are to be obtained. In general, all data analysis is preceded by data reduction, and each step can be further divided into additional steps, depending on the ultimate goal to be achieved from the analysis performed.

To better understand the phenomenon of turbulent flow about a simulated block building, the experiment described herein has been designed to gather data from which conclusions about the flow field can be inferred. Much research, both analytical and experimental, has been conducted relative to turbulent fluid motion. Turbulence, in its own respect, is proving to be one of the most complicated problems to solve in present-day scientific research.

To classify fluid motion as random or "turbulent" might be debated in many cases from a philosophical point

of view. It could be argued that no physical process is truly deterministic since at any time an unforeseen event could occur which would alter supposedly predictable results. On the other hand, it might be argued that turbulent fluid motion, or any physical process, is deterministic since no process is random in the sense that mathematical models might be possible if a sufficient knowledge of the underlying mechanisms of the phenomenon producing the data were known.

Even if exact mathematical models did exist, it would be physically impossible to verify them. To accurately measure the motions of the turbulent flow field with an in-situ instrument, it is necessary to extract kinetic energy from the medium and, in so doing, alter the flow. Any such instrument used to measure the flow will "always" disturb the flow; thus the measured quantity is always modified by the simple act of measurement, and in principle no exact measurement can be made. Faced with this dilemma, it might be asked exactly how any empirical results should be used to verify theoretical models.

Measurement of turbulent motion is a process, however, including the sampling of a quantity from which the error obtained is the difference between the measurement and the corresponding "true value." When using an instrument, however, there is concern for the characteristics of the measurement process associated with that particular instrument. That is to say, a simple reading may be taken to

measure turbulence, but this is only a sample from a statistical population generated by the process of measuring the turbulence itself. If the characteristics of the process are known, it is possible to put bounds on the error of a single measurement, although it is not possible to know the error exactly, for to do so would mean the true or exact value being measured is known. At least some estimate can be made of this particular problem.

The process of measurement is not the theme of this paper, but the results obtained from measurements are of particular concern. This chapter is concerned with the process of reducing data and performing specific analyses. There are general procedures followed when evaluating random data, and these are explained in Section A.

A. DATA ACQUISITION AND PROCESSING

Appropriate techniques for the acquisition and processing of random data (turbulent fluctuations) are heavily dependent upon the physical phenomenon represented by the data and the desired engineering goals of the processing. In general terms, however, processing performed in both the past and present has been divided into five primary categories: (1) collection, (2) recording and transmission, (3) preparation, (4) qualification, and (5) analysis.

Even though the operations are divided into these categories, each of the categories involves a number of sequential steps, as schematically illustrated in Figure 1-1.

Data Collection

The primary element in data collection is the instrumentation transducer (the particular instruments and their specifications were given in Section II-D). For some applications it is possible to perform all desired data processing directly on the transducer signals in real time. However, this was not the case for this particular experiment.

Data Recording and Transmission

During the experiment magnetic tape recorders were used to record all data. A detailed explanation of the procedures used is given in Section III. Magnetic tape recorders are more convenient than other types of recorders because they can both store the large quantity of data and reproduce them in electrical form for easy transmission and processing by computer systems.

Data Preparation

The next key step in data acquisition and processing is preparation of the raw analog data for detailed analysis. The raw data is supplied from an analog tape in the form of voltage time histories. A number of operations are

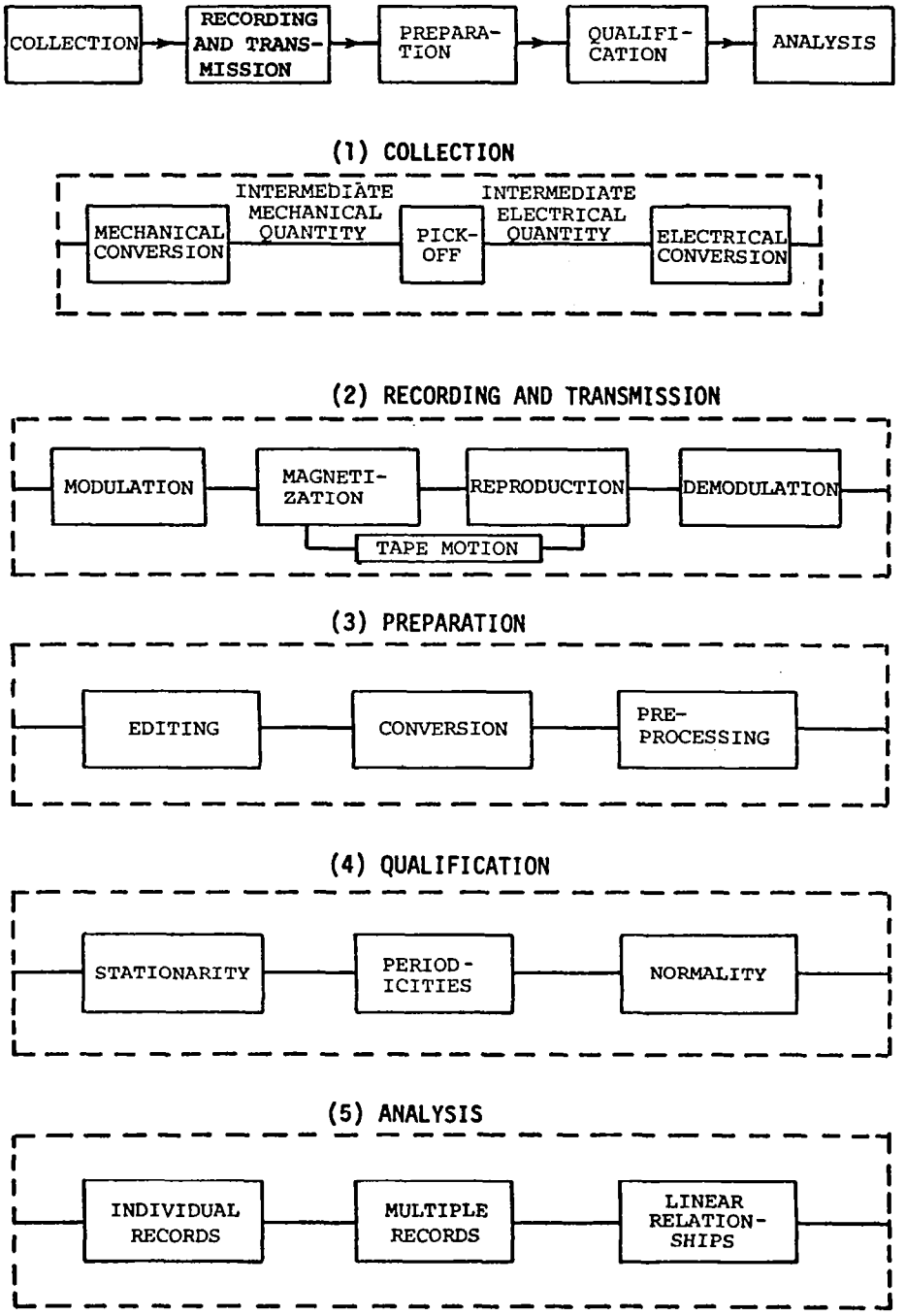

Figure 3-1 Key steps in data acquisition and processing.

needed at this point to transform the voltage time histories suitably for further processing and analysis.

Data editing. The data editing performed on the analog tapes is a pre-analysis procedure designed to detect and eliminate spurious and/or degraded data signals which might have resulted from acquisition and recording problems such as excessive noise, signal dropout, loss of signal due to instrumentation malfunction, etc.

Once the bad data has been eliminated, the voltage signals are converted into engineering units (calibration). This step includes the necessary scaling factor for conversion and the actual process of calculating the new values by means of multiplying the appropriate scaling factor. The scaling factor will depend on the particular units used to express the data (MKS units in this experiment).

Digitization. The next step, digitization, requires special attention. This process consists of two separate and distinct operations: (a) sampling and (b) quantization. These two operations must remain separate and distinct even though occurring practically simultaneously. Many problems and limitations exist when data has been digitized. An explanation of these problems will provide an understanding of the usefulness and limitations placed on any digitized data.

The sampling of analog data is ideally performed at equally spaced intervals, as illustrated in Figure 3-2.

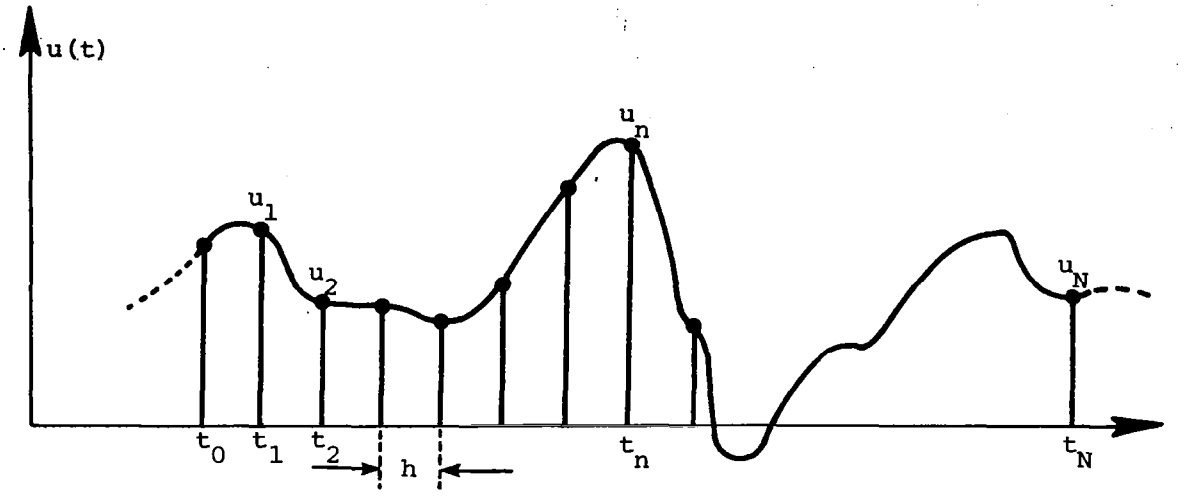

Figure 3-2 Sampling a continuous record.

Generally there is a problem in determining the appropriate interval, h, for sampling. On the one hand, sampling at points which are too close (small h) will yield correlated and highly redundant data, thus unnecessarily increasing the labor and cost of calculations. On the other hand, sampling at points which are too far apart (large h) will lead to confusion between the high and low frequency components of the original data. This latter problem, generally referred to as aliasing, is inherent in all digital processing which is preceded by an analog to

digital conversion, as in the case of this experimental operation.

If the sampling is at every interval, h, as illustrated in Figure 3-2, then the sampling rate is 1/h samples per second. However, at least two samples per cycle are required to define a frequency component in the original data. Hence, the highest frequency which can be defined by sampling at a rate of 1/h samples per second is 1/2h Hz. Any frequencies in the original data above 1/2h Hz will be folded back into the frequency range 0 to 1/2h Hz and will be confused with data in this lower range. Because of this phenomenon, the cutoff frequency,

$$f_c = \frac{1}{2h}$$

is defined as the Nyquist frequency or folding frequency. There are two practical methods by which this aliasing problem can be reduced or possibly avoided. The first method is to choose h sufficiently small so that it is physically unreasonable for data to exist above the associated cutoff frequency, f_c. The second method is to filter the data prior to sampling so that information above a maximum prescribed frequency is no longer contained in the filtered data. Then choosing f_c equal to the maximum frequency of interest will produce accurate results for frequencies below f_c. The first of the two methods was used in this study because it saves computing time and costs.

A similar problem associated with frequency, but not necessarily with digital data, is the maximum length of the recorded signal (t_N in the case of digital data). With this limitation (finite record length) there exists an equivalent lower recognizable frequency, which is

$$f_\ell = \frac{1}{t_N}$$

However, trends may still exist in the data due to frequencies whose wavelength is longer than f_ℓ. Trend removal, a process which improves the stationarity of the data, will be discussed later in this chapter and more specifically in Section IV.

Since the magnitude of each data sample must be expressed by some fixed number of digits, only a finite set of levels are available for approximating the infinite number of levels in the original continuous data. No matter how fine the scale, a choice between two consecutive levels or values will be required. By performing the quantization properly, the true level will be approximated by the quantizing level closest to it. The accuracy of the approximating process is a function of the number of available levels. The present digitizer produces binary outputs compatible with the computer system used and described in Section IV. The analog to digital conversion system produces 6 to 16 bits, which corresponds to a range of 64 to 65,536 levels. Other errors which occur during

the digitization process include aperture error, jitter and nonlinearities. These common errors encountered with any digitization process will not be discussed; however, very descriptive explanations of these problems and their associated error analyses are given by Sebestyan [11] and Oppenheim [12].

After the data are digitized, further operations must be performed on the data prior to any actual analysis. The first operation, reformatting, is theoretically trivial but requires considerable effort to get the data in optimum form for computer usage. Present-day computer operating systems accept system-generated formats; but the types of formats generated by the analog to digital conversion system are nonstandard and require special machine language formats. (These are described briefly in Section IV.) A detailed explanation is not given here; Section IV describes the final data format on the digital tapes so that future researchers have the information needed to reduce complications.

The next operation performed is conversion of the digitized data to physical units. The digitizing procedure produces information in units that are related to the true physical units (speed, direction, etc. in meters per second, degrees, etc.). A reference or calibration signal is recorded at the beginning of each tape when the data are recorded. To provide an indication of operating status,

a zero calibration is also included on each tape prior to the actual recording periods.

The final step, pre-qualifying the data, involves the detection and removal of isolated outliers, level shifts and trends. The actual process used is schematically illustrated in Section IV.

Data Qualification

The correct procedures for reducing random data, as well as interpreting or analyzing the results, are strongly influenced by certain basic characteristics which may or may not be exhibited by the data. The three most important of these basic characteristics are the stationarity of the data, the presence of periodicities in the data, and the normality of the data.

Standard analysis procedures apply to only the stationary data, whereas nonstationary data require special analysis for each situation. Procedures to determine whether the data are stationary and to remove nonstationary trends are discussed later. Periodicities in the data are identified to avoid erroneous interpretation of the results. Autocorrelations and spectral analysis are used to evaluate predominant periodicities in the data and are discussed in general later in this chapter. The procedures for computations are given in Section D. The validity of the assumption that the data have a Gaussian probability density function is investigated since the normality assumption is vital to some analytical applications of random data.

Stationarity. There are several means of defining stationarity of random data; generally, in the strictest sense, the definition incorporates ensemble averages and ensemble probability distributions. For the purposes of this experiment, where only a single sample record is available, the assumption of ergodicity is evoked. It can be shown that ergodic data (by definition) satisfy stationarity. The stationarity of data can be estimated crudely by visual observation of the data or can be tested by investigating a single record as follows:

1. Divide the sample record into N equal time intervals where the data in each interval may be considered independently.
2. Compute a mean square value (or mean value and variance) separately for each interval and align the sample values in the same time sequence as they occur in the original data.
3. Test the sequence of mean square values for the presence of underlying trends or variations other than those due to expected sampling variations (sometimes performed using the run test).

The mathematical calculations which require the assumption of stationarity are given at the end of Section III.

Periodicity. Intense periodic components in the data can usually be detected by visual inspection; however, less intense periodic components in random data are not normally detected by visual inspection. This less intense periodicity can often be detected by inspection of either the power spectral density function, the probability density function, or the autocorrelation function of the respective sample record. Each method used to detect periodicity expresses it in a different manner, and further details can be obtained from [12].

Normality. The most direct way to test samples of stationary random data for normality is to measure the probability density function of the data and compare it to the theoretical normal distributions. (This is done by calculating the skewness and kurtosis and plotting the curve using the theoretical equation and the calculated variance.) This was performed for each record and plotted (Section IV presents examples of such plots) along with the computed skewness and kurtosis, which are presented in tabular form above each plot.

Data Analysis

The procedures for analyzing the properties of sample records and/or random data may be divided logically into two categories: analysis of individual sample records and analysis of a collection of sample records,

given the properties of the individual records. Applicable data analysis procedures for these two categories are outlined below.

Individual records. A sample procedure for analyzing the statistical properties of individual time history records is presented in Figure 3-3. It should be noted that many of the suggested steps in the procedure might be omitted for some applications, while additional steps might be required for other applications. Further, the data qualification step discussed previously is incorporated into the procedures to help clarify how these two parts of the overall data processing problem interact.

All of the analysis techniques discussed in this report apply to sample records of only stationary data. However, if data are determined to be nonstationary during the qualification phase of the processing, special analysis techniques will be required, as indicated by Block E of Figure 3-3 (included for completeness). Since only stationary data are considered herein, no discussion of the techniques for nonstationary and transient data analysis is given, but they are discussed in [12]. Various other analyses of individual time history records are often required, depending upon the specific goals of the data processing. For example, studies of fatigue damage in

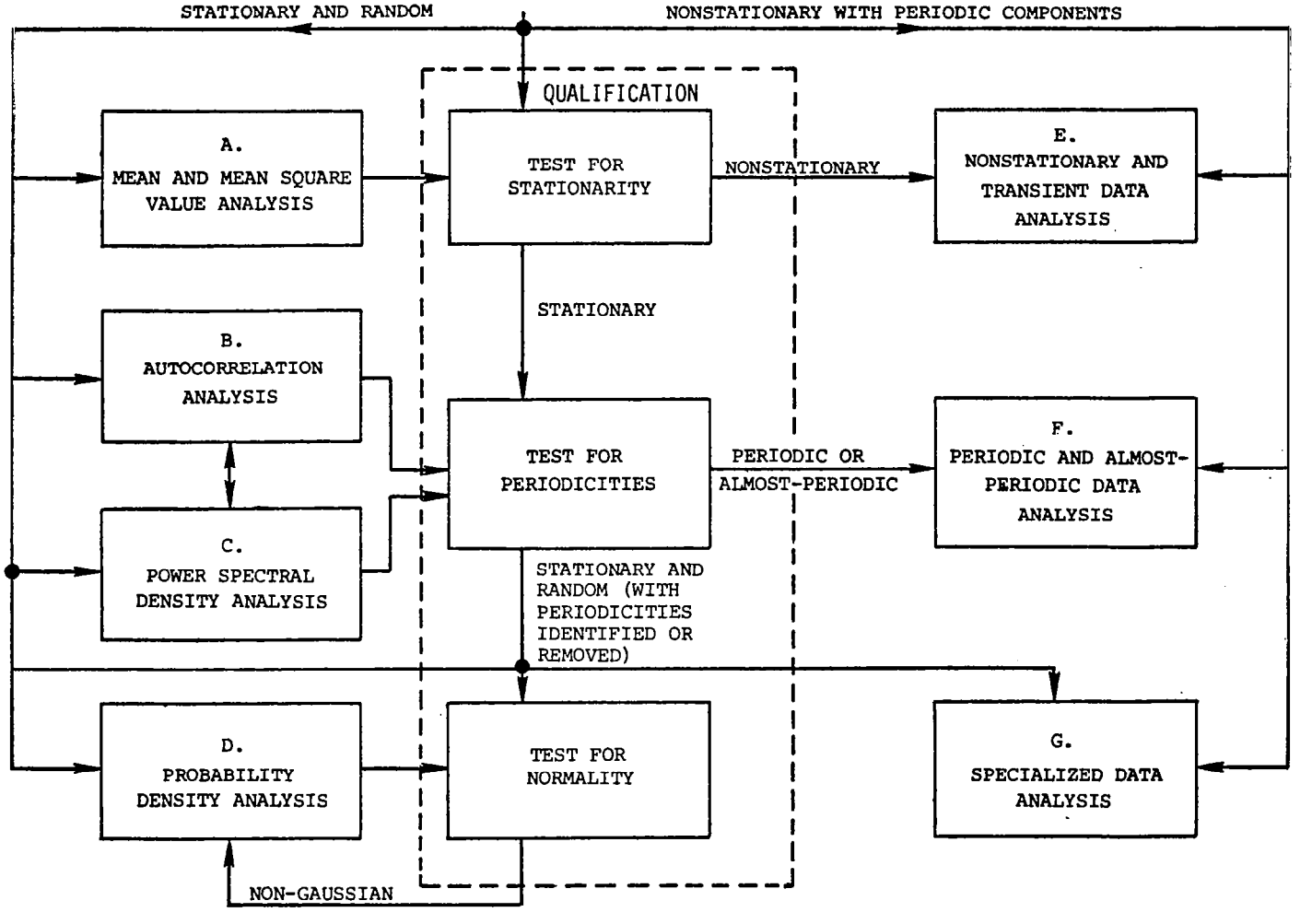

Figure 3-3 General procedures for analyzing individual sample records.

mechanical systems and gust gradient analysis involve the peak probability density functions of strain data, as discussed by Frost et al. [13] relative to wind turbine generator development. An investigation of zero crossings or arbitrary level crossings might be warranted for certain fatigue analysis of wind turbines experiencing velocity gusts whose magnitude will induce structural damage with repeated occurrence.

A collection of records. In the preceding, a discussion for analyzing each individual sample record from an experiment was given. A procedure for further statistical analyses of a collection of sample records is presented in Figure 3-4. The first step in the procedure is to analyze the pertinent statistical properties of the individual sample records, as outlined in Figure 3-3. Hence, the applicable portions of Figure 3-3 constitute Block A in Figure 3-4.

The next step in analyzing the records is to test for correlation among them. As in the case of autocorrelation and power spectral density functions, the cross-correlation and cross-spectral density functions are Fourier transform pairs. The measurements of a cross-correlogram will technically not yield any new information from that given by a cross-spectrum. However, since it may present desired information in a more convenient format it will be addressed in Section V, where Taylor's hypothesis

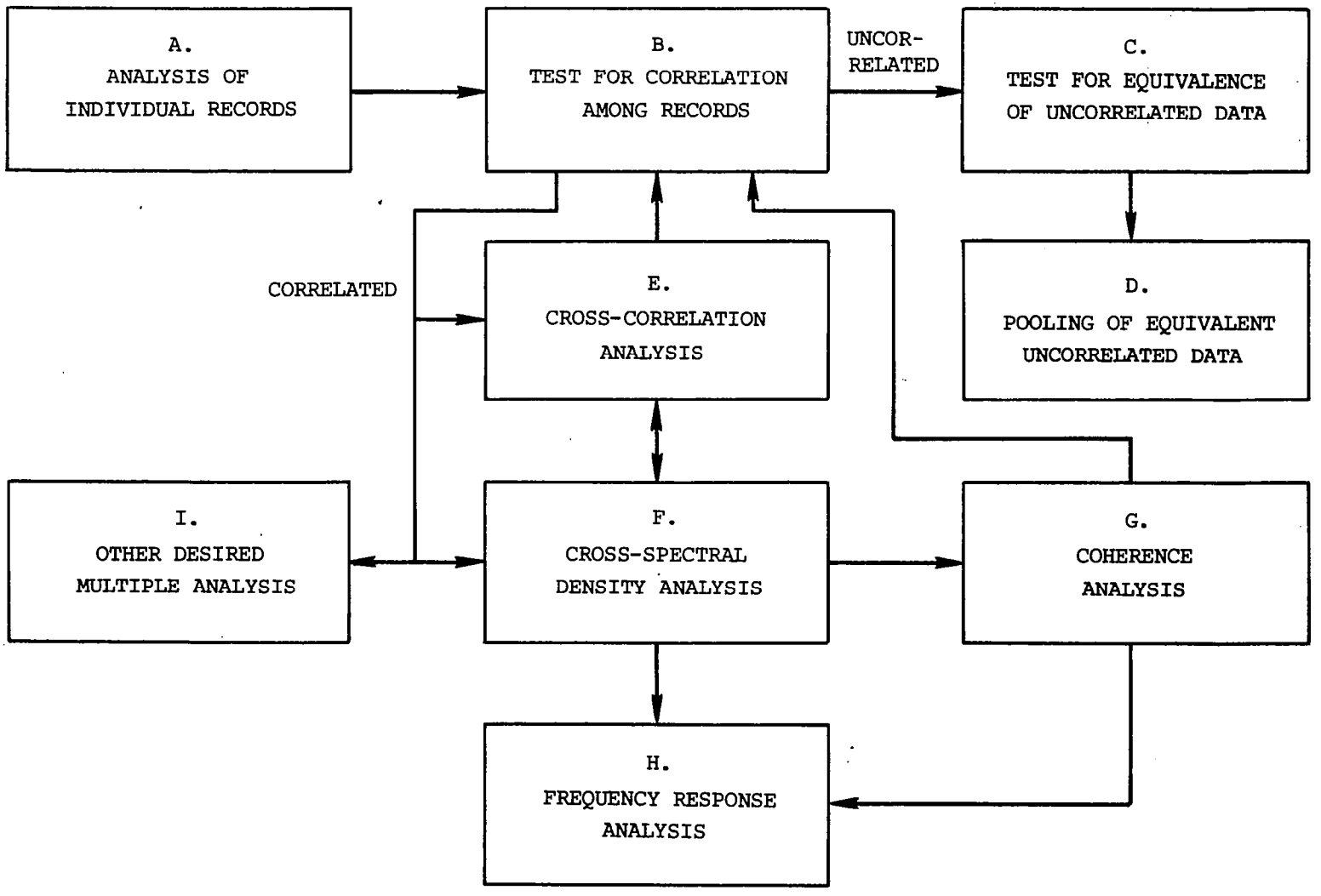

Figure 3-4 General procedure for analyzing a collection of sample records.

is described and tested using the data sets of this report. The cross-spectral density and coherence function analyses will aid in the test for correlation among the collection of sample records. The coherence function tells not only whether the records are correlated, but to what degree they are correlated as a function of frequency, as well as how much lag time exists between the two records as a function of frequency. The cross-spectral and coherence analyses were not performed during the research reported.

B. DIGITAL DATA ANALYSIS PROCEDURES

This section discusses the digital techniques (distinct from analog data analysis procedures) developed for analyzing the data tapes obtained from MSFC. Most formulae assume the data to be processed as discrete time series values representing sample records from stationary (ergodic) random processes. This discussion includes only methods used to compute the mean, the standard deviation, the removal of trends, the Fourier Transform, the Fast Fourier Transform, the correlation functions, and the spectral density function. Many procedures commonly used in digital data processing are not discussed in this section but can be found in [12].

Let a single continuous random record u(t) be sampled at points $\Delta t = h$ apart. These points determine a Nyquist folding frequency, f_c, given by

$$f_c = \frac{1}{2h} \tag{3.1}$$

as discussed in the previous section. Let

$$\{u_n\} \quad ; \; n = 1,2,3,\ldots,N \tag{3.2}$$

be the data values found at the N points

$$t_n = t_o + nh \quad ; \; n = 1,2,3,\ldots,N \tag{3.3}$$

where the initial point t_o is arbitrary and does not enter into the later formulae unless the sequence is assumed to start at n = 0 and end at n = N - 1 as a matter of convenience. In equation form, the original data values (illustrated in Figure 3-2, page 33) are

$$u_n = u(t_o + nh) \quad ; \; n = 1,2,3,\ldots,N \tag{3.4}$$

Arithmetic Quantities

The sample mean value is given by

$$\bar{u} = \frac{1}{N} \sum_{n=1}^{N} u_n \tag{3.5}$$

where N is the number of data samples and u_n represents the data values. The quantity $\bar{u}$ calculated here is an unbiased estimate of the mean value μ of the total population being sampled. In order that subsequent formulae and calculations may be simplified, the data is now transformed to have a zero mean value. A new time history record $x(t) = u(t) - \bar{u}$ is therefore defined where x(t) has data values $\{x_n\}$ given by

$$x_n = x(t_o + nh) = u_n - \bar{u} \quad ; \; n = 1,2,3,\ldots,N \tag{3.6}$$

Note that $\bar{x} = 0$. The original data values are represented

by $\{u_n\}$ instead of by $\{x_n\}$ so that the $\{x_n\}$ notation indicates a zero sample mean value. As appropriate, subsequent formulae will be stated in terms of the transformed data values $\{x_n\}$.

The sample standard deviation is given by

$$S = \left[\sum_{n=1}^{N} \frac{(x_n)^2}{N-1}\right]^{1/2} = \left[\frac{1}{N-1} \sum_{n=1}^{N} (x_n)^2\right]^{1/2} \tag{3.7}$$

where N is the number of data samples. The quantities S and S^2 are unbiased estimates of the standard deviation and variance σ_x and σ_x^2, respectively, of the total population being sampled.

A further transformation of the data is convenient at this time if the computer calculations are to be performed with fixed point, as opposed to floating point arithmetic. Multiplying the transformed values x_n by 1/S yields

$$Z_n = x_n/S \quad ; \; n = 1,2,3,\ldots,N \tag{3.8}$$

This results in final data with a sample mean of zero and a sample standard deviation of unity. This is generally performed to reduce overflow and underflow errors when using fixed point computer calculations.

Trend Removal

A special correction is needed to remove any trends which might be in the data, defined as any frequency components whose periods are longer than the record length ($f < 1/t_N$). In particular, this type of component cannot

be removed by highpass digital filtering [12]. Hence, special trend removal techniques must be applied. Least squares procedures can be employed for the linear as well as the higher order polynomial trends. To remove linear trends only an alternative method, which is not as accurate as least squares procedures, is the average slope method. In this experiment the trend was removed by taking a least squares fit of a polynomial throughout the data. This procedure is defined in detail in Section IV.

Autocorrelation Estimates Via Direct Computations

For N data values $\{x_n\}$, n = 1,2,...,N, from a transformed record x(t) which is stationary with $\bar{x} = 0$, the estimated autocorrelation function at the displacement rh is defined by the formula

$$\hat{R}_r = \hat{R}_x(rh) = \frac{1}{N - r} \sum_{n=1}^{N-r} x_n x_{n+r} \quad ; \quad r = 0,1,2,...,m \tag{3.9}$$

where r is the lag number, m is the maximum lag number, and $\hat{R}_x(rh)$ is the estimate of the true value $R_x(\tau)$ at lag τ, corresponding to the displacement rh. Note that the maximum lag number m is related to the maximum time displacement of the estimate by

$$\tau_{max} = \tau_m = mh \tag{3.10}$$

Equation (3.9) was selected since it represents an unbiased estimated as compared to the following biased estimate.

$$\hat{R}_r = \hat{R}_x(rh) = \frac{1}{N} \sum_{n=1}^{N-r} x_n x_{n+r} \quad ; \quad r = 0,1,2,...,m \tag{3.11}$$

This estimate will provide very accurate results when N is much larger than m. When N is large and m is small with respect to N, then Equations (3.9) and (3.11) provide comparable results.

A normalized value for the autocorrelation function is obtained by dividing $\hat{R}_r$ by $\hat{R}_o$ where

$$\hat{R}_o = \hat{R}_x(o) = \frac{1}{N} \sum_{n=1}^{N} (x_n)^2 = \overline{x^2} \tag{3.12}$$

Note that the quantity $\hat{R}_o$ is a sample estimate of the true mean square value of the data. The quantity $\hat{R}_o$ is related to the sample variance S^2 by the relation

$$\hat{R}_o = \left[\frac{N - 1}{N}\right] S^2 \tag{3.13}$$

Thus for large N, there is negligible difference between $\hat{R}_o$ and S^2. When $\hat{R}_r$ is normalized, one obtains $\hat{R}_r/\hat{R}_o$ which is theoretically between plus and minus one; that is,

$$-1 \leq \hat{R}_r/\hat{R}_o \leq 1$$

The autocorrelation can also be computed by Fast Fourier Transform (FFT) techniques as discussed at the end of this section.

Cross-Correlation Functions

There are two basic approaches used for estimating cross-correlation functions, namely, the direct approach (discussed in this section) and the FFT approach (discussed later in this section).

Unbiased estimates of the sample cross-correlation functions at lag numbers r = 0,1,2,...,m are defined by

$$\hat{R}_{xy}(rh) = \frac{1}{N - r} \sum_{n=1}^{N-r} x_n y_{n+r} \tag{3.14}$$

$$\hat{R}_{yx}(rh) = \frac{1}{N - r} \sum_{n=1}^{N-r} y_n x_{n+r} \tag{3.15}$$

Note that the two cross-correlation functions $\hat{R}_{xy}(rh)$ and $\hat{R}_{yx}(rh)$ differ by the interchange of the x_n and y_n data values.

The sample cross-correlation function $\hat{R}_{xy}(rh)$ may be normalized to have values between plus and minus one by dividing by $\sqrt{\hat{R}_x(o)}\ \sqrt{\hat{R}_y(o)}$. This defines a sample cross-correlation coefficient

$$\hat{B}_{xy}(rh) = \frac{\hat{R}_{xy}(rh)}{\sqrt{\hat{R}_x(o)}\ \sqrt{\hat{R}_y(o)}} \quad ; \quad r = 0,1,2,...,m \tag{3.16}$$

which theoretically should satisfy $-1 \leq \hat{B}_{xy}(rh) \leq 1$.

Fast Fourier Transform

The FFT is an algorithm for fast computation of the Fourier transformations on a digital computer. A short history of the FFT, as well as its many applications, is provided in [12] and [14].

The FFT is a powerful tool for calculating spectral density functions, cross-spectra, autocorrelations and cross-correlations and is discussed here for later reference.

An infinite-range Fourier Transform of a real-valued or a complex-valued record x(t) is defined by the complex-value quantity

$$X(f) = \int_{\infty}^{\infty} x(t)\ \exp[-j2\pi ft]\ dt \tag{3.17}$$

Theoretically this transform, X(f), will not exist, [14], for an x(t) which is a representative member of a stationary random process when the "infinite" limits are used. However, by restricting the limits to a finite time interval of x(t), say in the range (o,T), the finite range Fourier Transform will exist, [8], as defined by

$$X(f,T) = \int_{o}^{T} x(t)\ \exp[-j2\pi ft]\ dt \tag{3.18}$$

For arbitrary f, the discrete version of Equation (3.18) [14] is

$$X(f,T) = h \sum_{n=0}^{N-1} x_n\ \exp[-j2\pi fnh] \tag{3.19}$$

The selection of discrete frequency values for the computation of X(f,T) is

$$f_k = kf_o = \frac{k}{T} = \frac{k}{Nh}\ ;\ k = 0,1,2,\ldots,N-1 \tag{3.20}$$

At these frequencies, the transformed values of the Fourier components are defined by

$$X_k = \frac{X(f_k,T)}{h} = \sum_{n=0}^{N-1} x_n\ \exp\left[-j\ \frac{2\pi kn}{N}\right]\ ;\ k = 0,1,2,\ldots,N-1 \tag{3.21}$$

where h has been included with X(f,T) to have a scale factor

of unity before the summation. Note that results are unique only out to k = N/2 since the Nyquist cutoff frequency occurs at this point. A Fast Fourier Transform method has been developed [14] and a modified version of the subroutine is given in Figure 3-5. This subroutine computes the FFT of N data values. It requires N to be an integral power of 2. For example, $N = 2^a$ where "a" is a positive integer. A complete explanation of the original subroutine is given in [14]. The present FFT subroutine was modified to also calculate the inverse FFT by changing the signs of the imaginary parts of x(t) (noted as XI in the subroutine). If the value of NGG is equal to 1, the subroutine computes the FFT; otherwise it computes the inverse FFT. This subroutine was used extensively in the computation of the autocorrelations, cross-correlations and spectral density functions present in this thesis. The following sections describe briefly the indirect FFT technique for computation of the autocorrelation and cross-correlation functions.

Autocorrelation Via FFT Computations

An indirect method for computing autocorrelation function estimates is to first compute the power spectral density function directly by FFT and to then compute the autocorrelation by the inverse FFT of the result. The double use of the FFT procedure is in most cases more efficient than the direct procedure; of course, this depends upon the maximum lag values desired.

```
      SUBROUTINE FFT(N,NU,NGG)
      COMMON/ST3/XR(2048),XI(2048)
      IF(NGG.EQ.1) GO TO 321
      DO 320 I=1,N
  320 XI(I)=-XI(I)
  321 N2=N/2
      NU1=NU-1
      K=0
      DO 100 L=1,NU
  102 DO 101 I=1,N2
      P=IBITR(K/2**NU1,NU)
      ARG=6.283185*P/FLOAT(N)
      C=COS(ARG)
      S=SIN(ARG)
      K1=K+1
      K1N2=K1+N2
      TR=XR(K1N2)*C+XI(K1N2)*S
      TI=XI(K1N2)*C-XR(K1N2)*S
      XR(K1N2)=XR(K1)-TR
      XI(K1N2)=XI(K1)-TI
      XR(K1)=XR(K1)+TR
      XI(K1)=XI(K1)+TI
  101 K=K+1
      K=K+N2
      IF(K.LT.N) GO TO 102
      K=0
      NU1=NU1-1
  100 N2=N2/2
      DO 103 K=1,N
      I=IBITR(K-1,NU)+1
      IF(I.LE.K) GO TO 103
      TR=XR(K)
      TI=XI(K)
      XR(K)=XR(I)
      XI(K)=XI(I)
      XR(I)=TR
      XI(I)=TI
  103 CONTINUE
      IF(NGG.EQ.1) GO TO 121
      DO 124 I=1,N
      XR(I)=XR(I)/N
      XI(I)=XI(I)/N
  124 CONTINUE
  121 RETURN
      END
      FUNCTION IBITR(J,NU)
      J1=J
      IBITR=0
      DO 200 I=1,NU
      J2=J1/2
      IBITR=IBITR*2+(J1-2*J2)
  200 J1=J2
      RETURN
      END
```

Figure 3-5 FFT subroutine.

Care must be exercised in using this indirect method since the usual correlation function is not computed. Rather, this method computes a "circular" correlation function which is defined by the relationship

$$\hat{R}_x^c(rh) = \frac{(N - r)}{N} \hat{R}_x(rh) + \frac{r}{N} \hat{R}_x[(N - r)h] \qquad (3.22)$$

where $R_x(rh)$ has been defined by Equation (3.9) and

$$\hat{R}_x^c(rh) = \hat{R}_x^c[(N - r)h] \quad ; \quad r = 0,1,2,\ldots,m \qquad (3.23)$$

The "circular" correlation function can be avoided by adding zeros to the end of the original data. The effect on the correlation function by adding zeros to the data is to spread apart the two portions of the "circular" correlation function. In particular, if N zeros are added to the original N data values, the two portions will separate completely.

Power spectral estimates via FFT. Computation of the autocorrelation function estimate requires calculation of the power spectra, and the procedures used are discussed below.

For sampled data from a transformed record x(t) which is stationary with $\bar{x} = 0$, a raw estimate $\tilde{G}_x(f)$ of a true power spectral density function $G_x(f)$ [14] is defined for an arbitrary f in the range $0 \leq f \leq f_c$ by

$$\tilde{G}_x(f) = 2h\left[\hat{R}_o + 2\sum_{r=1}^{m-1} \hat{R}_r \cos\left(\frac{\pi r f}{f_c}\right) + \hat{R}_m \cos\left(\frac{\pi m f}{f_c}\right)\right] \qquad (3.24)$$

where h is the time interval between samples, R_r is the estimate of the autocorrelation function at lag r, m is the maximum lag number, and $f_c = 1/2h$ is the cutoff or Nyquist frequency as described earlier. However, the spectral estimate at discrete frequencies can also be obtained as follows:

$$\tilde{G}_k = \tilde{G}_x(f_k) = \frac{2}{Nh} |X(f_k,T)|^2 = \frac{2h}{N} |X_k|^2 \qquad (3.25)$$

where X_k was defined in Equation (3.21) and will be calculated using the FFT.

The following steps are recommended [12] to compute the power spectrum estimates via FFT procedures. (Steps 2 and 5 were not used since N is relatively large.) Assume that the sample size for the data sequence x_n is initially of arbitrary size N. (For this experiment the value of N is selected to be an integral power of 2 as described earlier.)

1. Truncate the data sequence or add zeros so that $N = 2^a$, where a is an integer.
2. Taper the resulting sequence using the cosine taper window.
3. Compute the X_k using the FFT subroutine for $k = 0,1,\ldots,N-1$.
4. Compute the $\tilde{G}_k$ of Equation (3.25) for $k = 0,1,\ldots,N-1$.

5. Adjust these estimates for the scale factor due to tapering [by replacing $\tilde{G}_k$ with $(1/0.875)\tilde{G}_k$ if the cosine tapering is used].

Using the above procedure to calculate the power spectra estimate, the autocorrelation function is computed as follows.

1. Augment the N data values of x_n, where $n = 0,1,\ldots,N-1$, with N zeros to obtain a new x_n sequence of 2N terms. Remember to initialize the imaginary values to zero if only real valued functions are being computed.
2. Compute the 2N-point FFT giving X_k for $k = 0,1,\ldots,2N-1$, using the FFT subroutine with 2N replacing N.
3. Compute the raw spectral estimates $\tilde{G}_k$ for $k = 0,1,\ldots,2N-1$, using Equation (3.25).
4. Compute the inverse FFT (NGG = 1) of $\tilde{S}_k = \tilde{G}_k/2$ to obtain $\hat{R}_x{}^c(rh)$ for $r = 0,1,2,\ldots,2N-1$.
5. Discard the last half of $\hat{R}_r$ to obtain results for $r = 0,1,\ldots,N-1$, and multiply by the scale factor $N/(N - r)$.

This procedure provides a very accurate estimate of the autocorrelation, as illustrated relative to the direct procedures in Section V, where both techniques are compared by plotting the results and determining the total computational time for different values of N.

Cross-Correlation Functions Via FFT

The procedure used to compute the cross-correlation function via FFT is similar to that of the autocorrelation, but some differences exist. The initial size of the sample for both x(t) and y(t) is assumed to be $N = 2^a$, where a is an integer. For these computations, the cross-correlation function is obtained from the cross-spectral density function and involves two separate FFT's, one for x(t) and one for y(t). These two FFT's can be computed simultaneously by using the following equations and procedures.

The FFT's of the two real-valued records are computed simultaneously by inserting one record x(n) as the real part and one record y(n) as the imaginary part of a complex record z(n). In equation form, let

$$z(n) = x(n) + jy(n) \quad ; \; n = 0,1,2,\ldots,N-1 \tag{3.26}$$

The Fourier transform of z(n) by Equation (3.19) is

$$Z(k) = \sum_{n=0}^{N-1} [x(n) + jy(n)] \exp\left[-j \frac{2\pi kn}{N}\right] \quad ; \; k = 0,1,\ldots,N-1 \tag{3.27}$$

This is computed by using the modified FFT subroutine described in the last section. It is assumed in Equations (3.26) and (3.27) that N data points in x(n) and y(n) are transformed into N frequency points which are spaced 1/T apart. For these situations, the Nyquist cutoff frequency occurs when k = N/2 so that for N even, unique results occur only for k = 0,1,2,...,(N/2)-1. To obtain X(k) and Y(k), observe that

$$\exp\left[j\,\frac{2\pi n(N-k)}{N}\right] = \exp\left[-j\,\frac{2\pi nk}{N}\right] \qquad (3.28)$$

since $\exp[j2\pi n] = 1$ for any n. Hence, if $Z^*(k)$ is the complex conjugate of $Z(k)$, then

$$Z^*(N-k) = \sum_{n=0}^{N-1} [x(n) - jy(n)] \exp\left[-j\,\frac{2\pi nk}{N}\right] \qquad (3.29)$$

From Equations (3.27) and (3.29) it follows that

$$Z(k) + Z^*(N-k) = 2\sum_{n=0}^{N-1} x(n) \exp\left[-j\,\frac{2\pi nk}{N}\right] = 2X(k)$$

$$Z(k) - Z^*(N-k) = 2j\sum_{n=0}^{N-1} y(n) \exp\left[-j\,\frac{2\pi nk}{N}\right] = 2jY(k)$$

From this the real valued records $x(n)$ and $y(n)$ have Fourier Transforms $X(k)$ and $Y(k)$ given by

$$X(k) = \frac{Z(k) + Z^*(N-k)}{2}$$

$$Y(k) = \frac{Z(k) - Z^*(N-k)}{2j} \qquad ; k = 0,1,\ldots,N-1 \qquad (3.30)$$

Using this final result the following procedure is used to compute the cross-correlation using the supplied FFT subroutine.

1. Store x_n in the real part and y_n in the imaginary part of $z_n = x_n + jy_n$, $n = 0,1,\ldots,N-1$.
2. Augment both the real and imaginary parts with N zeros to obtain a new z_n sequence of 2N terms.
3. Compute the 2N-point FFT giving $Z(k)$ for $k = 0,1,\ldots,2N-1$, using the supplied FFT subroutine.
4. Compute X_k and Y_k for $k = 0,1,\ldots,2N-1$, using Equation (3.30).

5. Compute the raw cross-spectral density estimate $\tilde{G}_{xy}(f_k)$ for k = 0,1,...,2N-1, where $\tilde{G}_{xy}(f_k) = \frac{h}{N} |X_k^* Y_k|$ and X_k^* is the complex conjugate of X_k.

6. Compute the inverse FFT of $\tilde{G}_{xy}(k)$ and multiply by the scale factor N/(N - r) to obtain $\hat{R}_{xy}(rh)$ for r = -N,-N+1,...,0,1,...,N-1. This scale factor is required because of a similar "circular" correlation effect as the auto-correlation function described earlier.

These procedures have been programmed using Fortran language to analyze the wind data stored on the MSFC magnetic computer tapes. A short discussion of these data tapes and the associated programs needed to obtain data from the tapes is given in Chapter IV, and some preliminary analyses and results of this experiment are given in Section V.

SECTION IV

DATA ORIENTATION, FORMATTING, AND TAPE ACCESSING

Prior to using any experimental data a particular frame of reference is needed. The orientation of the tower system with respect to the ground is given in Chapter II; however, it is necessary to explain the frame of reference by which data is recorded and the relatively simple procedures used to record and retrieve data. It is also appropriate at this time to explain the procedures and the associated computer programs developed for extracting data from the available magnetic data tapes. Finally, a few of the example plots and computer printouts of past data reduction and analyses performed by MSFC are illustrated. These plots are in general self-explanatory, and only a brief explanation of each is given. With this introduction and explanation the following section is intended for use by future researchers using MSFC data tapes.

A. DATA RECORDING AND INITIAL PROCESSING

The output from the sensors described in Section II-D is recorded on nine analog recorders located in the Instrumentation and Recording Station (Figure 2-1, page 10).

Recording Methods

Horizontal wind speed. Signals produced by the horizontal wind speed sensors (Climet Model 011-1, three-cup anemometers) are recorded on analog recorders 1, 2 and 3 (indicated in Table 4-1). The square wave with frequency proportional to the wind speed signal is utilized for this experiment.

Wind direction. Signals produced by the wind direction sensors (Climet Model 012-1 vanes) are recorded on analog recorders 4, 5 and 6 (indicated in Table 4-2) as a positive DC voltage whose amplitude is directly proportional to the wind direction.

Vertical velocity. Signals produced by the vertical velocity sensors (Gill Model 27100 propeller anemometers) are recorded on analog recorders 7, 8 and 9 (indicated in Table 4-3) as a positive or negative DC voltage whose amplitude is directly proportional to the vertical velocity.

Temperature. Signals produced by the temperature sensors (Climet Model 016-5 thermistors) are recorded on analog recorder 9 (indicated in Table 4-3) as a positive DC voltage that is directly proportional to the temperature.

Analog recorders. The nine analog recorders are Ampex Model CP-100 recorders. Each recorder has the

TABLE 4-1

METHOD OF RECORDING HORIZONTAL WIND SPEED

Recorder #1			Recorder #2			Recorder #3		
Channel #	Tower	Level	Channel #	Tower	Level	Channel #	Tower	Level
1	1	1	1	4	1	1	7	1
2	1	2	2	4	2	2	7	2
3	1	3	3	4	3	3	7	3
4	1	4	4	4	4	4	7	4
5	2	1	5	5	1	5	8	1
6	2	2	6	5	2	6	8	2
7	2	3	7	5	3	7	8	3
8	2	4	8	5	4	8	8	4
9	3	1	9	6	1	9 Blank		
10	3	2	10	6	2	10 Blank		
11	3	3	11	6	3	11 Blank		
12	3	4	12	6	4	12 Blank		
13 Time			13 Time			13 Time		
14 Voice			14 Voice			14 Voice		

TABLE 4-2

METHOD OF RECORDING WIND DIRECTION

Recorder #4			Recorder #5			Recorder #6		
Channel #	Tower	Level	Channel #	Tower	Level	Channel #	Tower	Level
1	1	1	1	4	1	1	7	1
2	1	2	2	4	2	2	7	2
3	1	3	3	4	3	3	7	3
4	1	4	4	4	4	4	7	4
5	2	1	5	5	1	5	8	1
6	2	2	6	5	2	6	8	2
7	2	3	7	5	3	7	8	3
8	2	4	8	5	4	8	8	4
9	3	1	9	6	1	9 Blank		
10	3	2	10	6	2	10 Blank		
11	3	3	11	6	3	11 Blank		
12	3	4	12	6	4	12 Blank		
13 Time			13 Time			13 Time		
14 Voice			14 Voice			14 Voice		

TABLE 4-3

METHOD OF RECORDING VERTICAL WIND SPEED

Recorder #7			Recorder #8			Recorder #9		
Channel #	Tower	Level	Channel #	Tower	Level	Channel #	Tower	Level
1	1	1	1	4	1	1	7	1
2	1	2	2	4	2	2	7	2
3	1	3	3	4	3	3	7	3
4	1	4	4	4	4	4	7	4
5	2	1	5	5	1	5	8	1
6	2	2	6	5	2	6	8	2
7	2	3	7	5	3	7	8	3
8	2	4	8	5	4	8	8	4
9	3	1	9	6	1	9 (Temp)	1	1
10	3	2	10	6	2	10 (Temp)	1	2
11	3	3	11	6	3	11 (Temp)	1	3
12	3	4	12	6	4	12 (Temp)	1	4
13 Time			13 Time			13 Time		
14 Voice			14 Voice			14 Voice		

capability of recording 12 channels of data plus voice and time. The allocation of the data to the respective channels is indicated in Tables 4-1, 4-2, and 4-3.

Test description. A test consists of the simultaneous recording of the output of each of the 100 sensors for approximately 1.5 hours. Each of the analog tapes are calibrated prior to the start of each test with approximately 30 seconds minimum and maximum calibration. These calibrations represent 0.0 and 100.0 percent levels for each sensor output. When each test is completed, the data tape is internally processed by the computer center and prepared for distribution to the user.

Hardware Systems

The hardware systems necessary to process and reduce the analog data are a cycle counter, an SDS station, a DDP-224 computer, and a DDP-116 computer. The following paragraphs describe the processing performed by each of the systems.

Cycle counter. The cycle counter is used to digitize the wind speed data contained on analog recorders 1, 2 and 3. This system counts the frequency of the square wave signal on the analog tapes for a fixed time increment (0.1 second) and outputs the count on a magnetic tape as a function of time.

SDS station. The SDS station is used to digitize the wind direction data on analog tapes 4, 5 and 6; the vertical velocity data on analog tapes 7, 8 and 9; and the temperature data on analog tape 9. This system converts the DC voltages recorded on these analog tapes to digital counts at a specified sample rate (10 per second). These digital data are then written on a magnetic tape as a function of time.

The calibrations on each analog tape are digitized using the above procedures. These calibration data are then written as the first two files on the digital data tapes to insure all units are working properly. (Malfunction is easily detected by analyzing the first two records containing the calibration results.)

To digitize all 68 channels of data on analog tapes 4-9, six runs on the SDS station are required (one for each data tape).

DDP-224. The DDP-224 is used to convert the data from the above stations from raw counts to engineering units and to prepare the data for analysis using the DDP-116 system. The data is later edited.

DDP-116. The DDP-116 is used to compute the several statistical properties of turbulence described in Section III.

Software Used in Preparing Master Digital Tapes

In response to a request from MSFC, the Computer Applications Section, Data Reduction Department of Computer Sciences Corporation has developed the software required to support the internal data reduction. This software is comprised of three DDP-224 programs and one DDP-116 program.

DDP-224 programs. The DDP-224 programs are used to do all preliminary processing required to prepare the data for analysis. There are three main programs used in the DDP-224; namely,

1. Merge program.
2. Lon-Lat program.
3. Filter-Edit program.

The merge program uses as input the 14 tapes created at the Analog to Digital (A/D) Stations. The program converts the data from raw counts to engineering units and merges the data into a time history stored on the disk for output to tape. This program also does a preliminary edit of each data channel for data out of range and compiles a parity history for each input tape. The program may be restarted with any number of the input tapes if there are problems encountered while merging.

The Lon-Lat program uses the output tape generated by the merge program to compute an overall mean for each data channel and the components of turbulence contained in the data. The components of turbulence are output on tape as a function of time.

The Filter-Edit program uses as input the tape generated by the Lon-Lat program. These components of turbulence are filtered and edited for missing data and data flagged as out of range during the merge process. The Filter-Edit program will linearly interpolate for up to 2.0 seconds of bad or missing data on each channel. Data channels that contain more than 2.0 seconds of erroneous data are flagged as being permanently missing. These data channels receive no further processing, however, they are retained for future inspection. This Filter-Edit program outputs the filtered data on tape as a function of time for processing on the DDP-116 system.

DDP-116 program. The DDP-116 program uses as input the tape generated by the Filter-Edit program. This system (DDP-116) is used to analyze the components of turbulence and to display the analysis in a form that is easily interpreted by a researcher having an adequate background in statistical techniques and representations. The program used in the DDP-116 computes statistics, autocorrelation functions, and power spectral densities of the turbulence. These results are plotted using an SC-4020 plotter. The program also outputs the analysis on magnetic tape for future reference.

Magnetic Tape Reduction Summary

The data reduction process for the MSFC eight tower array can best be described as a sequence of events in which

the status of each event determines the action required for initiation of the next event. The initial magnetic tape reduction and analysis process can be divided into eight events as follows:

1. Receive nine data tapes for each run and enter in permanent log all pertinent information necessary for internal computer operations.
2. Run request submitted by MSFC to Computer Application Section, Computer Sciences Corporation.
3. Digitize the analog tapes.
4. Indicate reel's start and stop time for submission to the merge program.
5. Merge the digitized data and convert from raw counts to engineering units.
6. Convert digital data from speed and direction to longitudinal and lateral (Lon-Lat) components. (The details of this conversion are given in Section B of this chapter.)
7. Filter and edit the components of turbulence.
8. Analyze the components of turbulence.

The complete process of producing the digital magnetic tapes and preliminary data reduction and statistical analysis is presented in Figure 4-1. It must be remembered that this process is necessary for each

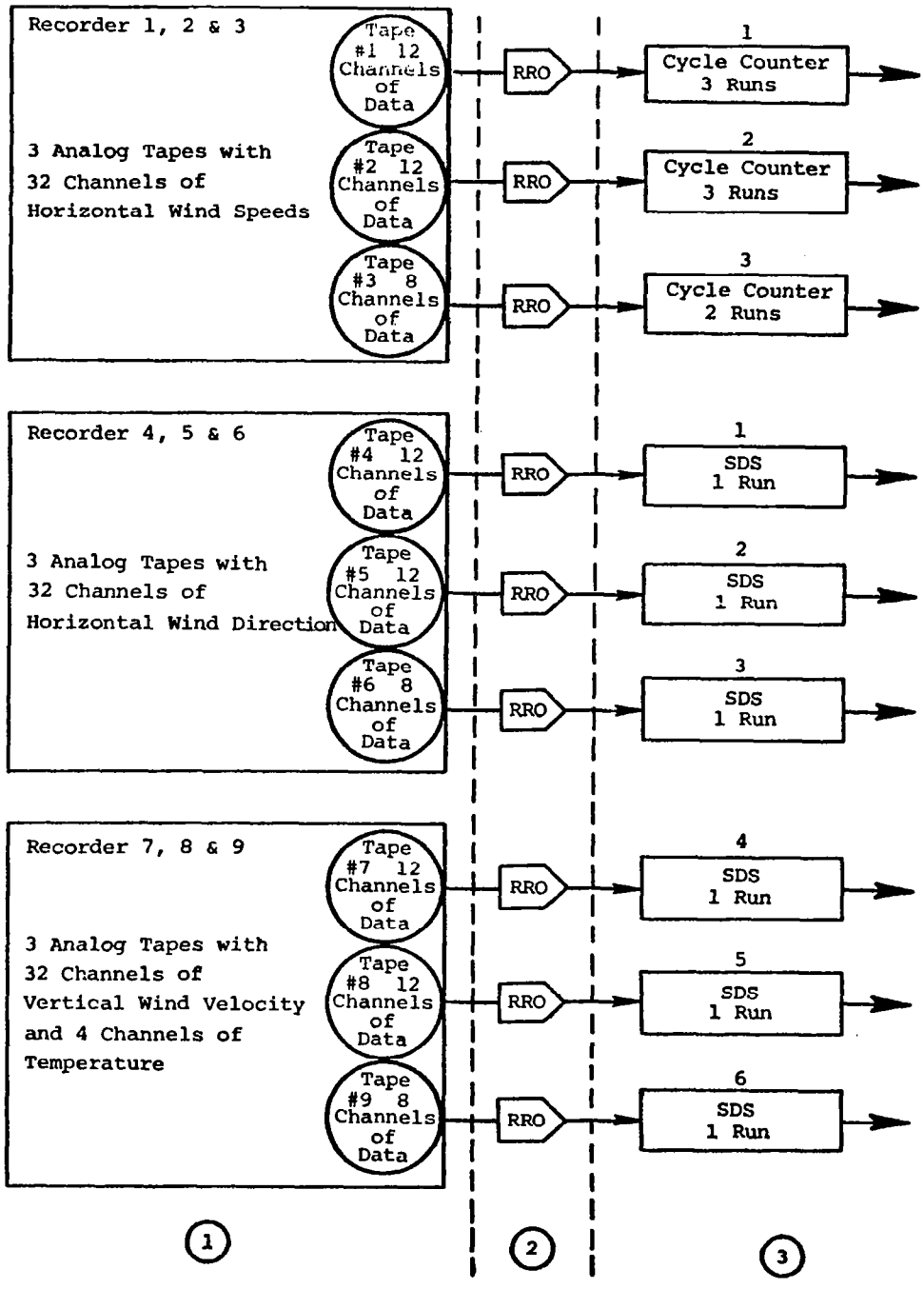

Figure 4-1 Flow chart showing data processing of magnetic tape for an individual run.

experimental run and that certain plots are produced and a digital magnetic tape for future reference and analysis of the data is generated.

Data Channels and Tower Representation

The reported data for the various instrumentation locations are listed according to channel numbers. There are 96 channels, which are arranged as follows: Channels 1-32 record horizontal wind speed, channels 33-64 record wind direction, and channels 65-96 record vertical wind speed. Table 4-4 indicates the corresponding channels, towers and levels recorded on tape and used in determining the various plots produced by the MSFC data systems laboratory.

It should be noted that the instrumentation on T3, level 4, (T3L4) has been moved to the 9 meter level and recorded on channels 12, 44 and 76, which correspond to the longitudinal, lateral and vertical velocity components, respectively. Also, short towers (SILJ, where I and J represent tower and level numbers respectively) S1, S2, S3 and S4 are recorded as T6L1 - T8L4 in ascending order and listed in Table 4-5. This method of recording was accomplished by simply moving the appropriate sensors to their perspective towers and levels and noting the change in the log for future reference.

TABLE 4-4

TOWERS AND LEVELS ASSOCIATED WITH THE GIVEN CHANNEL NUMBER

Data	Recorder #-Channel	Data Systems Lab Output: Data Channel	Data Systems Lab Output: Type Data	Tower and Level
Wind	1-1	1	Longitudinal	T1L1
Speed	1-2	2	Component	T1L2
↓	1-3	3	Spectra	T1L3
	1-4	4	↓	T1L4
	1-5	5		T2L1
	1-6	6		T2L2
	1-7	7		T2L3
	1-8	8		T2L4
	1-9	9		T3L1
	1-10	10		T3L2
	1-11	11		T3L3
	1-12	12		T3L4
	2-1	13		T4L1
	2-2	14		T4L2
	2-3	15		T4L3
	2-4	16		T4L4
	2-5	17		T5L1
	2-6	18		T5L2
	2-7	19		T5L3
	2-8	20		T5L4
	2-9	21		T6L1
	2-10	22		T6L2
	2-11	23		T6L3
	2-12	24		T6L4
	3-1	25		T7L1
	3-2	26		T7L2
	3-3	27		T7L3
	3-4	28		T7L4
	3-5	29		T8L1
	3-6	30		T8L2
	3-7	31		T8L3
	3-8	32		T8L4
Wind	4-1	33	Lateral	T1L1
Direction	4-2	34	Component	T1L2
↓	4-3	35	Spectra	T1L3
	4-4	36	↓	T1L4
	4-5	37		T2L1
	4-6	38		T2L2

TABLE 4-4 (Continued)

Data	Recorder #-Channel	Data Systems Lab Output: Data Channel	Data Systems Lab Output: Type Data	Tower and Level
Wind	4-7	39	Lateral	T2L3
Direction	4-8	40	Component	T2L4
↓	4-9	41	Spectra	T3L1
	4-10	42	↓	T3L2
	4-11	43		T3L3
	4-12	44		T3L4
	5-1	45		T4L1
	5-2	46		T4L2
	5-3	47		T4L3
	5-4	48		T4L4
	5-5	49		T5L1
	5-6	50		T5L2
	5-7	51		T5L3
	5-8	52		T5L4
	5-9	53		T6L1
	5-10	54		T6L2
	5-11	55		T6L3
	5-12	56		T6L4
	6-1	57		T7L1
	6-2	58		T7L2
	6-3	59		T7L3
	6-4	60		T7L4
	6-5	61		T8L1
	6-6	62		T8L2
	6-7	63		T8L3
	6-8	64		T8L4
Vertical	7-1	65	Vertical	T1L1
Wind	7-2	66	Component	T1L2
Speed	7-3	67	Spectra	T1L3
↓	7-4	68	↓	T1L4
	7-5	69		T2L1
	7-6	70		T2L2
	7-7	71		T2L3
	7-8	72		T2L4
	7-9	73		T3L1
	7-10	74		T3L2
	7-11	75		T3L3
	7-12	76		T3L4
	8-1	77		T4L1
	8-2	78		T4L2

TABLE 4-4 (Continued)

Data	Recorder #-Channel	Data Systems Lab Output: Data Channel	Data Systems Lab Output: Type Data	Tower and Level
Vertical	8-3	79	Vertical	T4L3
Wind	8-4	80	Component	T4L4
Speed	8-5	81	Spectra	T5L1
↓	8-6	82	↓	T5L2
	8-7	83		T5L3
	8-8	84		T5L4
	8-9	85		T6L1
	8-10	86		T6L2
	8-11	87		T6L3
	8-12	88		T6L4
	9-1	89		T7L1
	9-2	90		T7L2
	9-3	91		T7L3
	9-4	92		T7L4
	9-5	93		T8L1
	9-6	94		T8L2
	9-7	95		T8L3
	9-8	96		T8L4

TABLE 4-5

SHORT TOWERS RECORDED AS TALL*

Short Tower		Tall Tower	
Tower	Level	Tower	Level
S1	L1	T6	L1
S1	L2	T6	L2
S1	L3	T6	L3
S2	L1	T6	L4
S2	L2	T7	L1
S2	L3	T7	L2
S3	L1	T7	L3
S3	L2	T7	L4
S3	L3	T8	L1
S4	L1	T8	L2
S4	L2	T8	L3
S4	L3	T8	L4

*The method of recording was accomplished by simply moving the appropriate sensors from the tall towers (were disassembled) to the newer short towers and recording on magnetic tape as indicated above.

B. DIGITAL DATA PROCESSING

The analog to digital convertor, described generally in Chapter II along with the digitization procedure explained in Chapter III is used to produce a digital signal having 0.1 second averages. Tapes containing these data are produced by the NASA/MSFC computer laboratory. The data include horizontal, lateral and vertical components of wind speed (and temperature as described in Section II). The original digital data, prior to processing, was in the form of 0.1 second averages of the horizontal wind speed, V, horizontal wind direction, θ, and vertical wind speed, w. The principle used for digitization is illustrated in Figure 4-2. Let V_n be the average value of V(t) over the time increment Δt between t_n and t_{n-1}. The frequency of sampling, η, now essentially becomes $\eta = 1/\Delta t$. The mean velocity is then given by

$$\overline{V} = \frac{1}{N} \sum_{n=1}^{N} V_n \tag{4.1}$$

where N is the total number of time increments $(t_N - t_o)/\Delta t$. The time $t_p = (t_N - t_o)$ is the total time period of the data record recorded. The same computation is performed for the vertical velocity obtaining

$$\overline{w} = \frac{1}{N} \sum_{n=1}^{N} w_n \tag{4.2}$$

All digitized data is first bulk-averaged with the following relationships

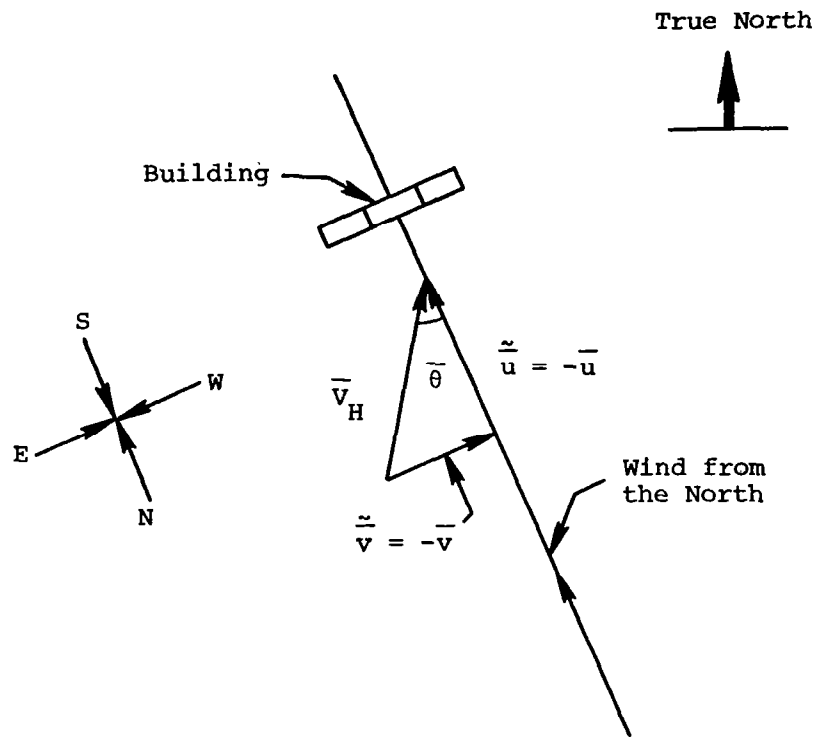

Note: Wind from 0 degree is from the north, and wind from 180 degrees is from the south.

Figure 4-3 Definition of average wind speed and respective wind direction.

array (from T1 to T5) as shown also in Figure 4-3. Then $\bar{v}$ is a positive wind component from the west or a positive wind component toward the east. In a similar manner, $\bar{u}$ is a positive wind component toward the north or equally a positive wind component from the south.

C. FLUCTUATING VELOCITY COMPONENTS

A new frame of reference is now used from which the fluctuating components are measured. Letting the mean horizontal wind velocity, V_H, be the longitudinal area of the new frame of reference, the fluctuating velocity components can be defined. The lateral and longitudinal velocity components are illustrated in Figure 4-4 relative to the horizontal mean velocity. The fluctuating components of the wind in the lateral direction, v', and in the horizontal direction, u', are perpendicular and parallel to the mean wind direction, respectively. The following relationships may be employed to compute v_k' and u_k' for the kth time increment, $t_k = t_o + (2k - 1)\ \Delta t/2$;

$$v_k' = V(t_k)\ \sin[\theta(t_k) - \bar{\theta}]$$
$$u_k' = V(t_k)\ \cos[\theta(t_k) - \bar{\theta}] - V_H \qquad (4.6)$$

The resulting fluctuating components will appear as shown in Figure 4-5 having in many cases a trend with time (usually non-linear). The trend results from diurnal variations. The procedure for removing the trend is to

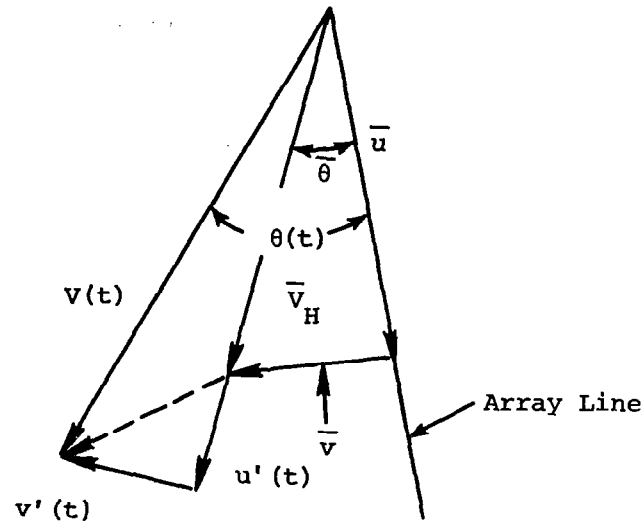

Figure 4-4 Definition of wind fluctuations u' and v'.

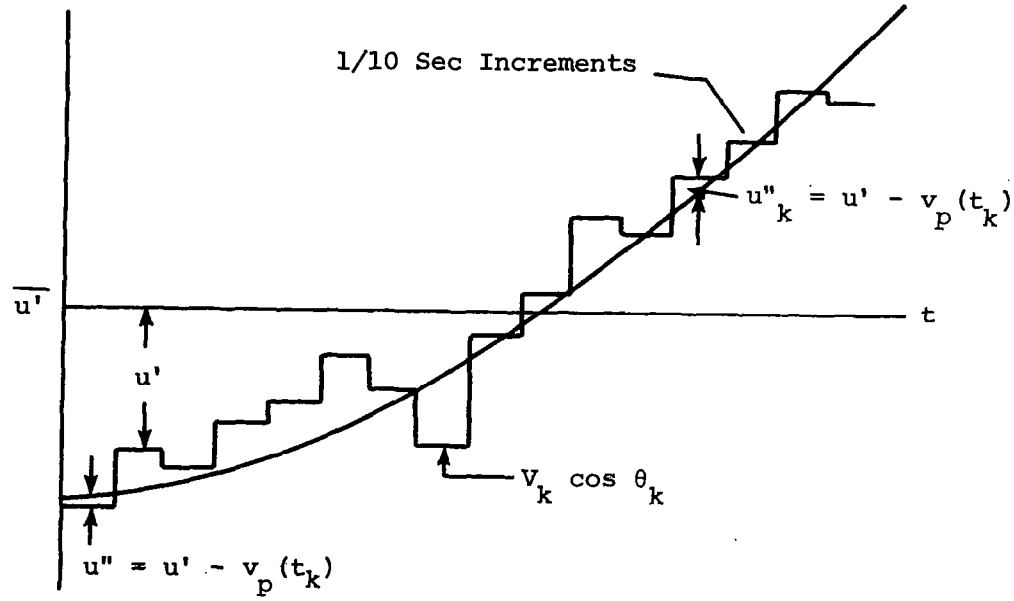

Figure 4-5 Illustration of trend removal.

take a least squares fit of a polynomial throughout the data, i.e., $v_p = C + Bt + At^2$. Where the values of A, B and C are obtained by solving the following system of equations;

$$\left.\begin{aligned} NC + B\Sigma t_k + A\Sigma t_k^2 &= \Sigma u_k' \\ C\Sigma t_k + B\Sigma t_k^2 + A\Sigma t_k^3 &= \Sigma t_k u_k' \\ C\Sigma t_k^2 + B\Sigma t_k^3 + A\Sigma t_k^4 &= \Sigma t_k^2 u_k' \end{aligned}\right\} \qquad (4.7)$$

where A, B, and C are unknown constant coefficients, $t_k = t_o + (2K - 1)\ \Delta t/2$ and u_k' is the kth value of u' or $u'(t_k)$. The mean of the fluctuating velocity u' is then calculated from

$$\overline{u'} = \frac{1}{N} \sum_{k=1}^{N} u_k' \qquad (4.8)$$

where N is the total number of data samples. The computed parabolic curve fit estimates the variations of the averaged data over the sampling interval. A similar procedure is carried out for $\overline{v'}$ and $\overline{w'}$ also. Thus, new random variables are defined as:

$$\left.\begin{aligned} u_k'' &= u_k' - \left(C + Bt_k + At_k^2\right) \\ v_k'' &= v_k' - \left(C_1 + B_1 t_k + A_1 t_k^2\right) \\ w_k'' &= w_k' - \left(C_2 + B_2 t_k + A_2 t_k^2\right) \end{aligned}\right\} \qquad (4.9)$$

Averaging the three components u", v", and w" we get

$$\left.\begin{aligned} \overline{u''} &= \frac{1}{N}\sum_{k=1}^{N} u''_k \\ \overline{v''} &= \frac{1}{N}\sum_{k=1}^{N} v''_k \\ \overline{w''} &= \frac{1}{N}\sum_{k=1}^{N} w''_k \end{aligned}\right\} \qquad (4.10)$$

In general, the mean value of these double prime quantities will not be zero, hence in order to obtain a mean value of zero the following triple prime quantities are defined:

$u''' = u'' = \overline{u''}$

$v''' = v'' = \overline{v''}$

$w''' = w'' = \overline{w''}$

such that $\overline{u'''} = \overline{v'''} = \overline{w'''} = 0$.

These final triple prime quantities are digitally recorded on a magnetic tape in a format to be discussed in the following section.

D. TAPE FORMAT AND COMPUTER PROGRAMS

The data tapes received from the MSFC computer center were generated on a UNIVAC computer having a bit structure different from that of the IBM/360 used for retrieving data from the tapes and performing the data analysis reported herein. The data tapes from MSFC are nine track unlabeled tapes having unformatted records with a block size of 2300. These tapes have been retained as masters from which a working copy is produced on the IBM tape drives.

The working copy of all master data tapes is produced on a scratch data tape which has been initialized and labeled using the program listed in Figure 4-6. Scratch tapes are assigned to the programmer by the computer facilities but must be initialized and labeled prior to their use. In this example, tape number 8886 is a scratch tape previously assigned to a particular project code (TTTTTT is where the project code is indicated) and the programmer's code is indicated also in Figure 4-6 as PPPPPP. Any serial number could be logically written on the tape at the programmer's preference; however, serial numbers equal to the label number are convenient.

```
IIQIXII    II  1
//JOBNAME JOB (TTTTTT,PPPPPP,G-B),NAME
//*TAPE         008886,W
//*REMARKS      PLEASE MOUNT 8886 INSTEAD OF SCRATCH
// EXEC PGM=IEHINITT
//SYSPRINT DD SYSOUT=A
//TAPE DD DCB=DEN=3,UNIT=3400-4
//SYSIN DD *
TAPE INITT SER=008886
```

Figure 4-6 Initialization program.

Once the scratch tape has been initialized and a serial number has been logically written on the tape by the operating system, a working copy of the master tape can be produced. In order to convert from UNIVAC to IBM bit structure, a special PL/1 program was developed. This

66.	VERTICAL	COMPONENT	TOWER	1	LEVEL	1
67.	VERTICAL	COMPONENT	TOWER	1	LEVEL	2
68.	VERTICAL	COMPONENT	TOWER	1	LEVEL	3
69.	VERTICAL	COMPONENT	TOWER	1	LEVEL	4
70.	VERTICAL	COMPONENT	TOWER	2	LEVEL	1
71.	VERTICAL	COMPONENT	TOWER	2	LEVEL	2
72.	VERTICAL	COMPONENT	TOWER	2	LEVEL	3
73.	VERTICAL	COMPONENT	TOWER	2	LEVEL	4
74.	VERTICAL	COMPONENT	TOWER	3	LEVEL	1
75.	VERTICAL	COMPONENT	TOWER	3	LEVEL	2
76.	VERTICAL	COMPONENT	TOWER	3	LEVEL	3
77.	VERTICAL	COMPONENT	TOWER	3	LEVEL	4
78.	VERTICAL	COMPONENT	TOWER	4	LEVEL	1
79.	VERTICAL	COMPONENT	TOWER	4	LEVEL	2
80.	VERTICAL	COMPONENT	TOWER	4	LEVEL	3
81.	VERTICAL	COMPONENT	TOWER	4	LEVEL	4
82.	VERTICAL	COMPONENT	TOWER	5	LEVEL	1
83.	VERTICAL	COMPONENT	TOWER	5	LEVEL	2
84.	VERTICAL	COMPONENT	TOWER	5	LEVEL	3
85.	VERTICAL	COMPONENT	TOWER	5	LEVEL	4
86.	VERTICAL	COMPONENT	TOWER	6	LEVEL	1
87.	VERTICAL	COMPONENT	TOWER	6	LEVEL	2
88.	VERTICAL	COMPONENT	TOWER	6	LEVEL	3
89.	VERTICAL	COMPONENT	TOWER	6	LEVEL	4
90.	VERTICAL	COMPONENT	TOWER	7	LEVEL	1
91.	VERTICAL	COMPONENT	TOWER	7	LEVEL	2
92.	VERTICAL	COMPONENT	TOWER	7	LEVEL	3
93.	VERTICAL	COMPONENT	TOWER	7	LEVEL	4
94.	VERTICAL	COMPONENT	TOWER	8	LEVEL	1
95.	VERTICAL	COMPONENT	TOWER	8	LEVEL	2
96.	VERTICAL	COMPONENT	TOWER	8	LEVEL	3
97.	VERTICAL	COMPONENT	TOWER	8	LEVEL	4

Figure 4-8 (continued)

```
 98.  TEMPERATURE     TOWER 1     LEVEL 1
 99.  TEMPERATURE     TOWER 1     LEVEL 2
100.  TEMPERATURE     TOWER 1     LEVEL 3
101.  TEMPERATURE     TOWER 1     LEVEL 4


102.
   .     SECOND BLOCK OF DATA REPEATS THE RECORD FORMAT OF
   .     FLOATING WORDS 2 THROUGH 101.  TIME FOR THIS BLOCK
   .     OF DATA  IS EQUAL TO WORD 1 PLUS 0.1 SECONDS.
   .
201.
202.
   .     THIRD BLOCK.
   .
   .
301.
302.
   .     FOURTH BLOCK.
   .
   .
401.
402.
   .     FIFTH BLOCK OF DATA REPEATS THE RECORD FORMAT OF
   .     FLOATING WORDS 2 THROUGH 101.  TIME FOR THIS BLOCK
   .     OF DATA IS EQUAL TO WORD 1 PLUS 0.4 SECONDS.
   .
501.
502.  TEST NUMBER
503.  YEAR
504.  MONTH
505.  DAY
506.  TIME OF DAY TEST BEGAN
507.  STATION NUMBER
```

Figure 4-8 (continued)

data from the tape in a logical manner. An algorithm has been developed to extract data from the tapes in a sequential manner. It is possible to extract data from a single point by dimensioning an array by 507 and specifying the exact location of the data being sought. This in essence has been performed; however, instead of sampling only one of the velocity components, a subroutine program has been developed to sample four components with only one pass of the tape. Also, the option of selecting every time increment or to select only equally spaced time increments (every point, every other point, every third point, etc.) has been included. This program is illustrated in Figure 4-9. The argument contains all the information needed to read and control the magnetic tape. The data arrays W, X, Y, and Z are used to store the total number of data values, NDV, being read from each channel of the tape. NTW, NLW, and NCW, respectively, are the tower number (1-8), level number (1-4), and component number (1, 2 or 3 corresponding to the longitudinal, lateral and vertical components, respectively). NSTEP indicates the number of data time intervals to be skipped; for example 1 would cause every point to be extracted, 2 would cause every other point to be extracted, 3 would extract every third point, etc. NRUN is data passed back to the calling program and represents the run number of the tape. NT is a switch to indicate whether an end

```
      SUBROUTINE READT(NTW,NLW,NCW,NTX,NLX,NCX,NTY,NLY,NCY,
     *NTZ,NLZ,NCZ,NDV,NSTEP,NRUN,W,X,Y,Z,NT)
      DIMENSION T(507),W(NDV),X(NDV),Y(NDV),Z(NDV)
      IF(NT.LT.0) GO TO 90
      NW=(NTW-1)*4+NLW+1+(NCW-1)*32
      NX=(NTX-1)*4+NLX+1+(NCX-1)*32
      NY=(NTY-1)*4+NLY+1+(NCY-1)*32
      NZ=(NTZ-1)*4+NLZ+1+(NCZ-1)*32
      JJ=0
      NS=1
      K=-4
    3 READ(10,END=90) T
      K=K+5
    2 IF(NS.GT.K+4) GO TO 3
      NT=(NS-K)*100
      IF(T(NT+NW).GT.20.) T(NT+NW)=0.0
      IF(T(NT+NX).GT.20.) T(NT+NX)=0.0
      IF(T(NT+NY).GT.20.) T(NT+NY)=0.0
      IF(T(NT+NZ).GT.20.) T(NT+NZ)=0.0
      JJ=JJ+1
      W(JJ)=T(NT+NW)
      X(JJ)=T(NT+NX)
      Y(JJ)=T(NT+NY)
      Z(JJ)=T(NT+NZ)
      NS=NS+NSTEP
      IF(JJ.LT.NDV) GO TO 2
      NT=1
      NRUN=T(502)
      RETURN
   90 NT=-1
      REWIND 9
      RETURN
      END
```

Figure 4-9 Subroutine used to extract data from magnetic tapes.

of file has been reached (NT = 1 means no end of file had been reached and the subroutine finished normally, whereas when NT is returned as a - 1, then it indicates an end of file has been reached while reading the tape). This automatically rewinds the tape in the last branch of the subroutine. NTX, NTY, and NTZ are tower numbers; NLX, NLY, and NLZ are the corresponding levels; and NCX, NCY, and NCZ are the respective components for the other data arrays X, Y, and Z. It should be noted that this subroutine only rewinds the magnetic tape upon encountering an end of file, and if it is necessary to use data at the beginning of the tape repeatedly, a rewind statement must be used after the call statement. This is very important and should be remembered when any correlation or spectral functions are being computed. This subroutine can easily be modified to read any number of elements by simply reducing or increasing the number of arrays within the subroutine and associated statements.

E. GENERAL STATISTICAL RESULTS

Several statistics of the triple prime random variables developed in Section III are computed and plotted by the MSFC computer laboratory. A set of plots for each data channel for each run is provided by the MSFC computer facilities. A sample set of the plots for one channel is presented and described in this section. Similar data and plots are available for other channels

and runs and provide a good means of assessing the data prior to further analysis.

A typical plot of u''' versus time is given in Figure 4-10. This plot provides a visual indication of the fluctuating digital signal as a function of time. Information of significance is tabulated above the figure and includes test number, 8624; channel number, 1; sample rate, 2/sec; and the variance (erroneously labeled as RMS value), 0.938. Approximately 8.33 minutes are plotted of the full 40 minute time history available on magnetic tape.

The probability density distribution function is compared with a Gaussian distribution having the same variance, in Figure 4-11. The probability density function is computed by dividing the range of u''' into increments $\Delta u'''$. By scanning u''', summing the number of data points which lie in each $\Delta u'''$ increment, and dividing by the total number of data points, the probability density function is obtained. The density is then plotted versus $\tilde{u}'''/S$ as shown in Figure 4-10. $\tilde{u}'''$ is the midpoint value of the increment $\Delta u'''$. In addition to the standard information listed on all the computer plots; the mean, standard deviation, skewness and kurtosis, along with other statistical results, are tabulated above the plot in Figure 4-11.

The skewness is a tendency of a distribution to depart from a symmetrical form or to have a larger tail on

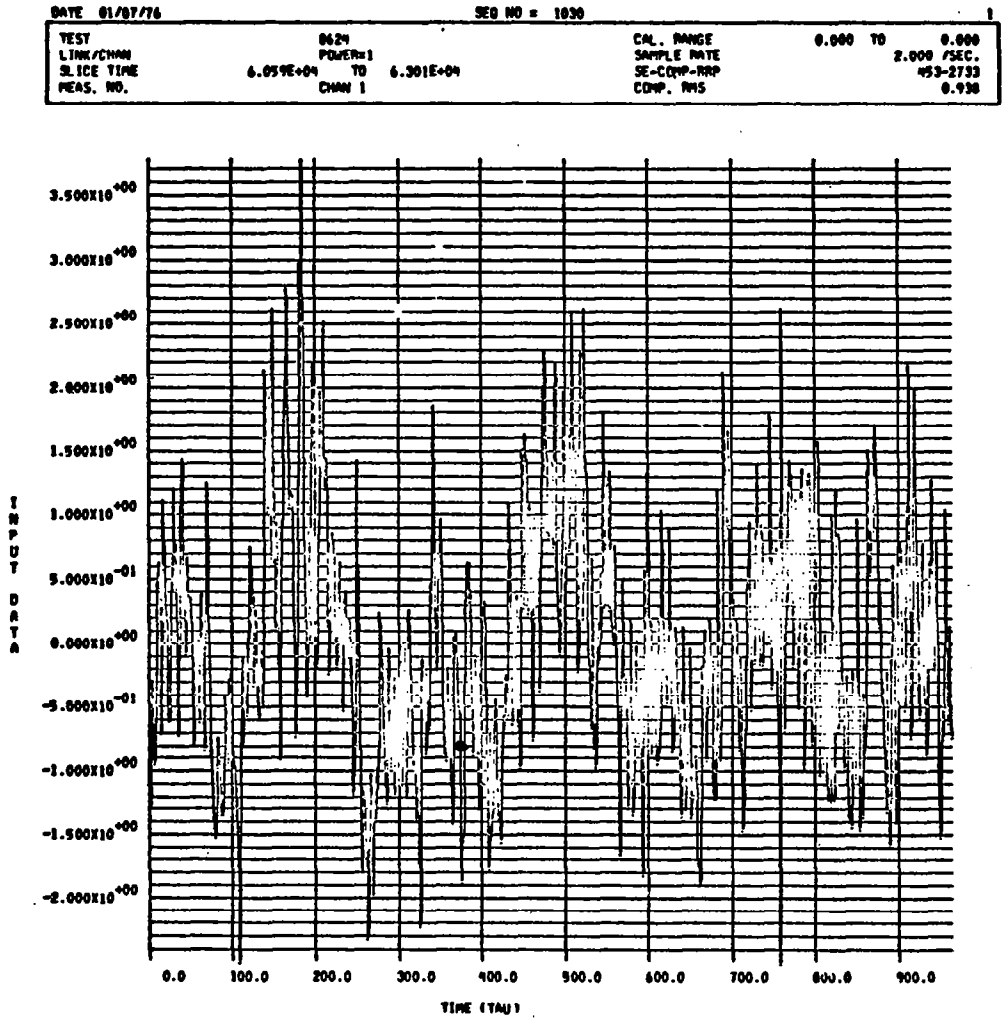

Figure 4-10 A typical plot of u''' versus time: TAU = 0.5 sec.; units of m s^{-1} (not a complete record).

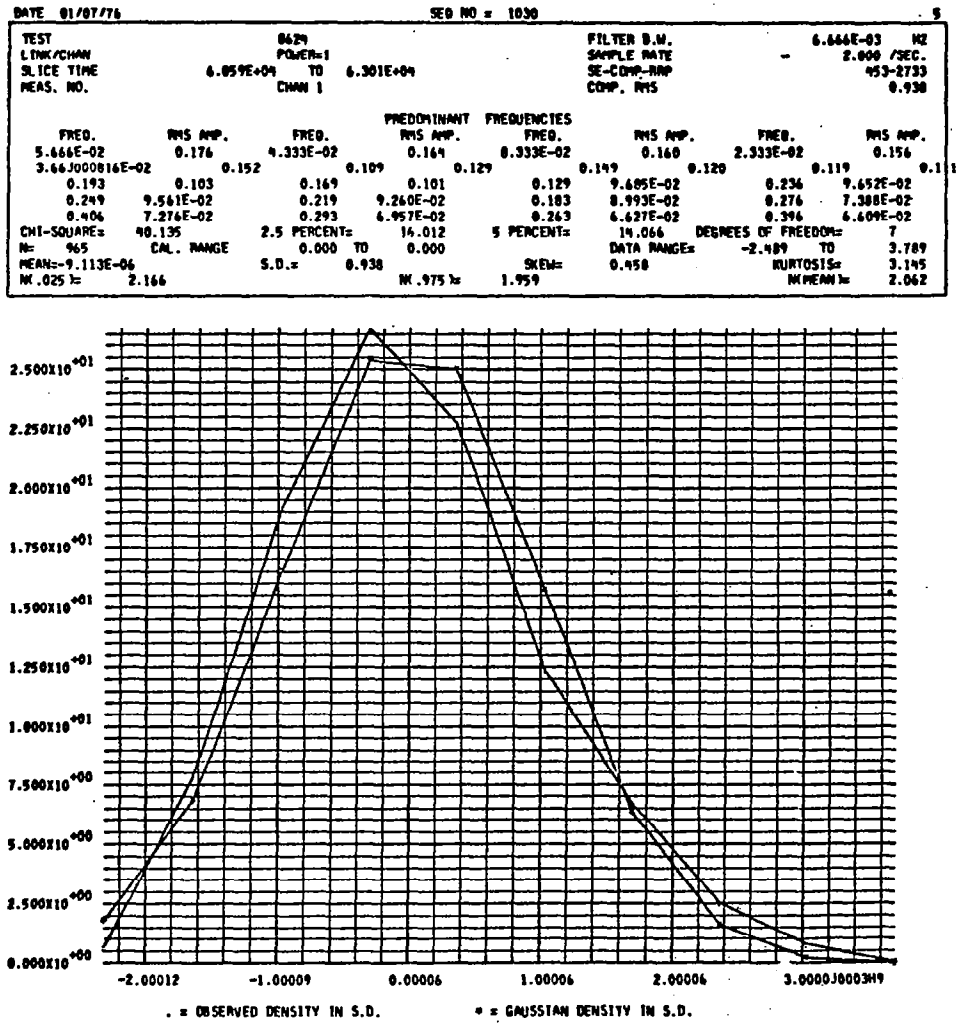

Figure 4-11 A typical plot of probability density compared with a Gaussian density.

one side or the other. Interest in this parameter lies in its measure of the amount of departure or skewness from a symmetrical probability distribution,

$$\text{Skewness} = \frac{1}{N} \sum_{k=1}^{N} (u_k''')^3/s^3$$

It can be seen in Figure 4-11 that the skewness is calculated to be 0.458, as compared to 0.0 for a Gaussian curve.

The probability density distribution may conceivably be perfectly symmetrical, yet differ from a normal curve as shown in Figure 4-12. The curve illustrated in case 1 is higher and narrower than the normal distribution and is labeled as being leptokurtic. This differs from case 2 where the curve is lower and wider than a normal distribution and is labeled as platykurtic.

$$\text{Kurtosis} = \frac{1}{N} \sum_{k=1}^{N} (u_k''')^4/s^4$$

The calculated value of the kurtosis is 3.145, Figure 4-11, and since it is slightly higher than the value of three for a true Gaussian curve, this particular data is leptokurtic.

The range of the u''' data is also listed in Figure 4-11. The maximum value of u''' (3.789) and the minimum value (-2.489) provide the extremes in the data over the range plotted. These values are tabulated above the plot in Figure 4-11.

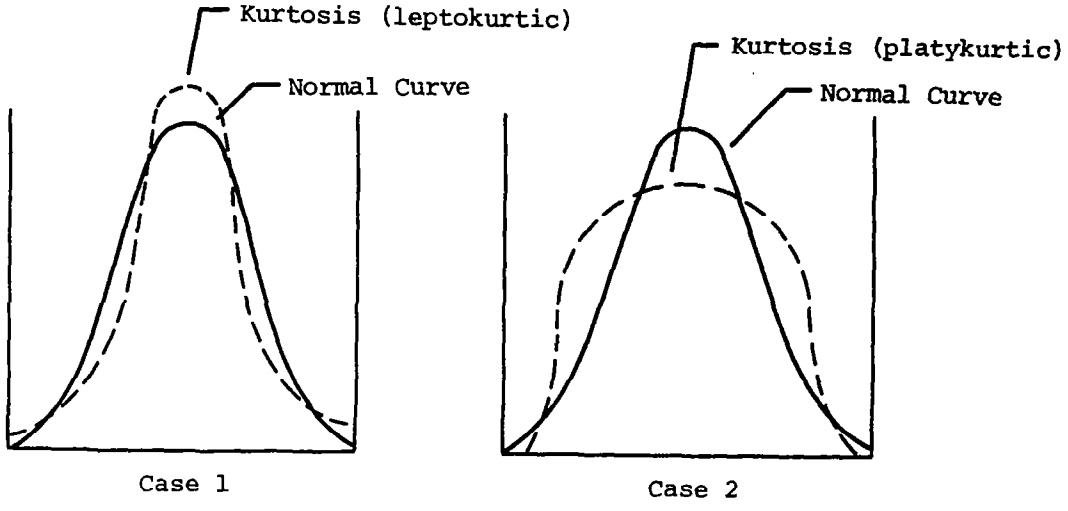

Figure 4-12 An example of leptokurtic and platykurtic curves as compared to a normal distribution.

A cumulative probability distribution of the data is plotted in Figure 4-13.

Plots of the autocorrelation function and power spectral density function are illustrated in Figure 4-14 and 4-15, respectively. Computation of these functions is described in Chapter III along with a brief explanation of their applications.

Mean values for each run are available in computer printouts. A typical printout of mean values for test run 8624 is illustrated in Figure 4-16. Data similar to those tabulated have been used in the past [1] to plot velocity profiles and velocity deficits behind the block building using a slightly different tower arrangement from that described in Figure 2-2, page 11.

The plots and printouts described in this section are valuable for quick reference prior to performing additional analyses. For more detailed analysis and for application of the data, however, the plots are not useful, and recomputation of the results is necessary.

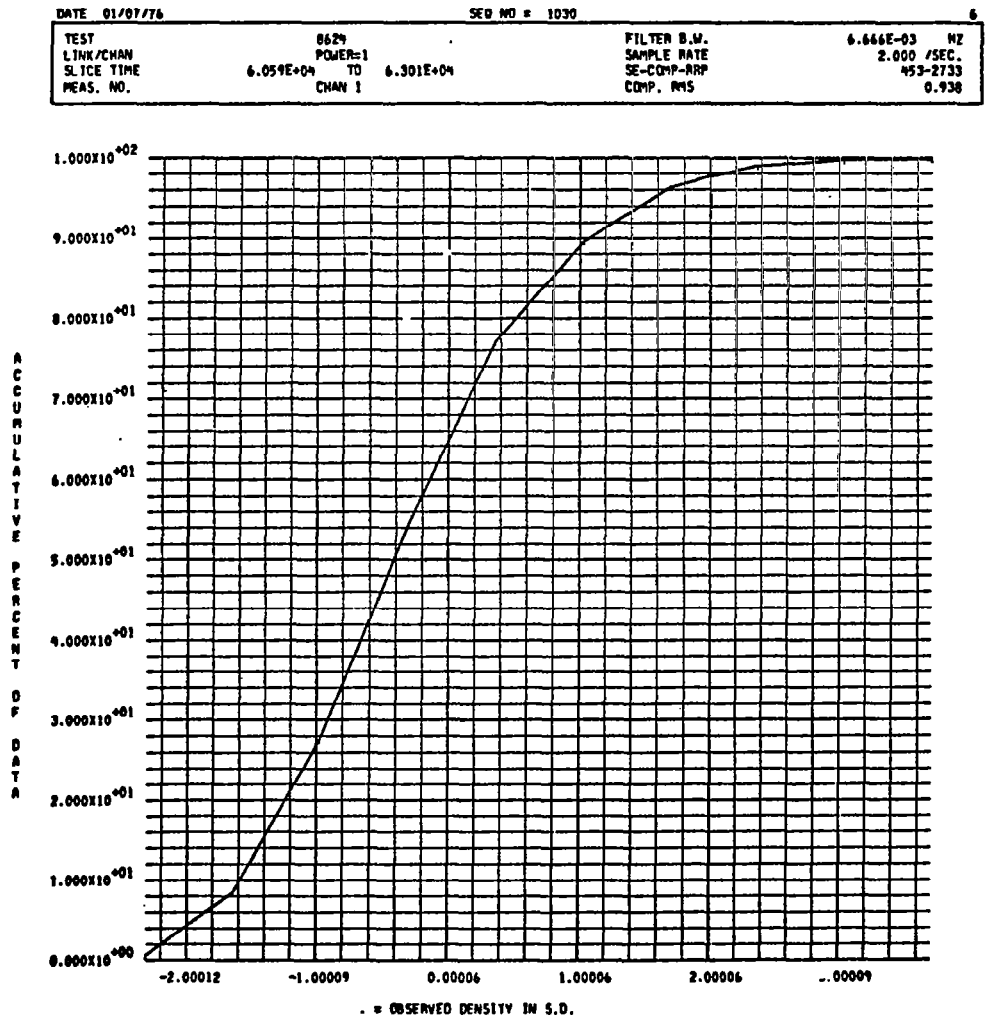

Figure 4-13 A typical plot of the accumulative percent of data.

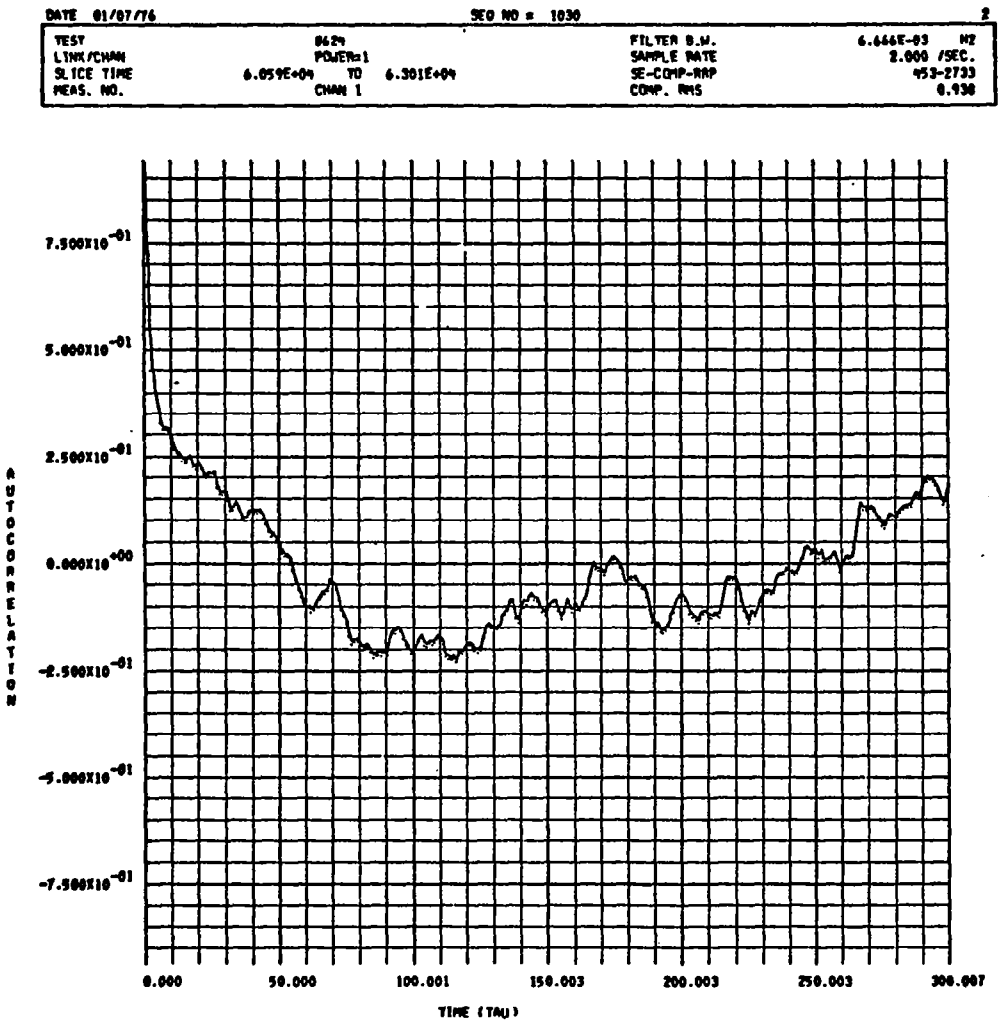

Figure 4-14 A typical plot of an autocorrelation function: TAU = 0.5 sec.; units of $m^2 s^{-2}$.

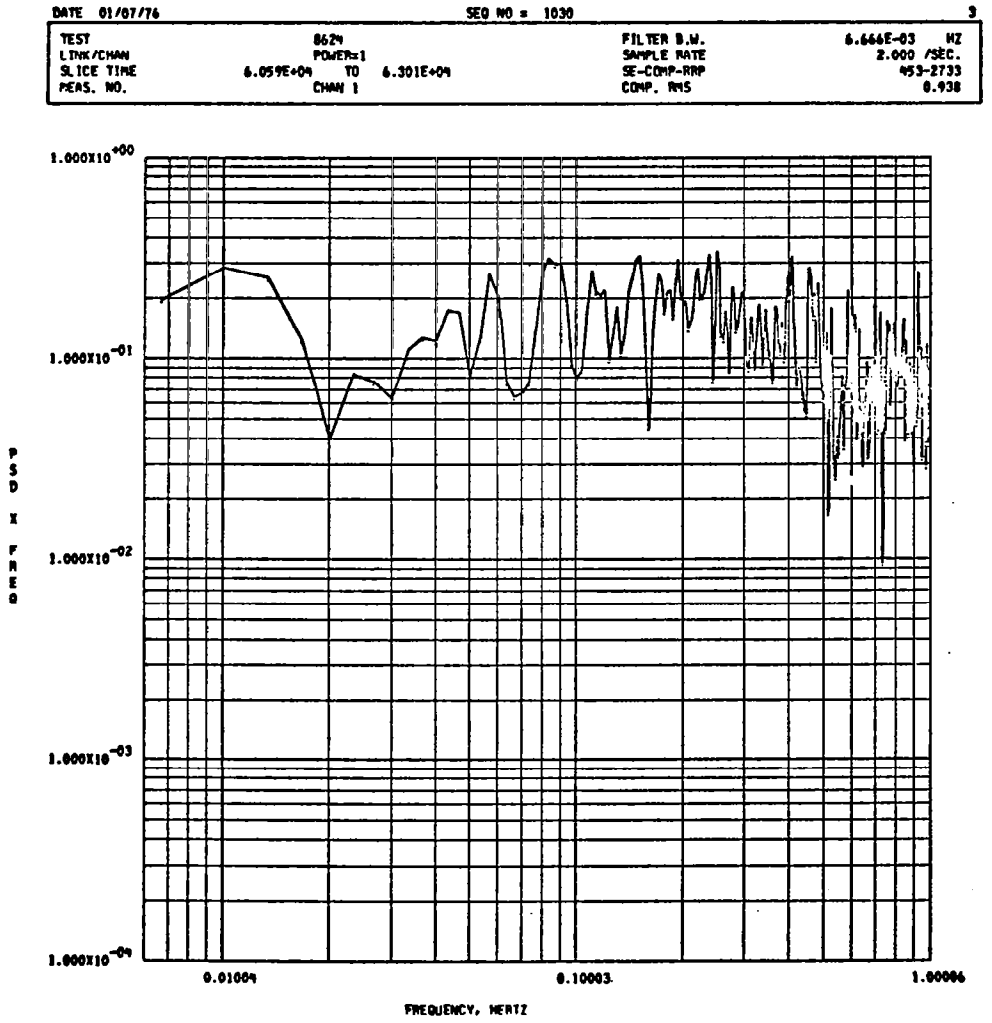

Figure 4-15 A typical power spectral density plot: units of m^2s^{-3}.

TEST NO. 8624 2/26/76 TIME 165000 STATION NO. 11001

TOWER	LEVEL	MEAN ZONAL	MEAN MERIDIONAL	MEAN SCALAR	MEAN DIRECTION	VERTICAL VELOCITY	--NO. OF OBSERVATIONS--- SPD. OR DIRECT.	VERTICAL
1	1	2.0487	2.9895	3.6241	214.4623	.0272	24245	24275
1	2	2.3735	3.4968	4.2263	214.2065	-4.8259	24245	24275
1	3	2.5700	4.4788	5.1638	209.8875	.1272	24245	24275
1	4	3.9971	4.7714	6.2179	219.9246	.2569	24245	24275
2	1	1.9003	2.1630	2.8792	221.3415	.2170	24245	24275
2	2	2.8733	3.0276	4.1743	223.5492	.5090	24245	24275
2	3	3.2904	3.6659	4.9260	221.9519	.4424	24245	24275
2	4	3.8427	4.9111	6.2357	218.0823	.2592	24245	24275
3	1	-.0169	-.2914	.2919	3.3279	-.0311	24245	24275
3	2	2.0917	4.0728	4.5740	207.1117	1.0011	24245	24275
3	3	2.5370	4.5621	5.2201	209.1173	-.1225	24245	24275
3	4	-2.7828	-4.0849	4.9427	34.2704	.0009	24245	24275
4	1	.9223	.3413	.9834	249.7402	-.0265	24265	24275
4	2	2.3095	3.2753	4.0077	215.2295	-.1064	24265	24275
4	3	3.2612	4.3579	5.4430	216.6496	.1676	24265	24275
4	4	2.4891	5.2211	5.7841	205.5273	.0070	24265	24275
5	1	3.2951	2.4210	4.0809	233.6546	.1119	24264	24275
5	2	3.2224	3.4132	4.6941	223.3969	.1422	24264	24275
5	3	-.0015	3.5265	3.5265	180.0093	.2154	24265	24275
5	4	2.9934	4.4481	5.3559	213.8905	-.2271	24265	24275
6	1	.9096	1.0851	1.4159	220.0140	-.1513	24265	24275
6	2	1.7511	2.2599	2.8590	217.8114	-.3075	24265	24275
6	3	2.3261	3.1165	3.8905	216.7596	.2740	24265	24275
6	4	.0408	-.4768	.4786	355.1710	-.4562	24265	24275
7	1	.4594	-.2393	.5180	297.5690	-.2601	24275	24275
7	2	3.1289	3.6387	4.7990	220.7332	.9213	24275	24275
7	3	.1528	-.6726	.6920	346.4559	.0126	24275	24275
7	4	.2662	.0937	.2841	250.7872	-.0462	24275	24275
8	1	2.1279	3.3562	3.9714	212.4383	-.1263	24275	24275
8	2	.4505	-.2266	.5043	296.7586	.0909	24275	24275
8	3	.4531	.5182	.6884	221.2112	-.0166	24275	24275
8	4	2.5293	2.7957	3.7686	222.1989	-.0049	24275	24275

Figure 4-16 A typical printout of mean values for a particular test run.

SECTION V

PRELIMINARY RESULTS AND CONCLUSIONS

Statistical results have been computed from the data described in the preceding chapters. Selected results are presented and explained. The results described in this chapter have been selected to emphasize the statistical characteristics of the turbulent flow field about a simulated block building.

The results presented consist of mean velocity profiles, velocity time histories, two-point spatial correlations (with and without lag times), and autocorrelations computed by the direct method and by the FFT method. It is possible to compute the autocorrelations by using the mean velocities, spatial correlations, and assuming Taylor's hypothesis when knowing the spatial distances separating each point in space. These results are presented with a brief explanation of the accuracy relative to the height of the measurement and the related building or surface protuberances.

The results presented are for the longitudinal velocity components only. For definition, the velocity components, after trend removal, are denoted by $u_{ij}(t)$, $v_{ij}(t)$, and $w_{ij}(t)$ for the longitudinal, lateral, and vertical wind speeds, respectively, where i and j represent the tower

position and level of the velocity measurement being discussed. The nomenclature (t) indicates the velocity is a function of time. For example, $u_{14}(t)$ represents the longitudinal wind speed at T1L4 for a particular time, t, relative to the beginning of the record. Each plot in Section V which utilizes $u_{53}(t)$ produces erroneous results as a result of spiking in the data and can be ignored (it has been included to illustrate its effect and methods of detection). The spiking in the data at T5L3 is possibly due to a malfunctioning transducer; however, the computational results clearly indicate this error.

A. COMPUTATIONAL RESULTS

Mean Velocities

Figures 5-1 and 5-2 are plots of the mean longitudinal velocities at each of the five towers nondimensionalized with respect to the level 4 value. For tower number 3 it was necessary to interpolate between the mean velocities $\bar{u}_{24}$ and $\bar{u}_{44}$ to determine the upper level nondimensionalizing velocity.

Near the building (run 8624) the velocity profile shows a pronounced deficit compared to the profiles farther from the building. The profile has practically recovered by the time it reaches T5. This phenomenon is not apparent in the no-building case (run 8704, Figure 5-2) where the profiles are similar at each tower. Other statistical work

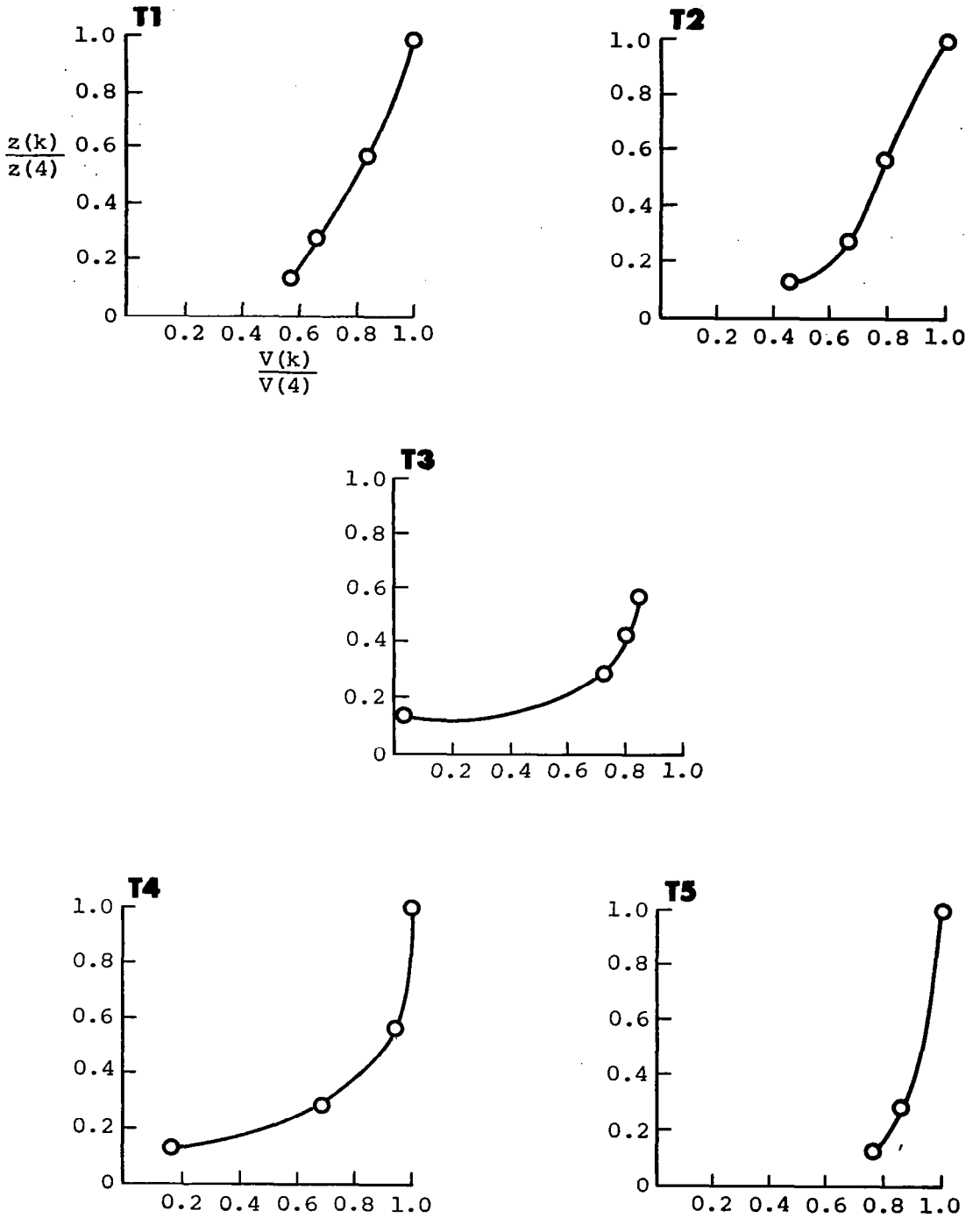

Figure 5-1 Mean non-dimensional velocities with the block building in the tower array, Run #8624.

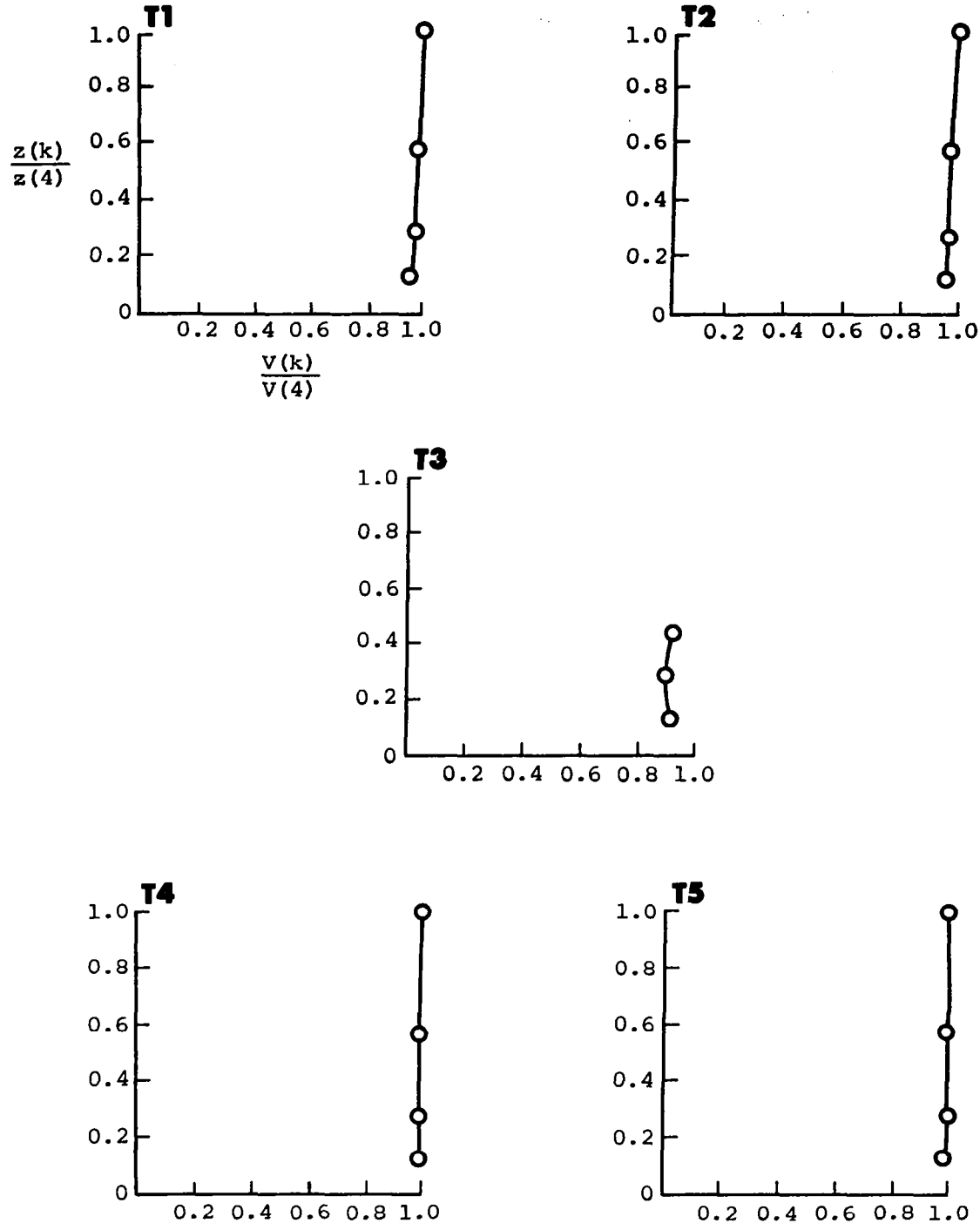

Figure 5-2 Mean non-dimensional velocities without the block building in the tower array, Run #8704.

related to mean velocities and velocity defects of the flow about surface obstructions is given by Frost, et al. [1,2]. In these studies good correlation with wind tunnel studies [3] was accomplished using a slightly different tower arrangement than the one used and described in Section II. Other velocity profiles were computed and plotted; however, they are not included for the sake of brevity and provide sufficient room for other results to be presented.

Time History Plots

To get some indication of the relative time histories for each level and tower, they have been plotted at their respective altitude in Figure 5-3. Visually inspecting these time history plots, some indication of the vertical correlations can be seen. A signal or turbulent fluctuation generally appears at the upper levels and is felt at the lower levels in descending order. Although not overly apparent from the time history plots, this becomes much more apparent when cross-correlations of the data are computed. Figure 5-3 clearly indicates spiking of the data for the $u_{53}(t)$ signal as mentioned earlier.

If the signals measured at the upper level (4) are plotted relative to each other or rather the time history plots of the upper levels are "stacked," one on top of the other, the signals' propagation downstream can be seen. This can be observed in Figure 5-4, where each time history plot

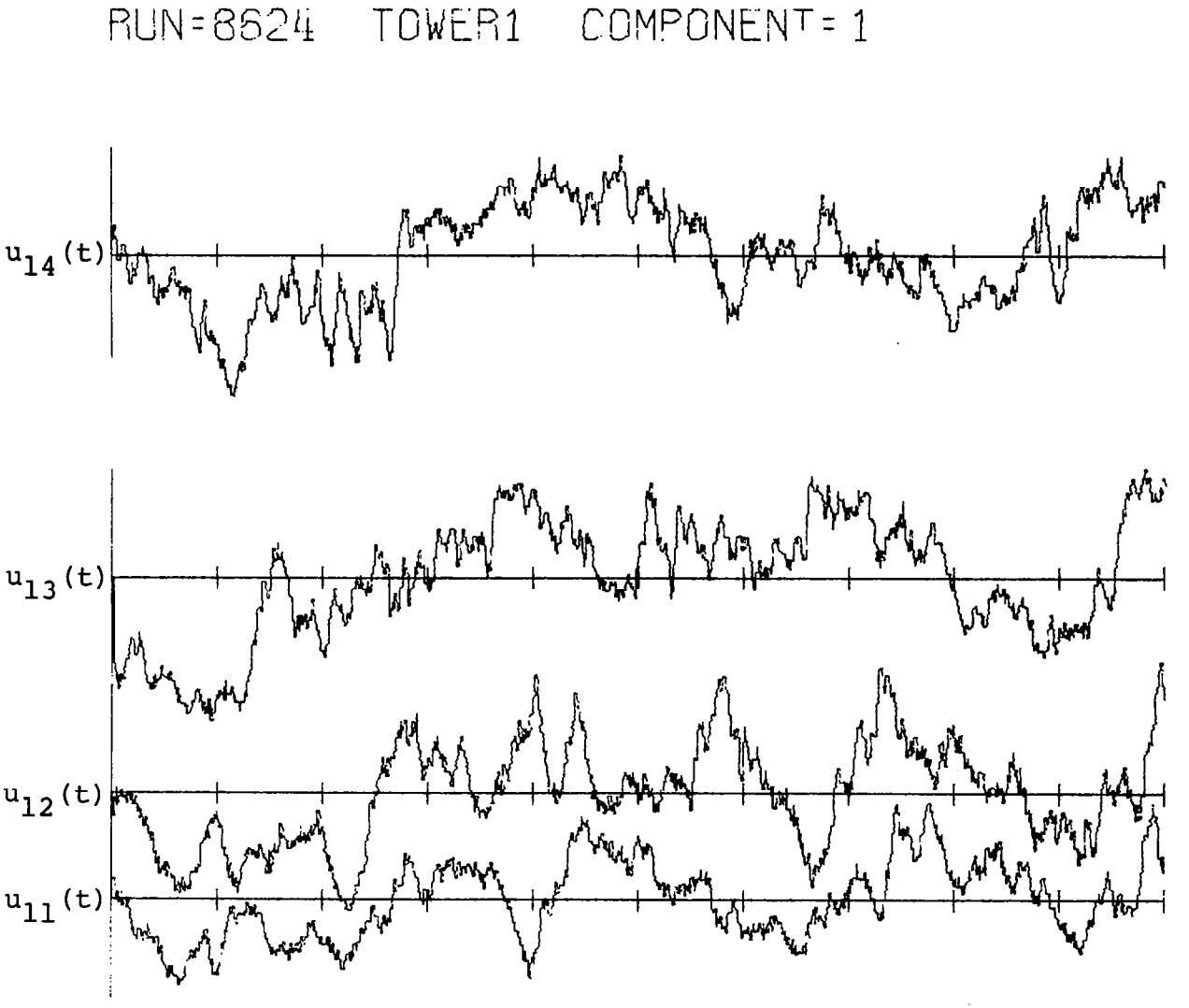

Figure 5-3 Time history signals of the different towers and levels. (Only 100 seconds for each level have been plotted.)

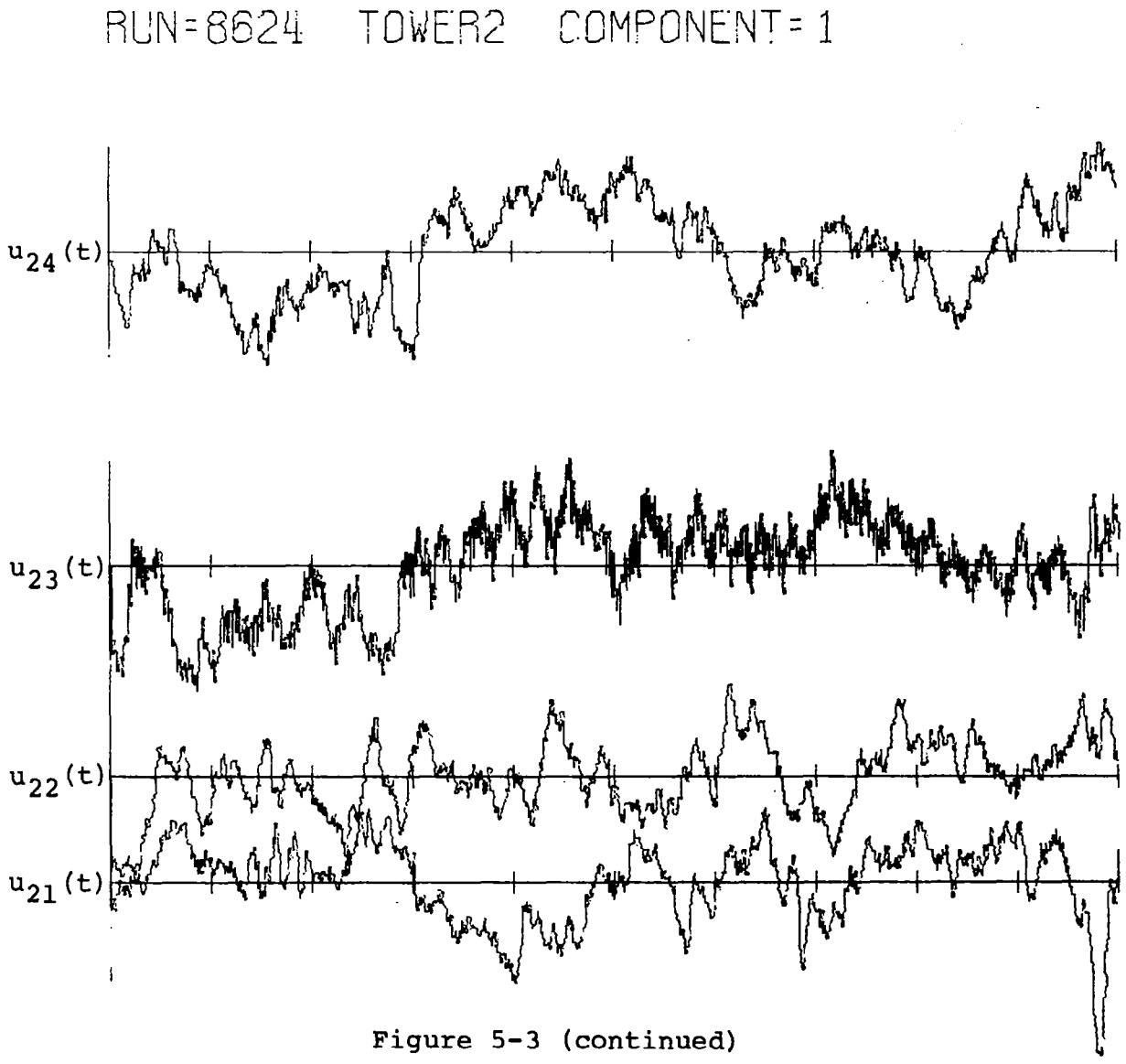

Figure 5-3 (continued)

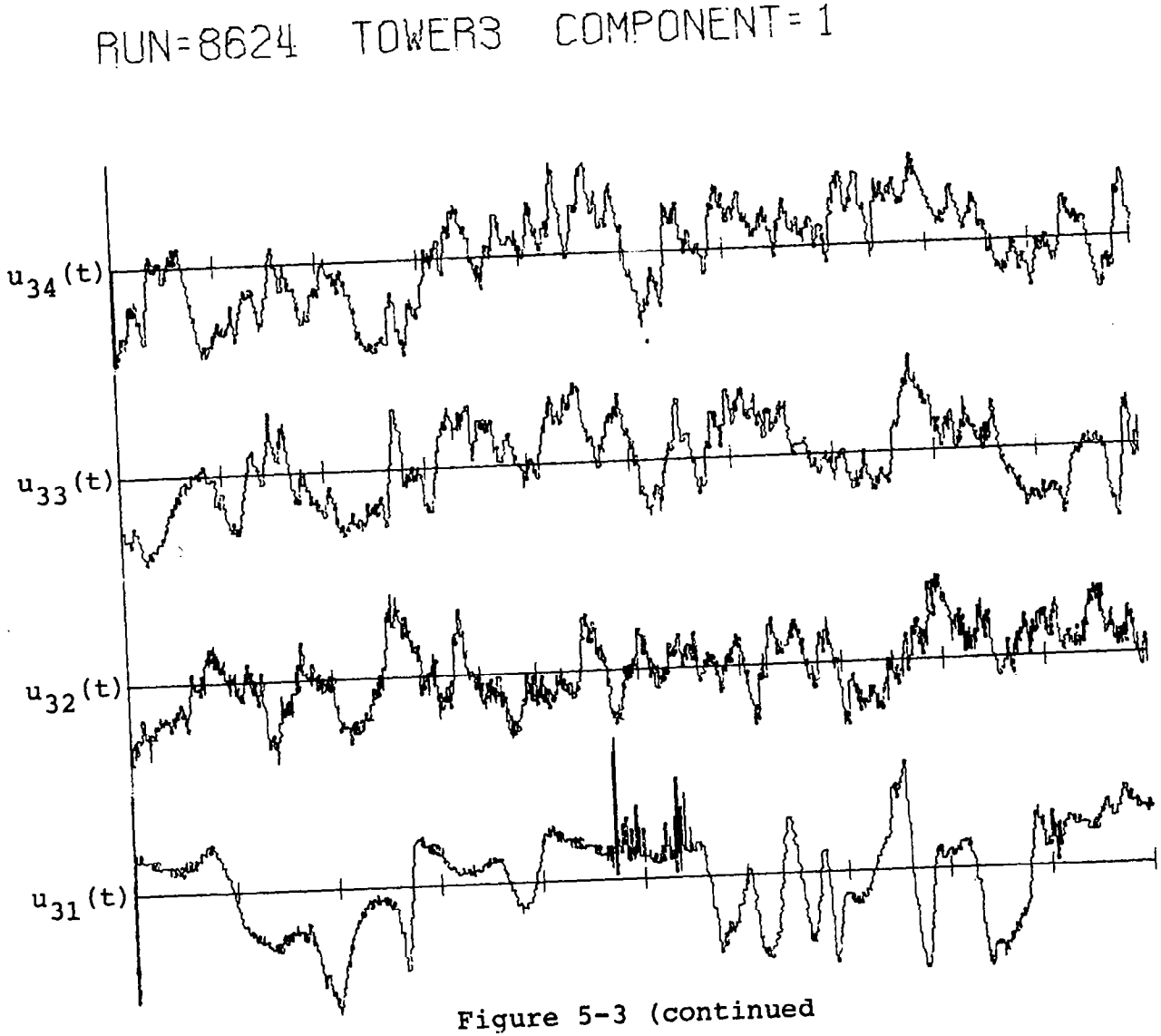

Figure 5-3 (continued

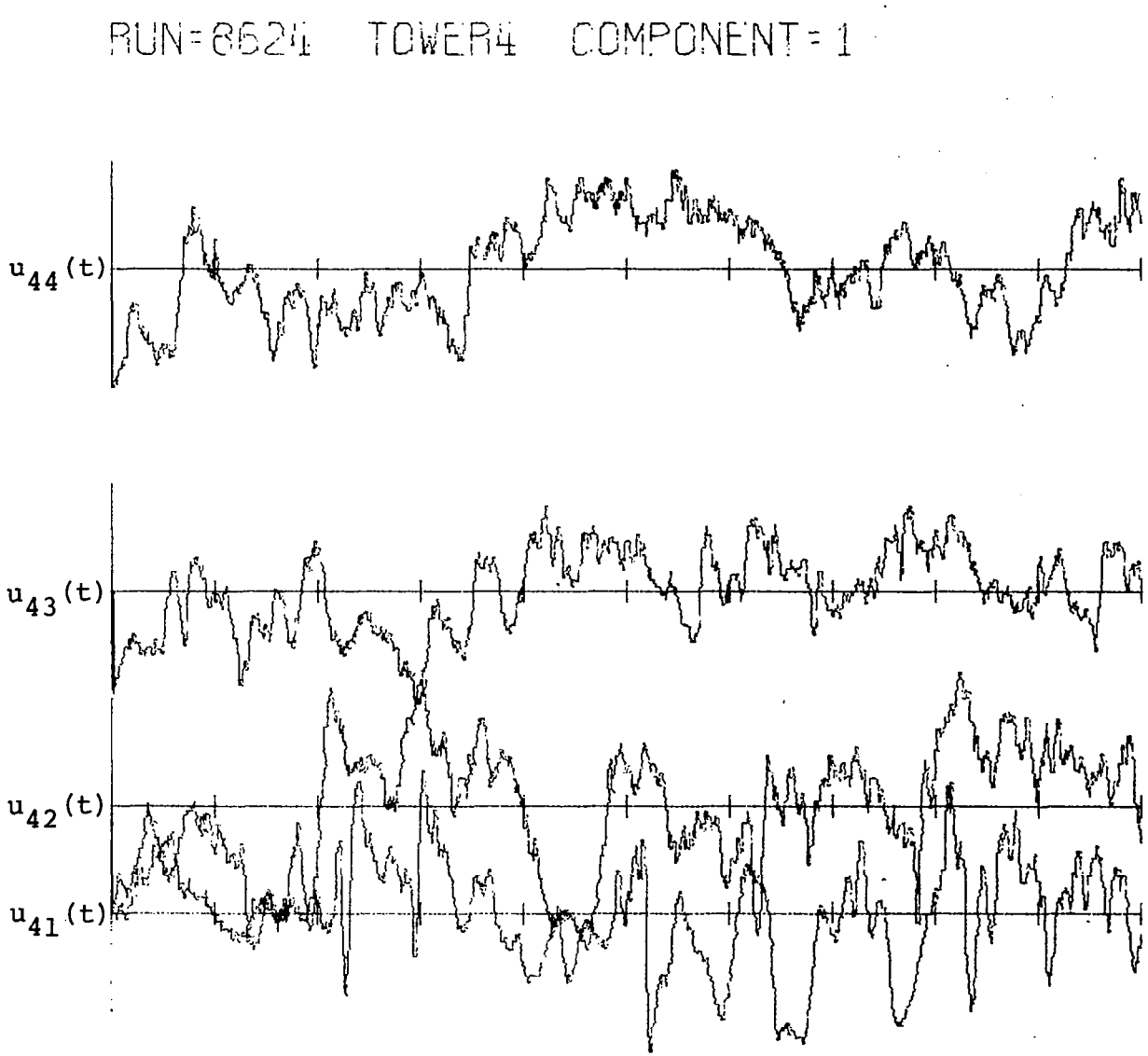

Figure 5-3 (continued)

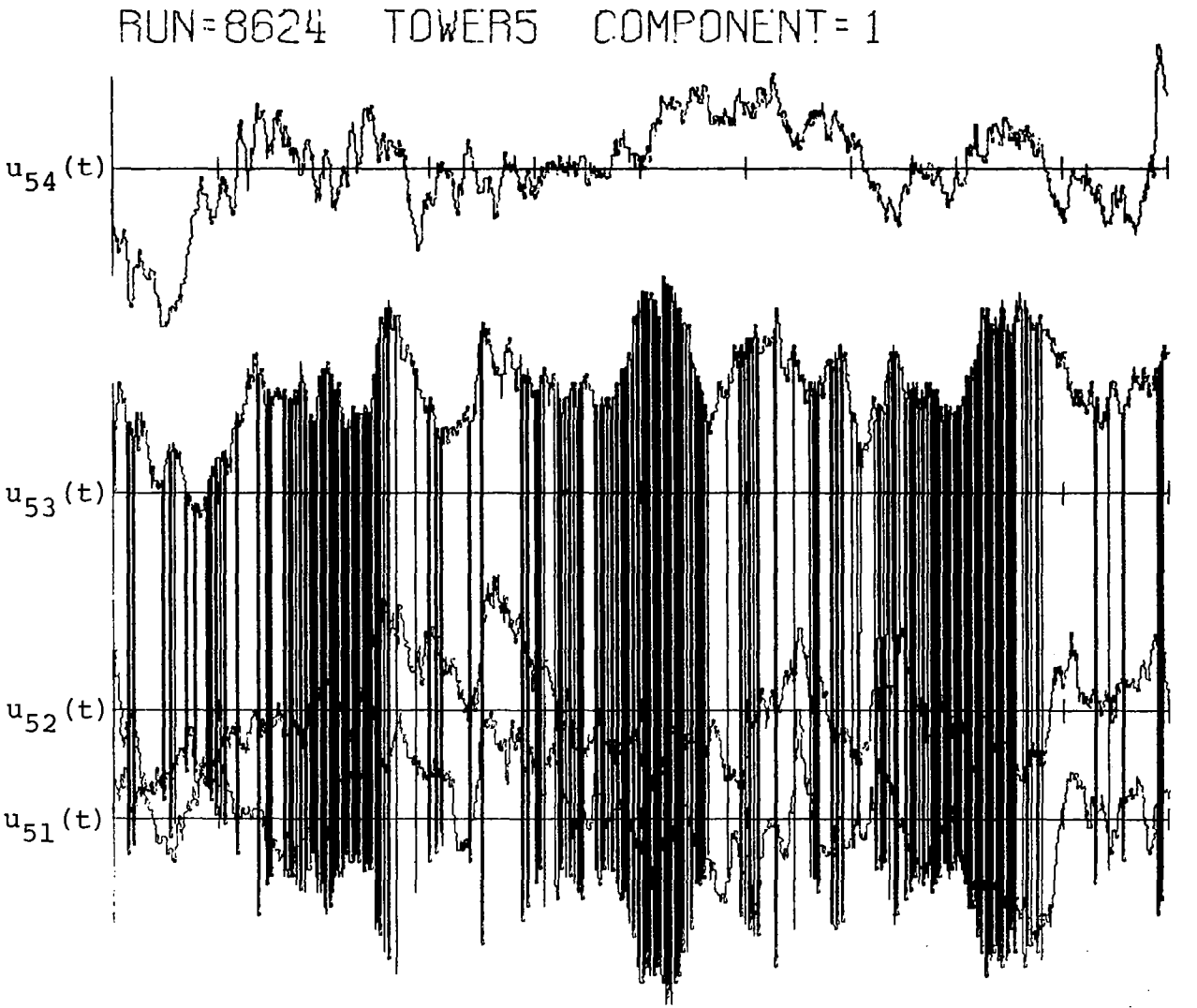

Figure 5-3 (continued)

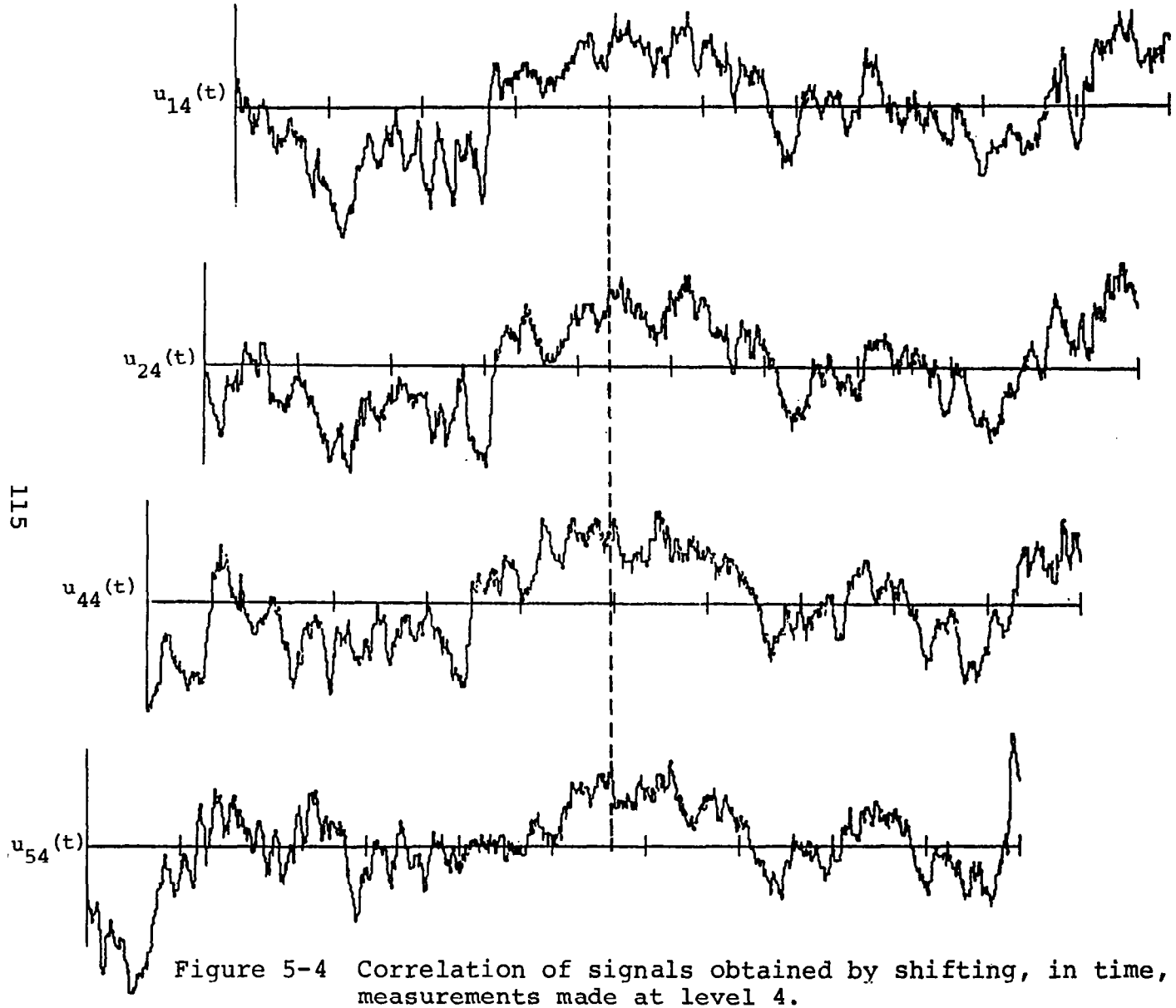

Figure 5-4 Correlation of signals obtained by shifting, in time, measurements made at level 4.

has been shifted, relative to $u_{14}(t)$, in time corresponding to the time it takes a signal to travel from one point to the next at the mean wind speed velocity (this time is proportional to the ratio of the distance to the mean wind speed).

A turbulence fluctuation existing at one point in space thus propagates in the mean wind direction and can be experienced downstream. The intensity and reproducibility of the signal will depend on several factors; for example, mean velocity, boundary conditions, spatial separation, etc. These will be discussed in detail when Taylor's hypothesis is examined near the end of this section.

Spatial Correlations

To get some indication of the effect surface obstructions have on the flow of air, it is necessary to measure the flow at selected points in space (Eulerian measurements) or to trace the position of air parcels in the flow as a function of time (Lagrangian measurements). The latter of these two measurements is rather difficult to make but is sometimes accomplished (not very successfully) by time-lapse photography of colored particles or radioactive tracer elements inserted at selected points in the flow field [9]. Usually, Eulerian velocities are measured by inserting a probe in the flow field and measuring its velocity relative to some position and time.

Two-point space-time correlations can be used to measure the general dependence of the flow field at one point in space relative to another point. This dependence can be a function of boundary conditions (flow direction and surface obstruction), of position in the flow field in which the measurements are being made, and of time (instantaneous effects or possibly effects after some lapse of time).

Two-point space-time correlations of the atmospheric flow about a simulated block building have been computed from the wind data described herein, some of which are presented in this section. In general, given two sets of data $x(t)$ and $y(t)$ with mean equal to zero [$\overline{x(t)} = \overline{y(t)} = 0$], then a correlation function $R_{xy}(\tau)$ is defined as

$$R_{xy}(\tau) = \lim_{T\to\infty} \int_{o}^{T} x(t)y(t + \tau)\, dt \qquad (5.1)$$

A correlation coefficient is then defined as

$$B_{xy}(\tau) = \frac{R_{xy}(\tau)}{\sigma_x \sigma_y} \qquad (5.2)$$

where σ_x and σ_y are the standard deviations of $x(t)$ and $y(t)$, respectively. As defined, $B_{xy}(\tau)$ is normalized and theoretically bound within the range $-1 \leq R_{xy}(\tau) \leq 1$. For the data described herein, digital techniques were used to compute the correlation coefficient and the method is explained in Section III. The digital estimate of $B_{xy}(\tau)$ is given as $\hat{B}_{xy}(rh)$ and is defined in Equation (3.16).

In this study, the symbol for the correlation coefficient, $B_{u_{ij}u_{k\ell}}(\tau)$, will be used where u_{ij} and $u_{k\ell}$ are longitudinal velocity components with u_{ij} being measured at tower "i" and level "j" and with $u_{k\ell}$ being measured at tower "k" and level "ℓ." When $i \neq k$ and $j \neq \ell$, $\hat{B}_{u_{ij}u_{k\ell}}(\tau)$ is called a two-point space-time correlation. The term coefficient is dropped throughout the remainder of this report for simplicity of presentation. If $\tau = 0$, then $B_{u_{ij}u_{k\ell}}(0)$ is called a two-point spatial correlation. If $i = k$ and $j = \ell$, then it is called a one-point correlation and will be written as $B_{u_{ij}}(\tau)$ to indicate only the tower and level at which the measurements were made. The terminology "auto-" and "cross-" correlations, used frequently in the literature, are used to denote velocity components. Since only the longitudinal velocity components are used for discussion in this paper, $R_{u_{ij}}(\tau)$ will be called an autocorrelation, whereas $R_{x_{ij}y_{ij}}$, where x and y are components (u,v,w) in different directions, will be called a cross-correlation. It should be noted that a cross-correlation can be measured at the same point spatially or, as often thought of, at different points in space.

In Figure 5-5 two-point spatial correlations have been plotted schematically, relative to their tower position and level. The correlations are computed relative to the position designated in the figure. For example, in the plot in Figure 5-5(a) the correlations have been computed

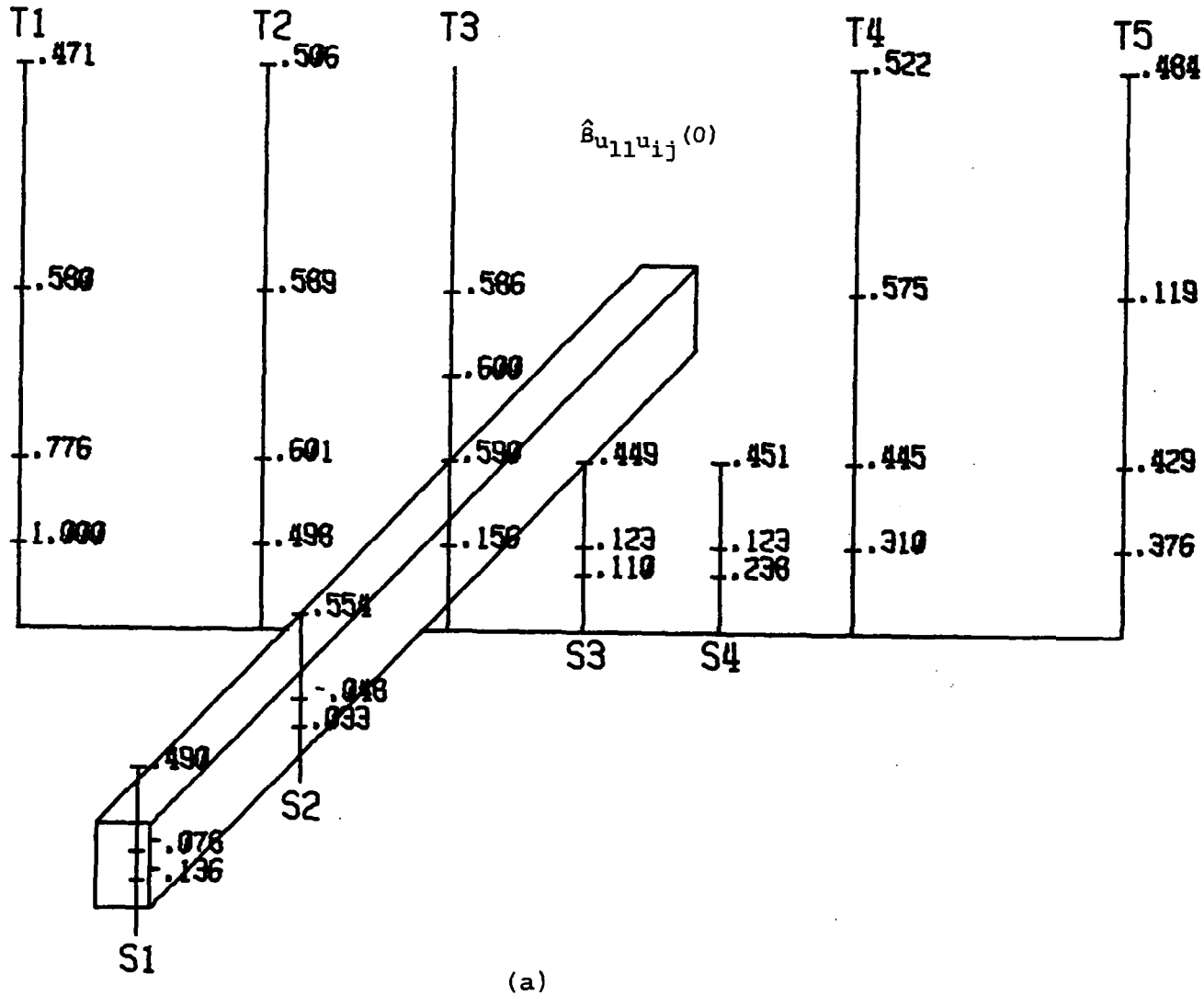

(a)

Figure 5-5 Spatial correlation relative to each tower and level.

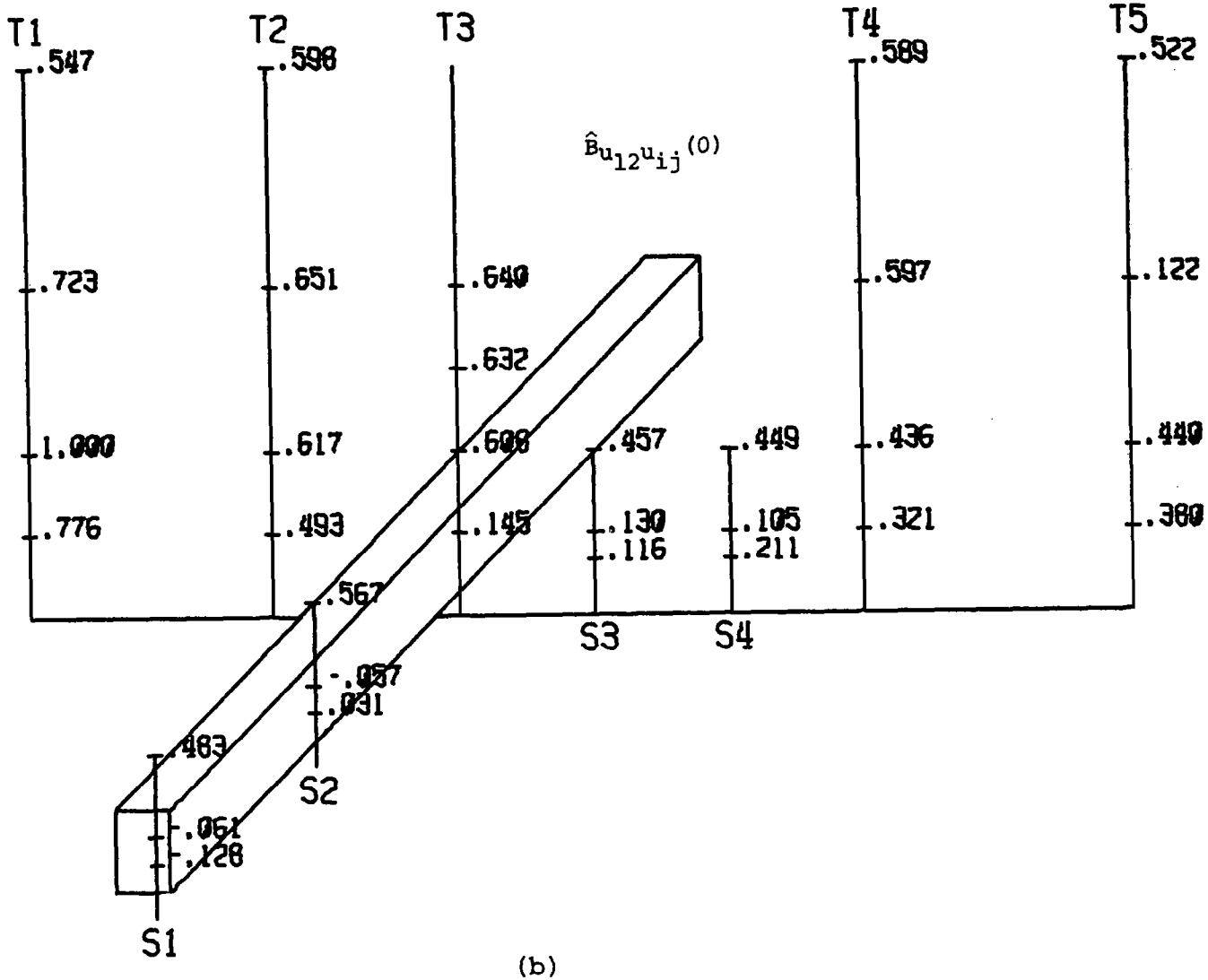

(b)

Figure 5-5 (continued)

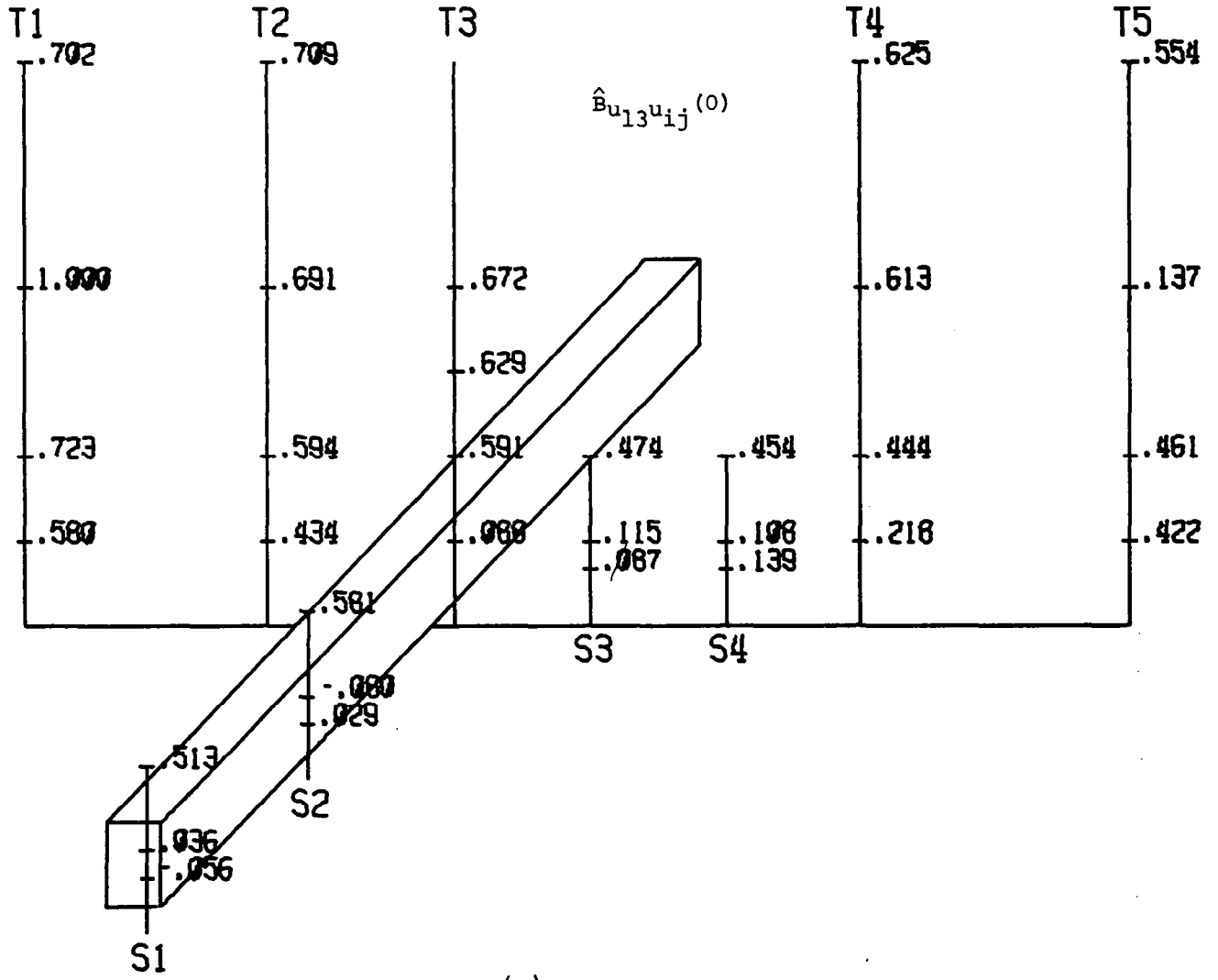

(c)

Figure 5-5 (continued)

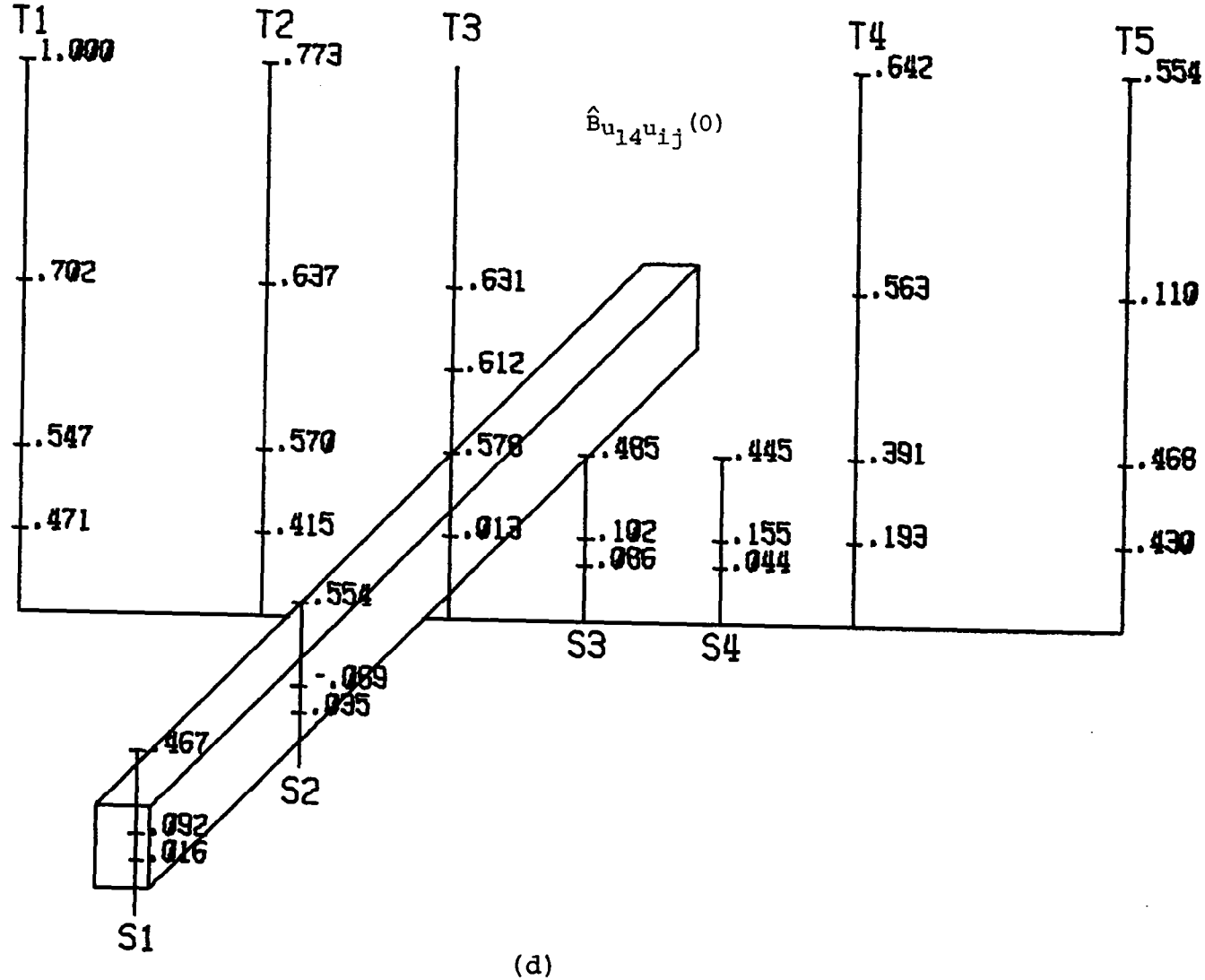

(d)

Figure 5-5 (continued)

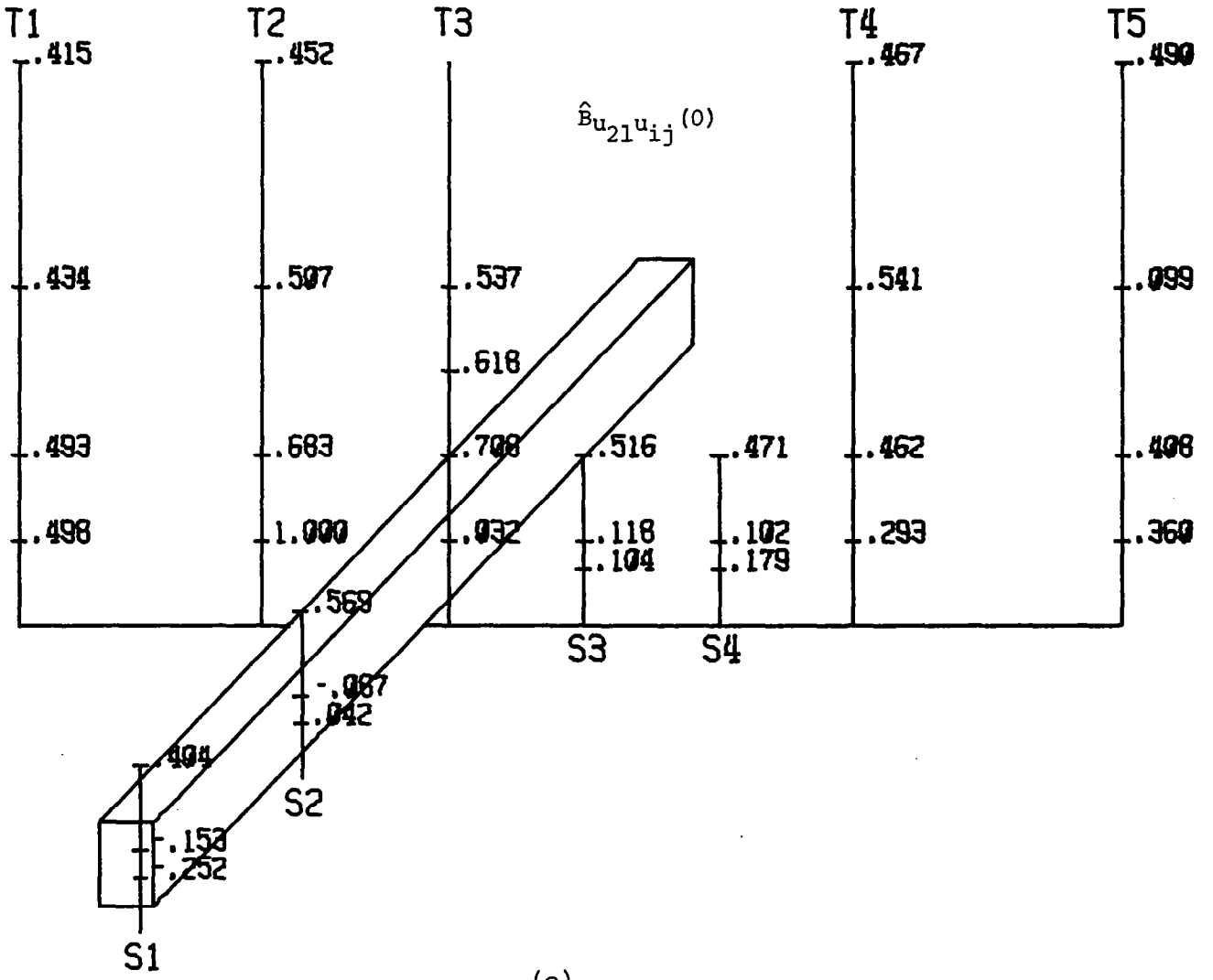

(e)

Figure 5-5 (continued)

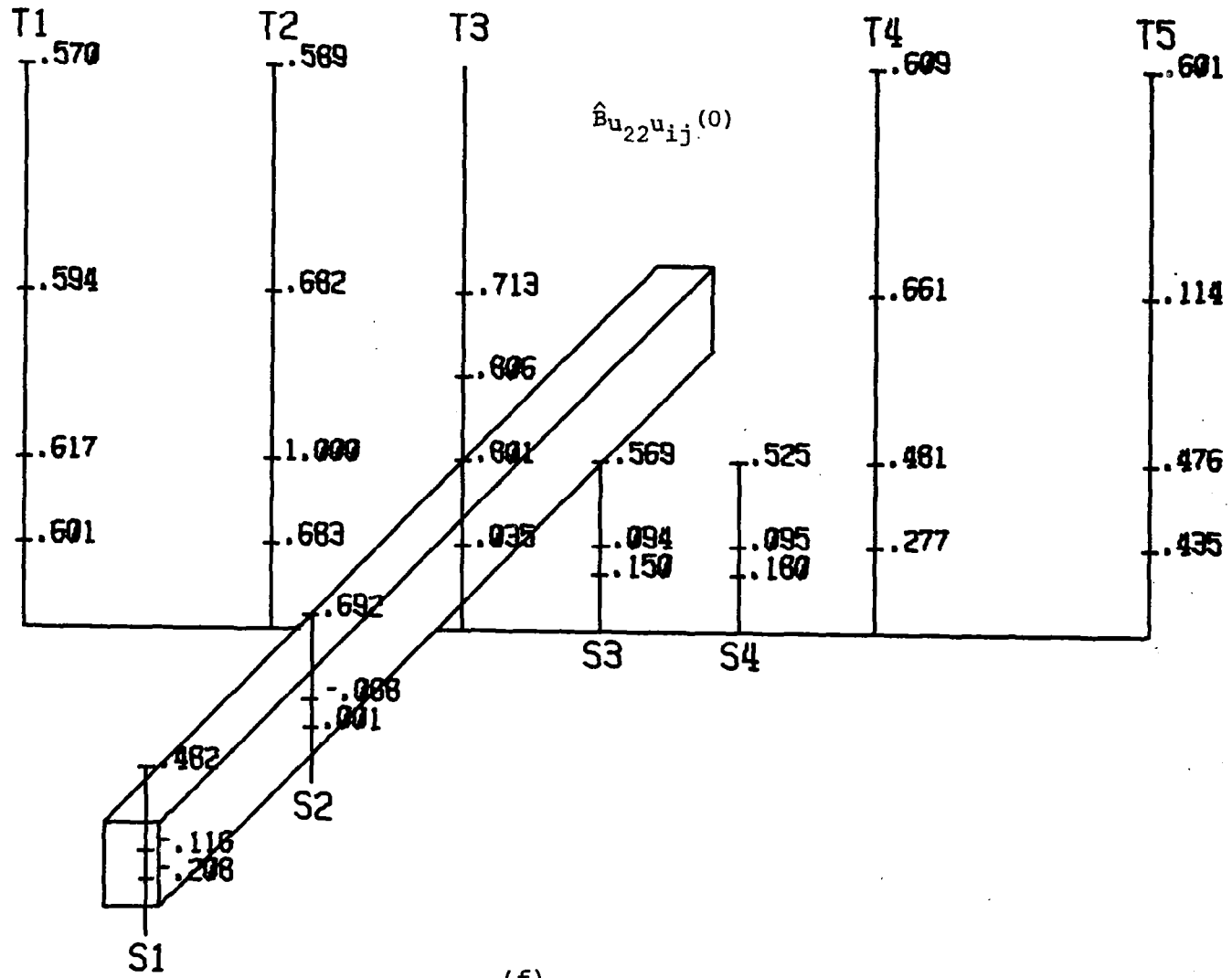

(f)

Figure 5-5 (continued)

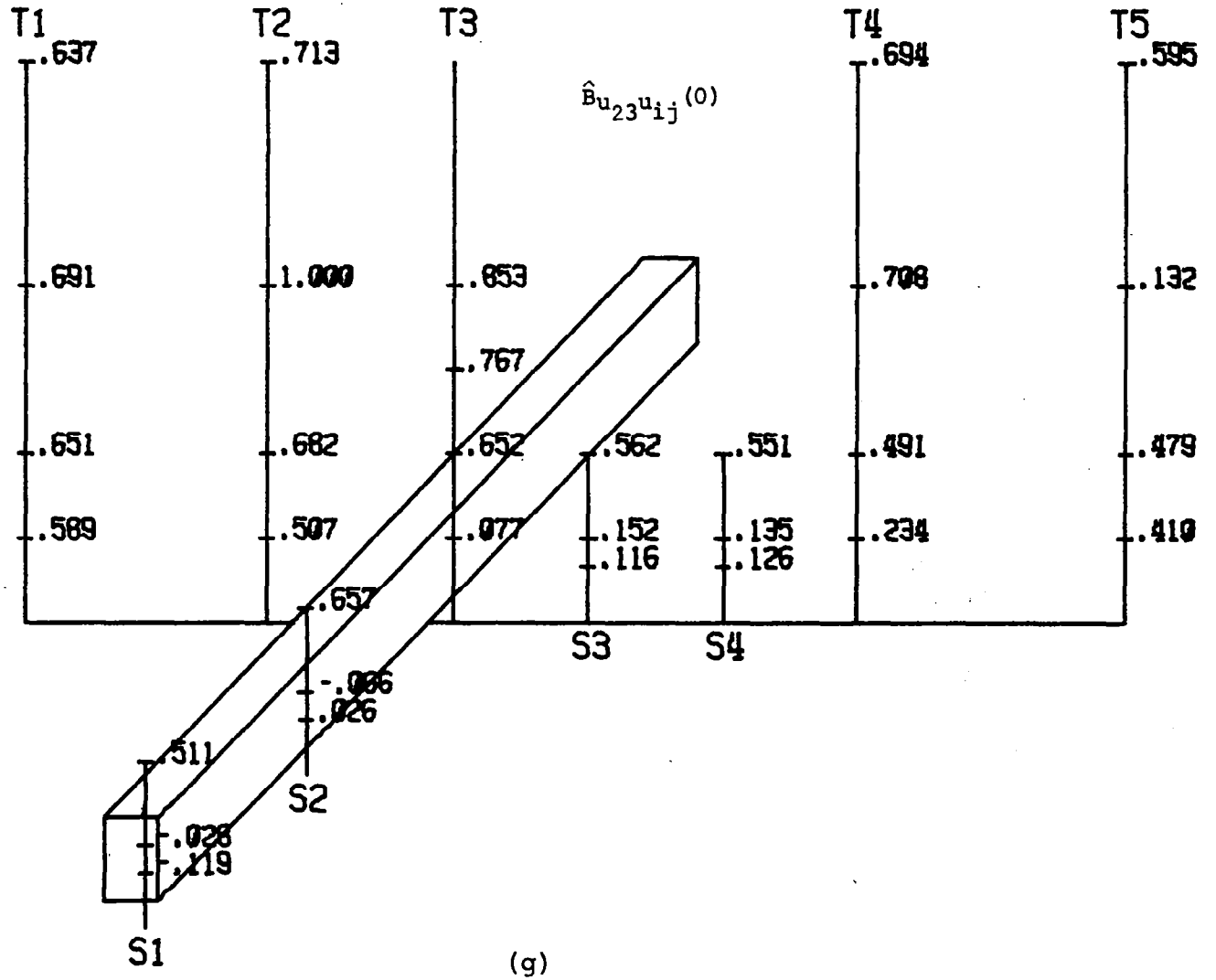

(g)

Figure 5-5 (continued)

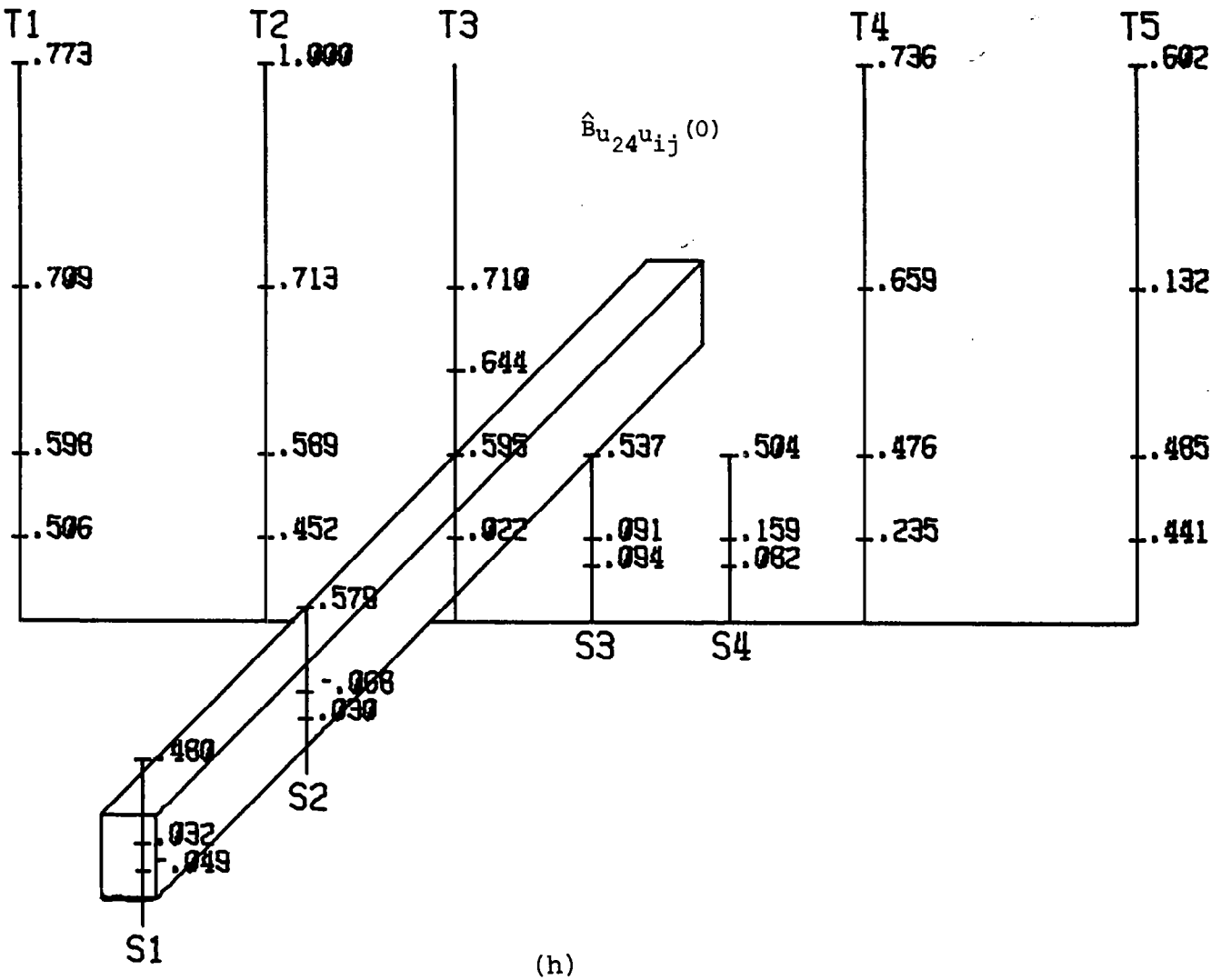

(h)

Figure 5-5 (continued)

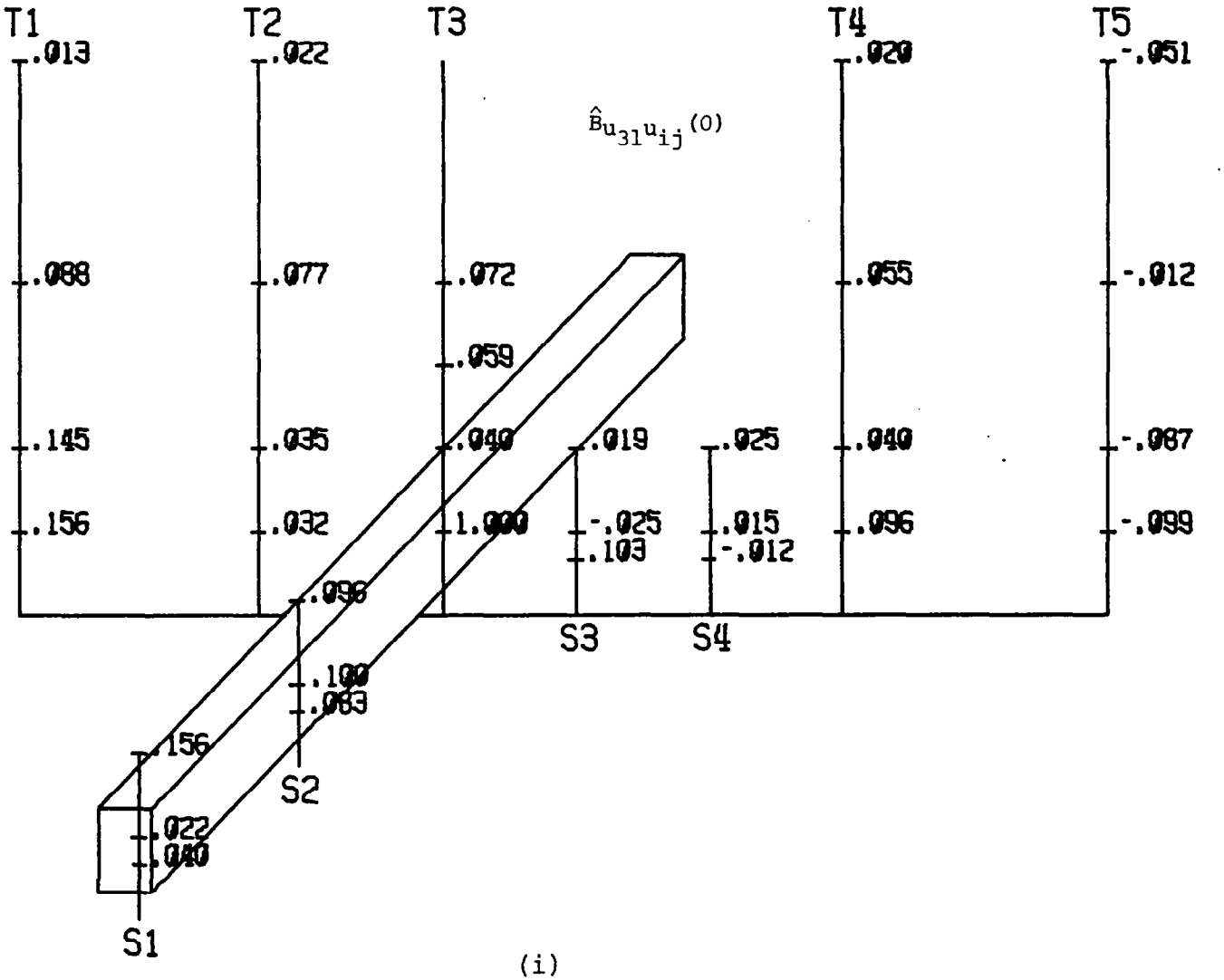

(i)

Figure 5-5 (continued)

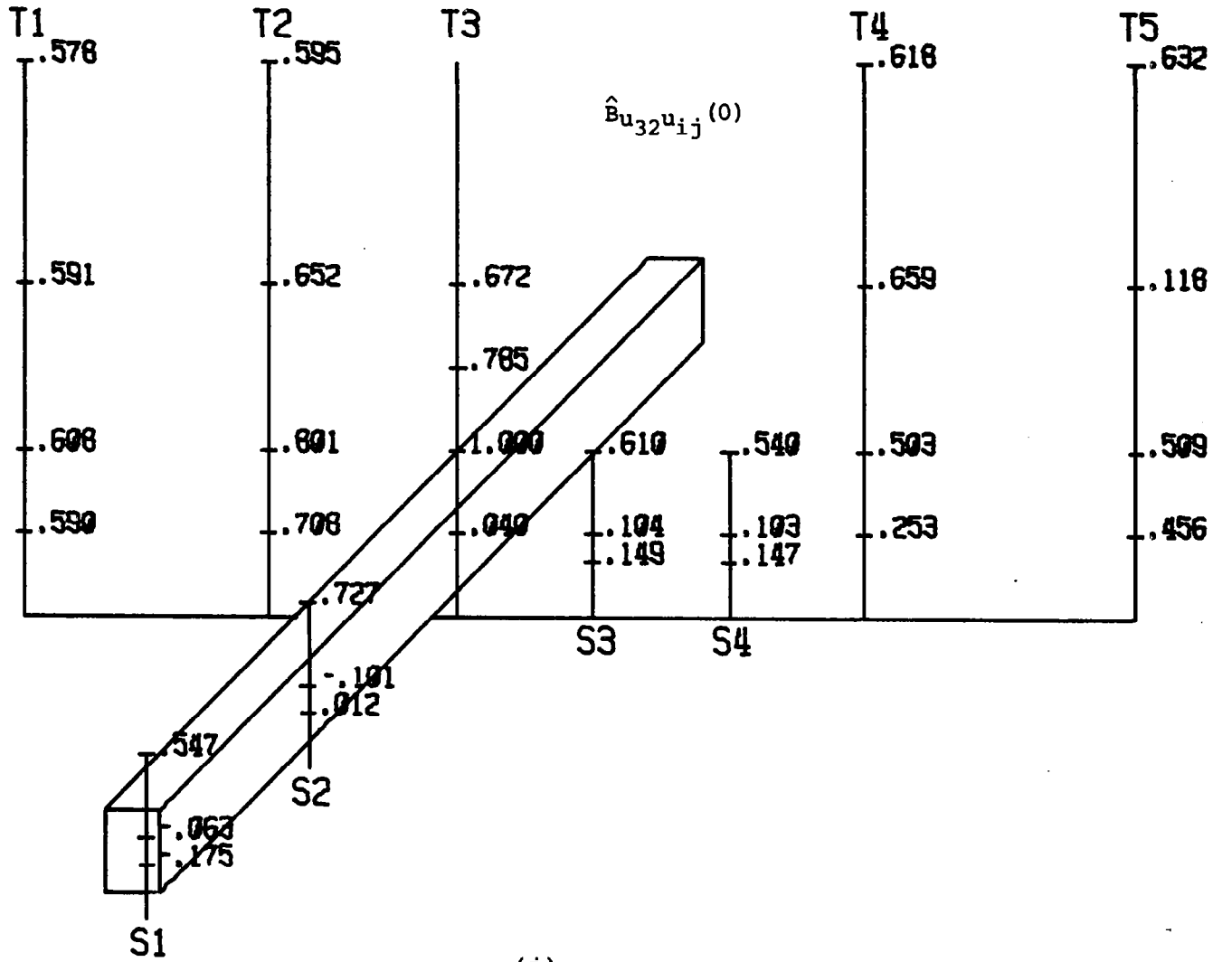

(j)

Figure 5-5 (continued)

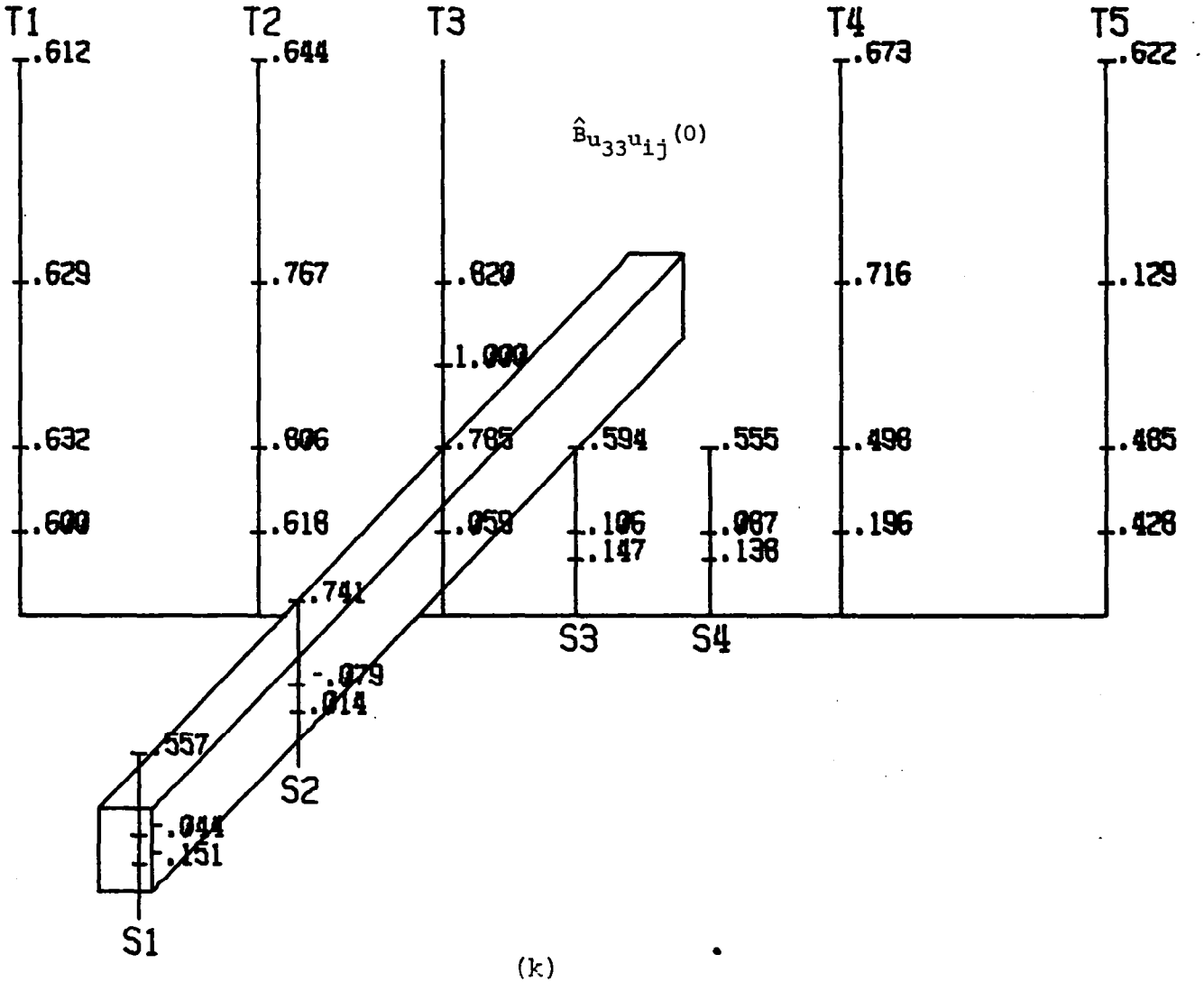

(k)

Figure 5-5 (continued)

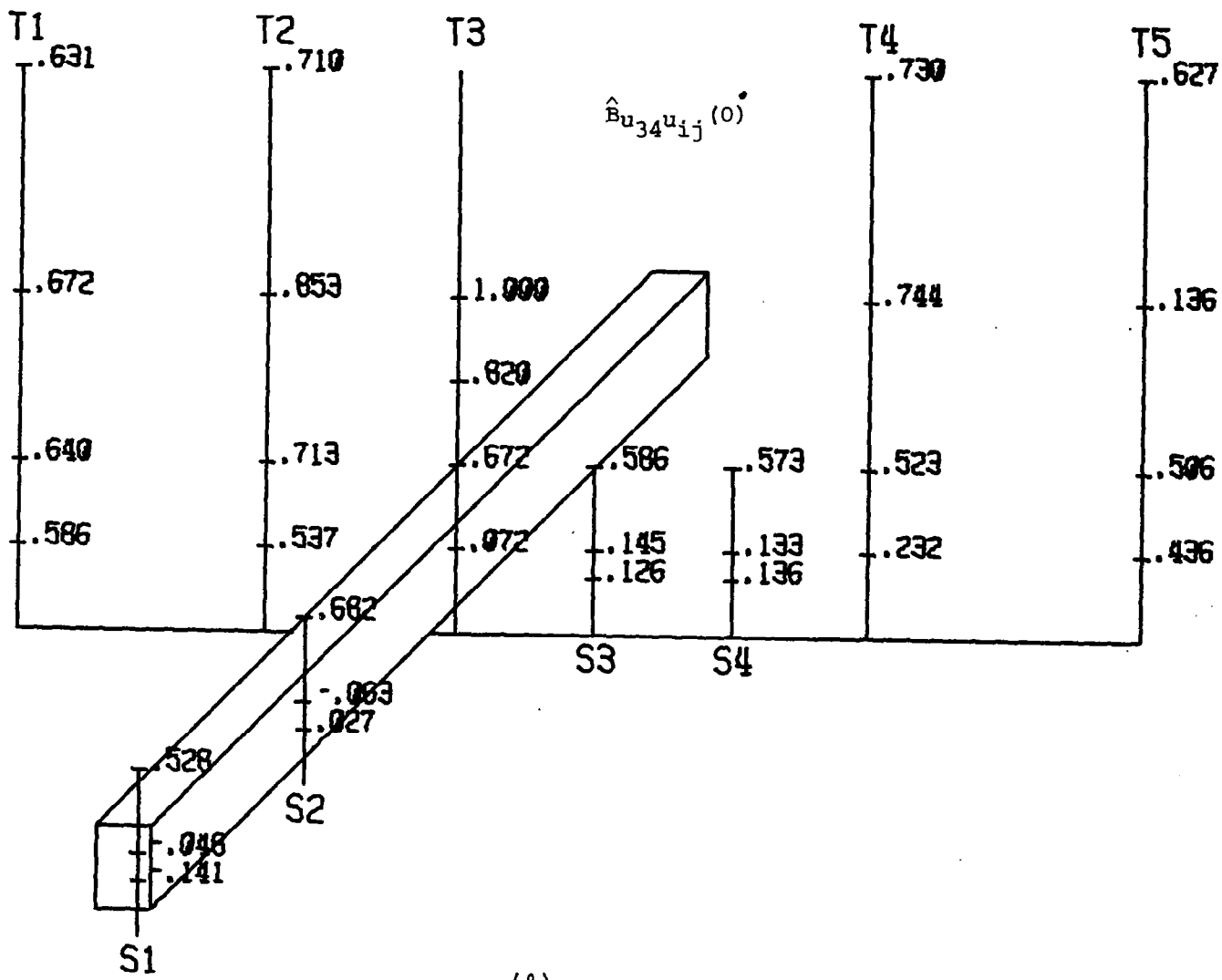

(ℓ)

Figure 5-5 (continued)

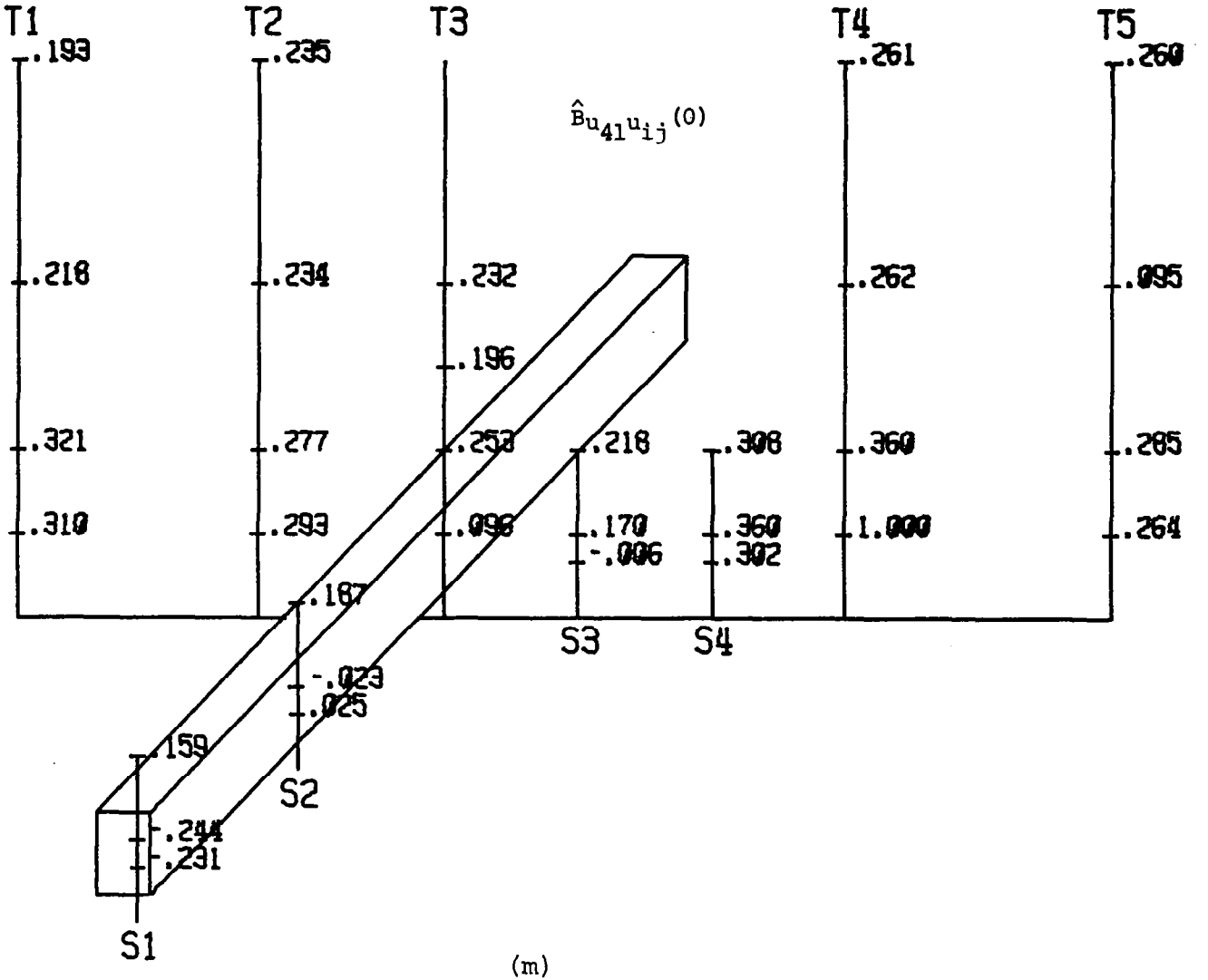

Figure 5-5 (continued)

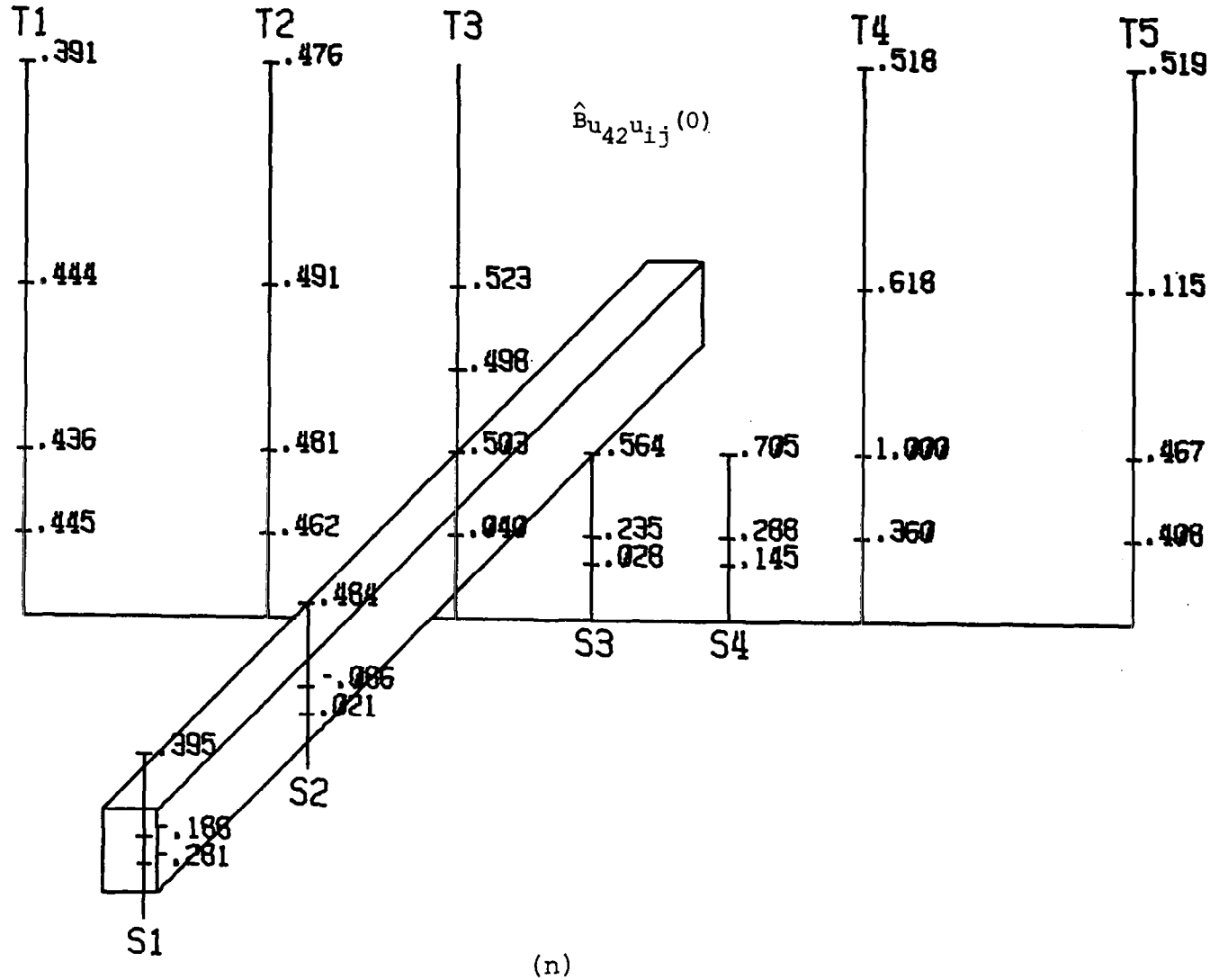

(n)

Figure 5-5 (continued)

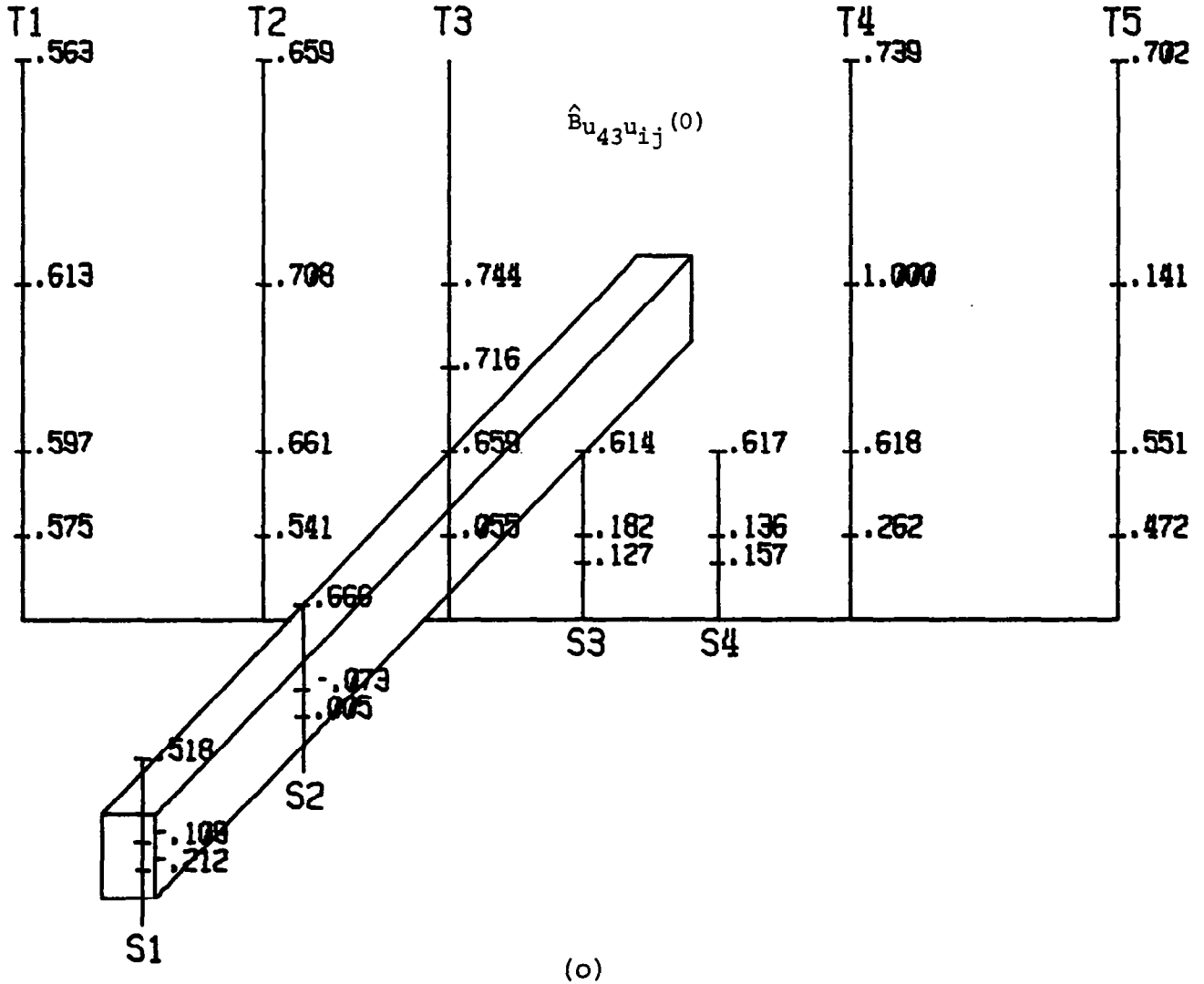

(o)

Figure 5-5 (continued)

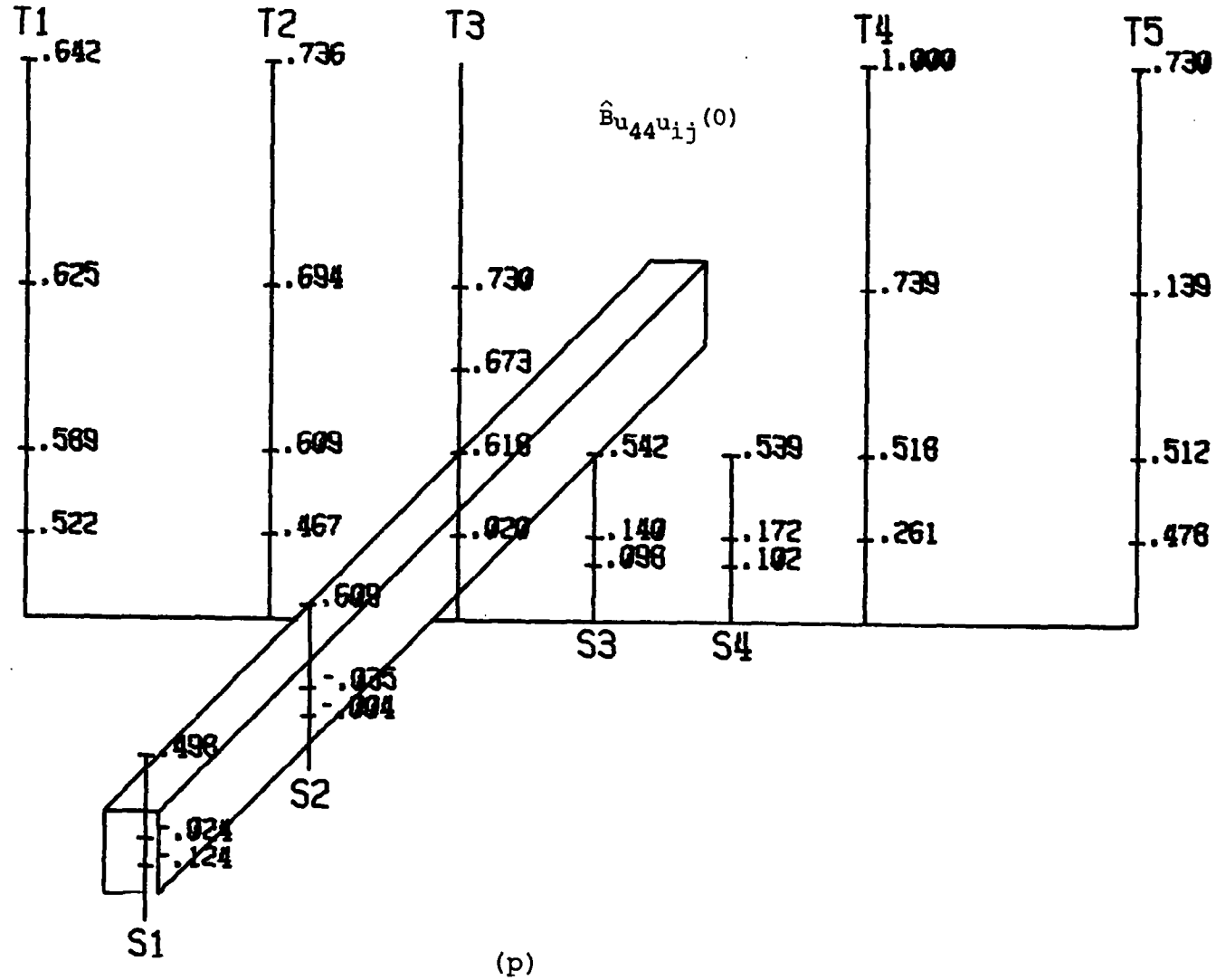

(p)

Figure 5-5 (continued)

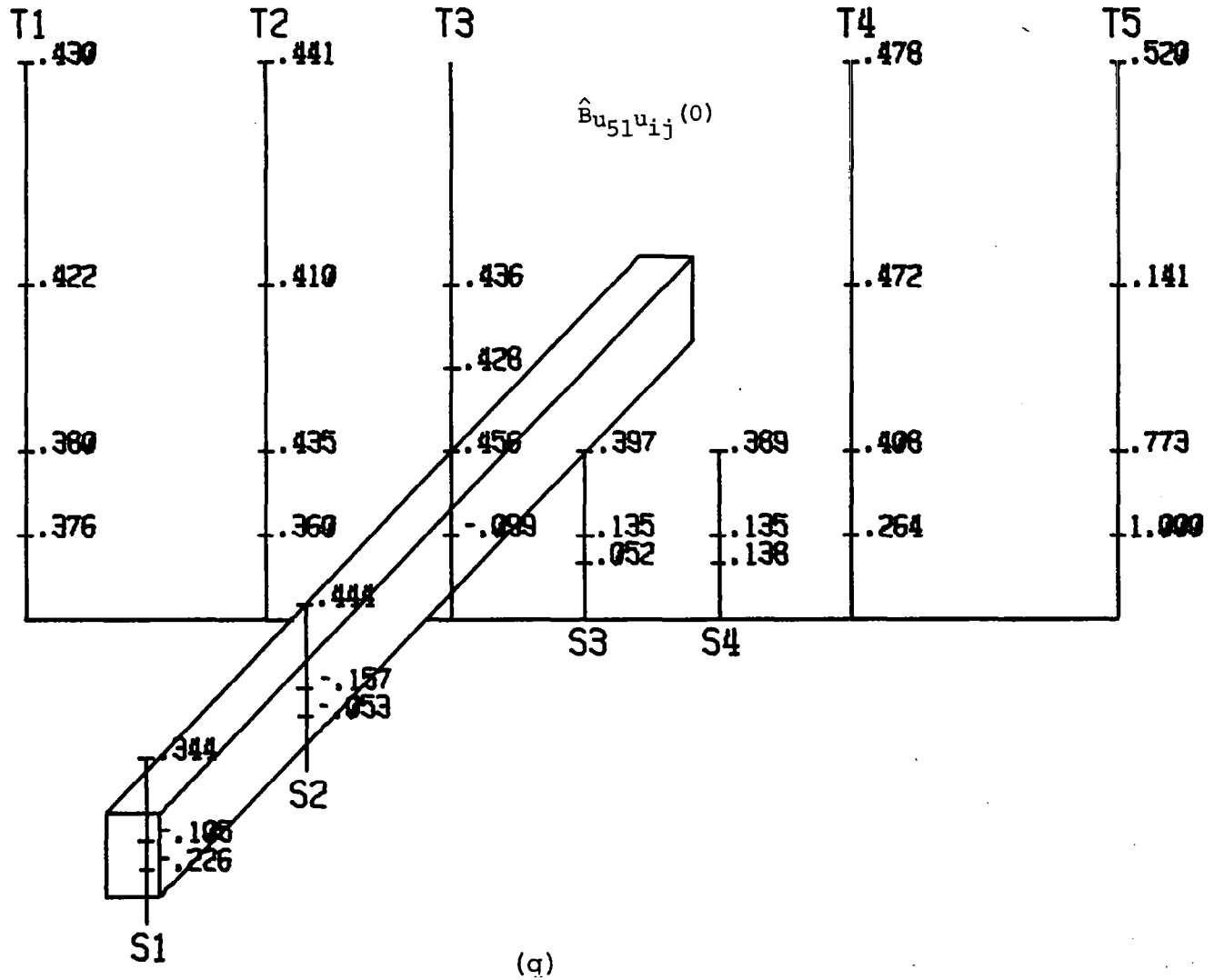

(q)

Figure 5-5 (continued)

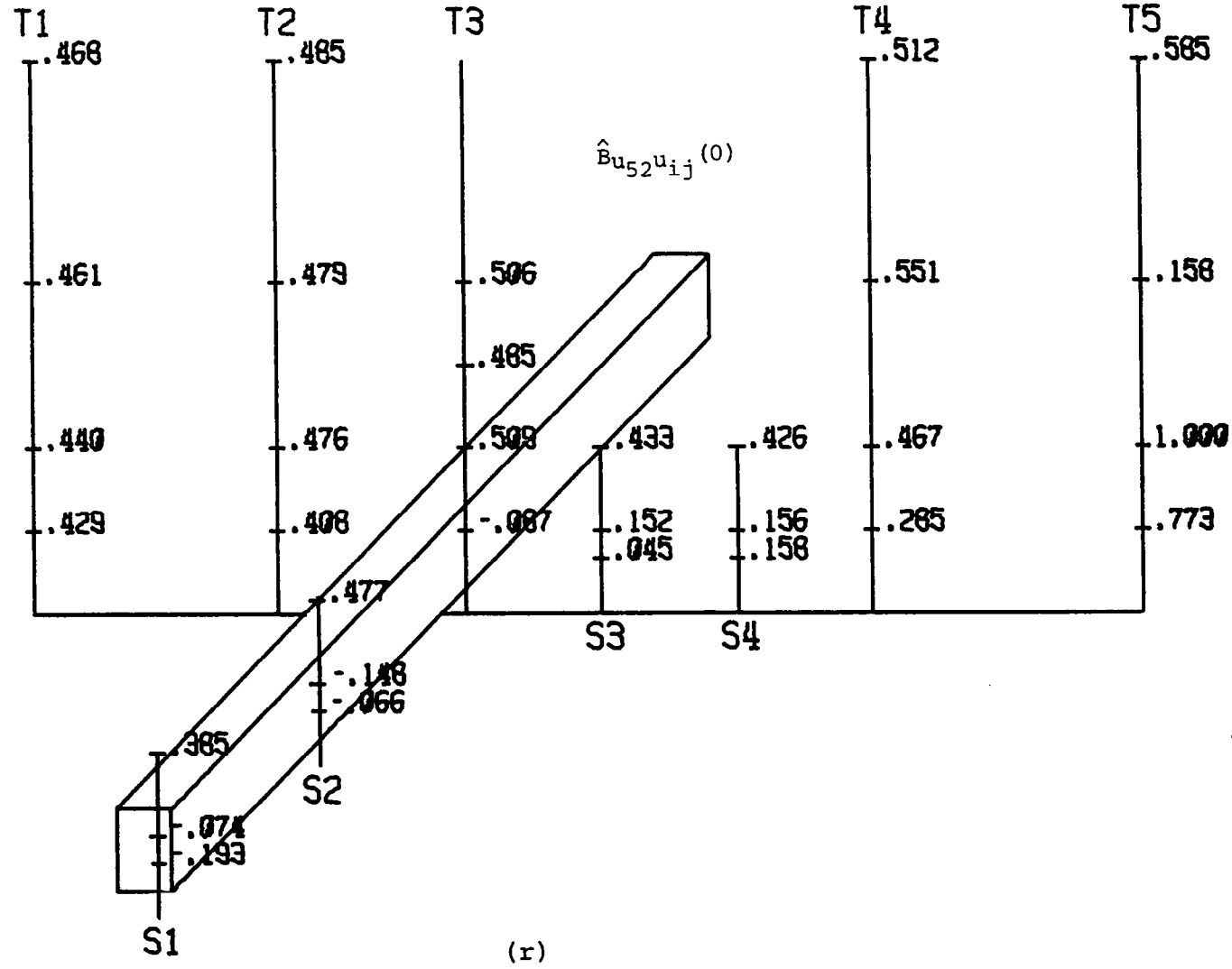

(r)

Figure 5-5 (continued)

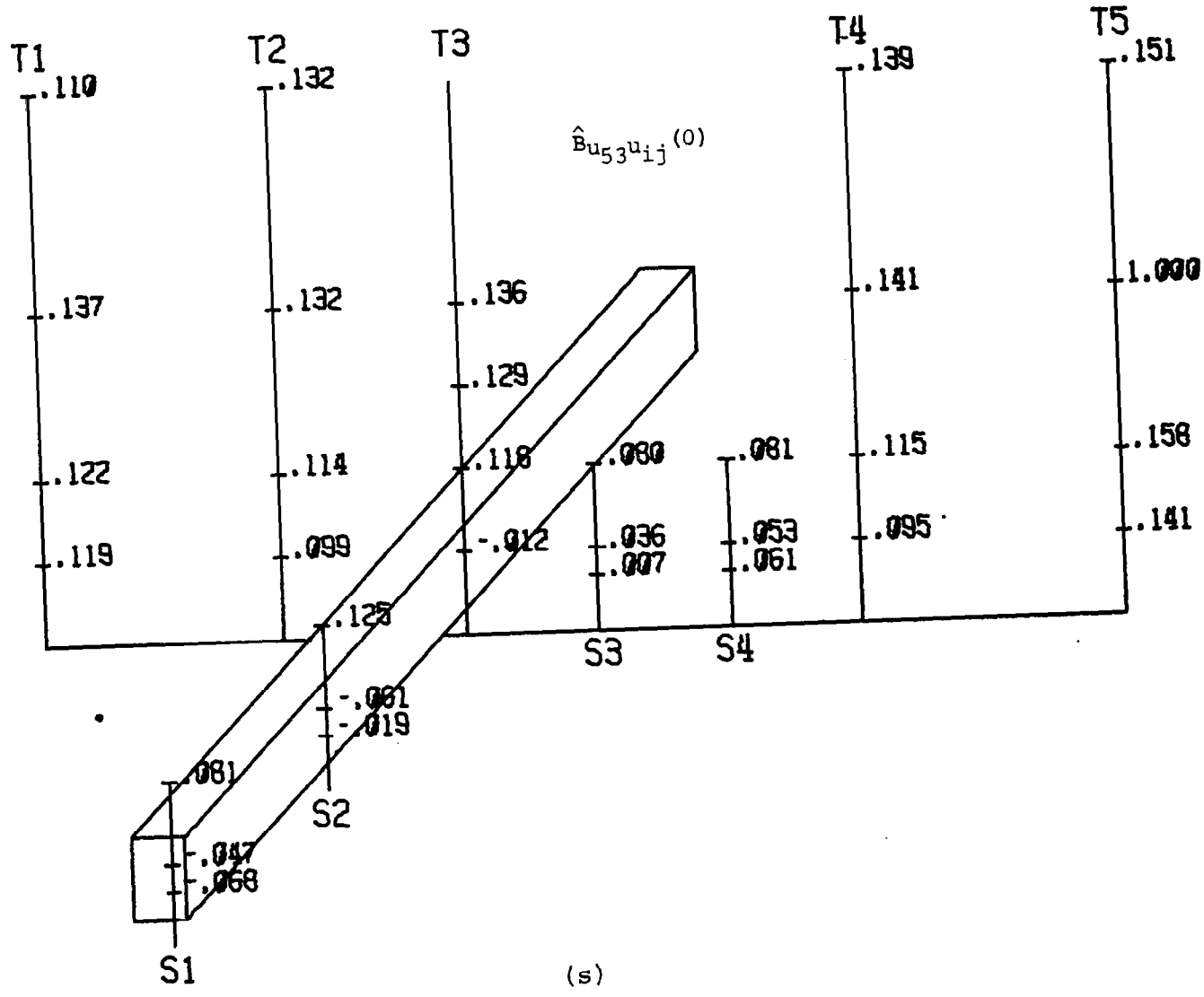

(s)

Figure 5-5 (continued)

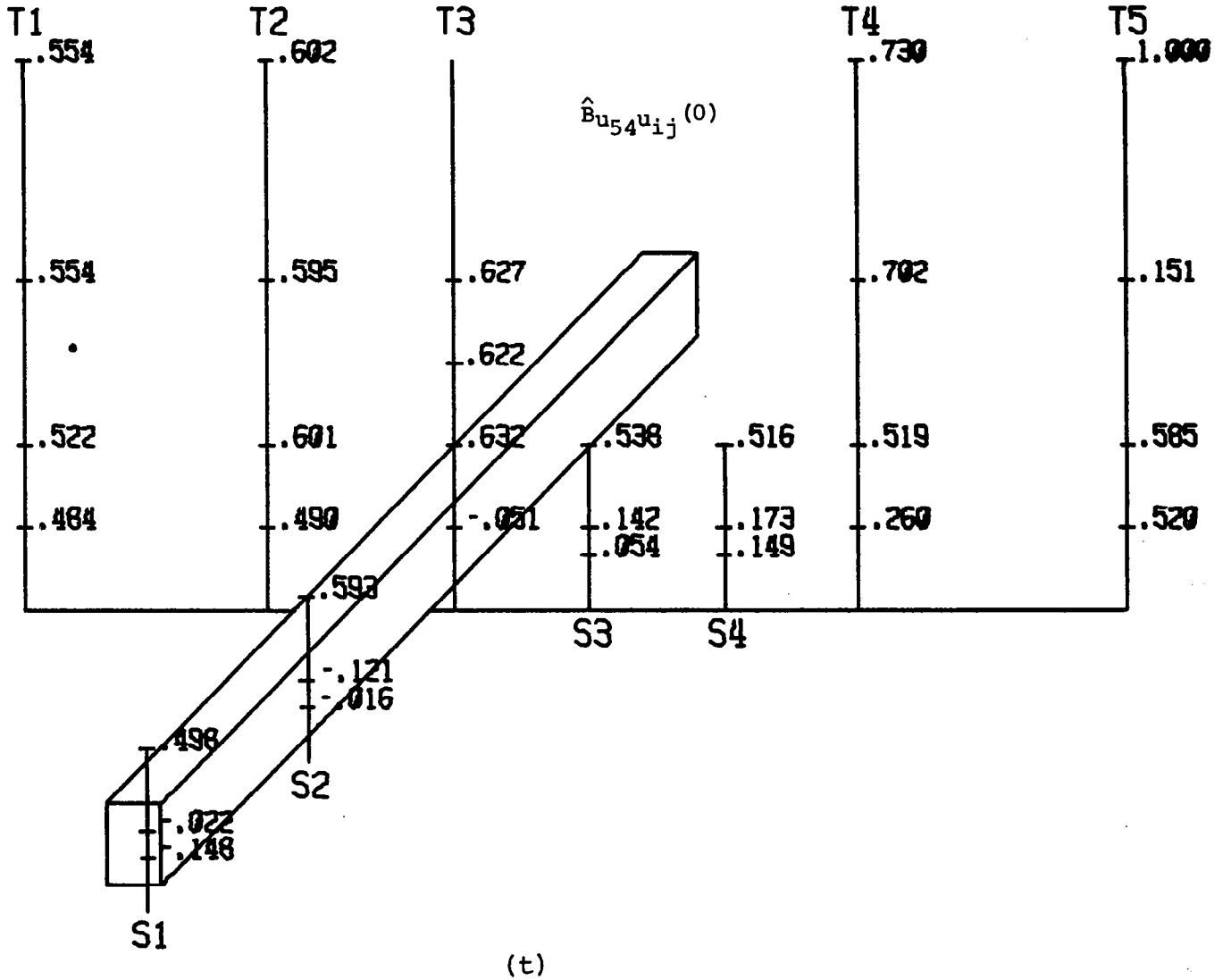

(t)

Figure 5-5 (continued)

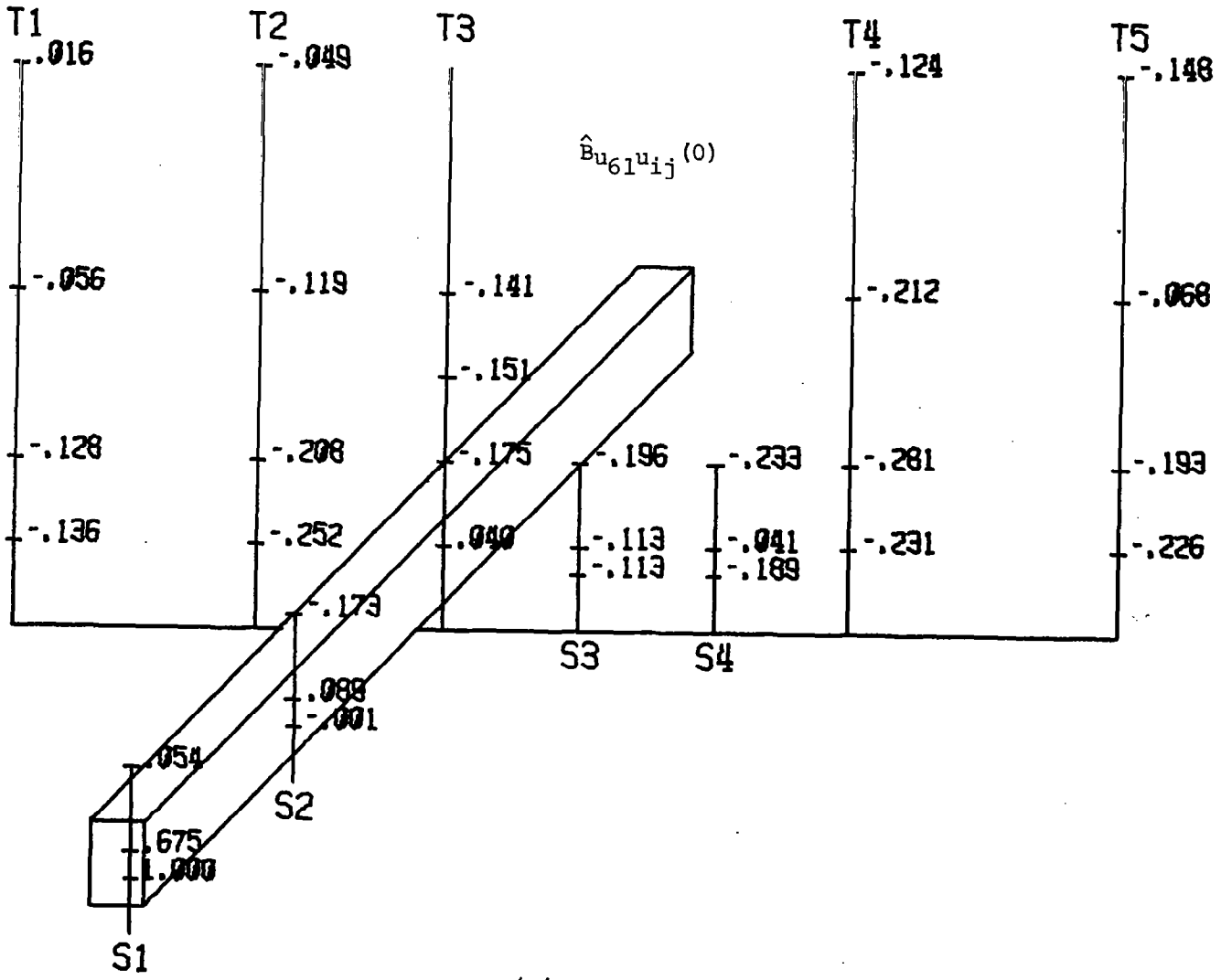

(u)

Figure 5-5 (continued)

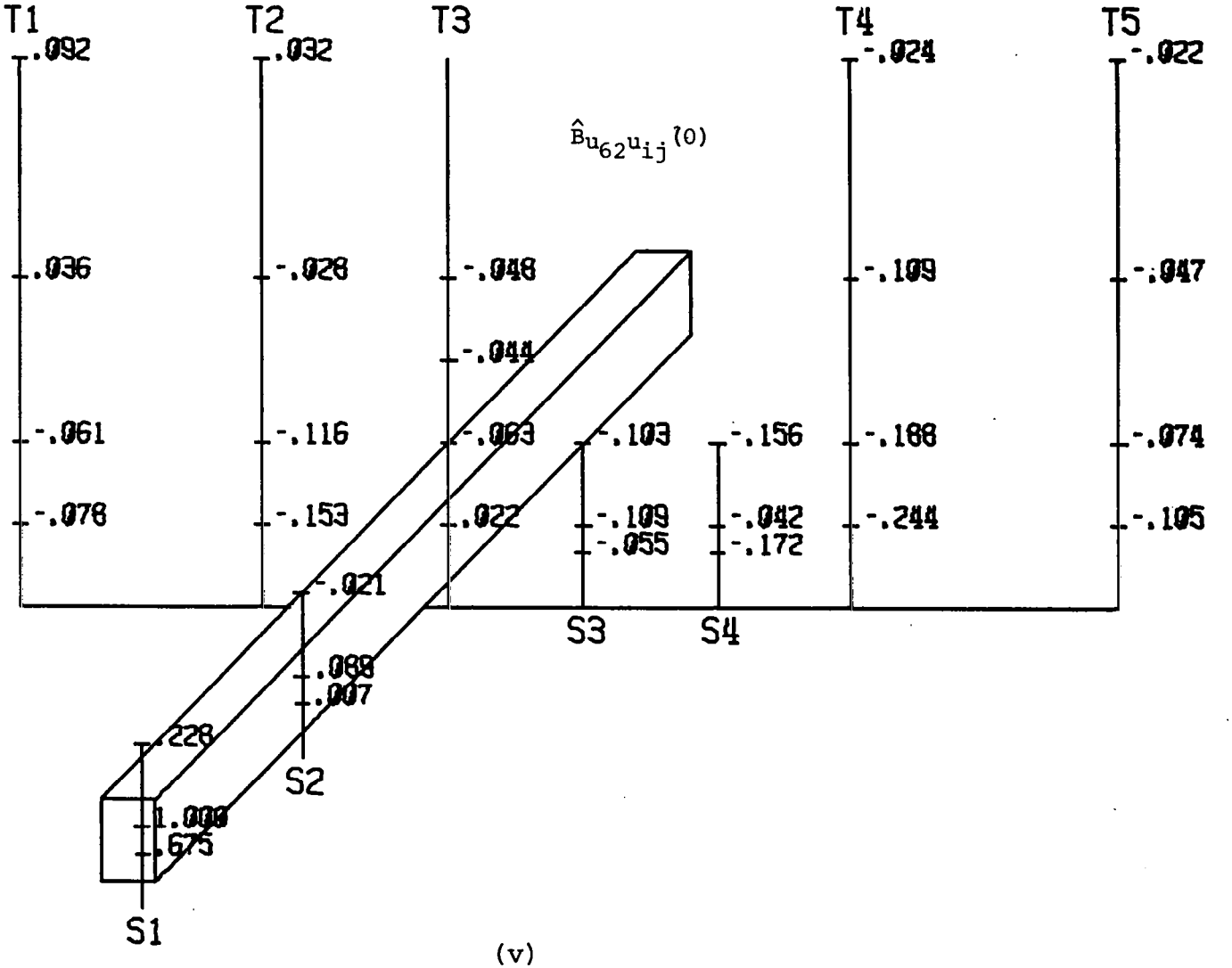

(v)

Figure 5-5 (continued)

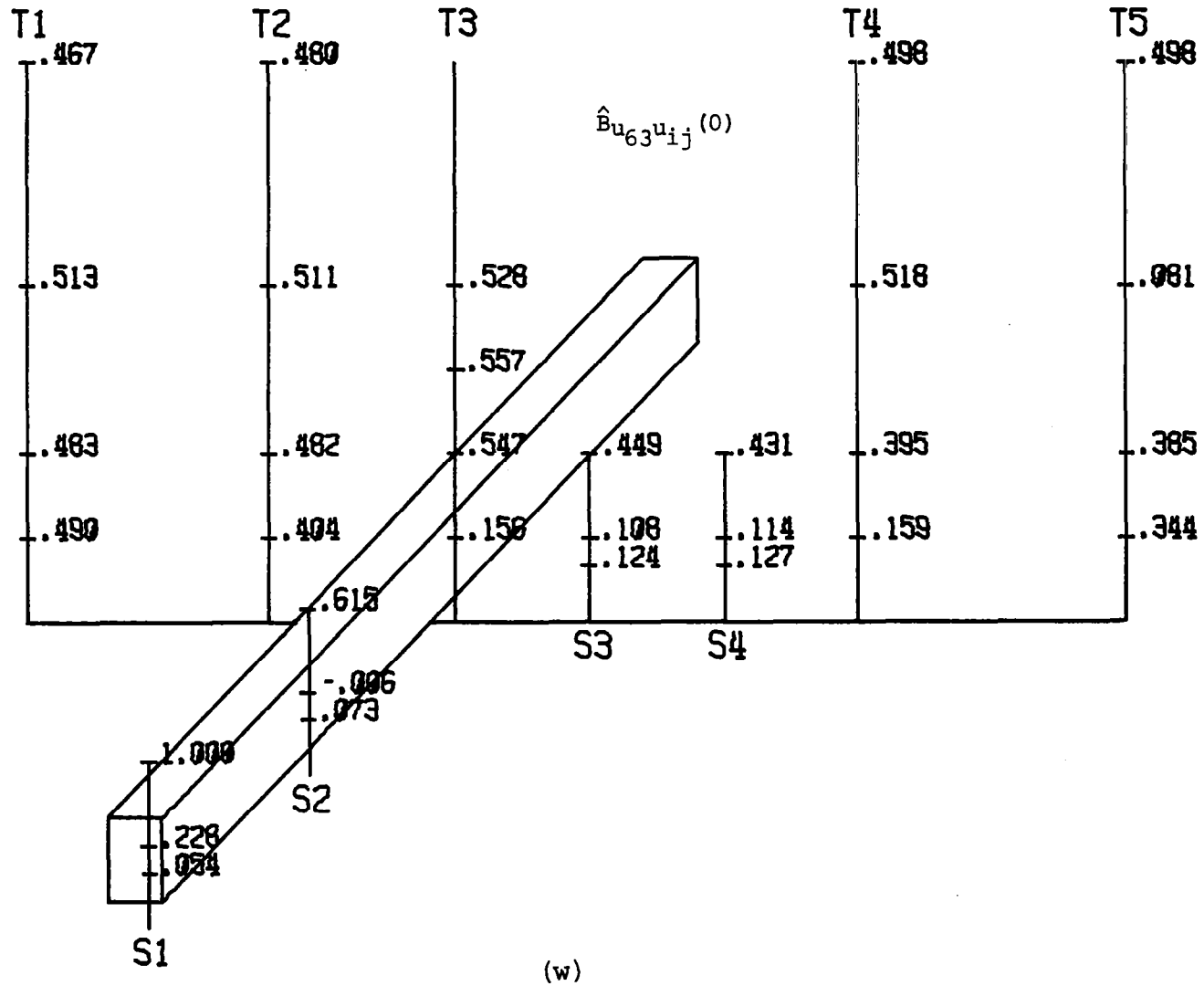

(w)

Figure 5-5 (continued)

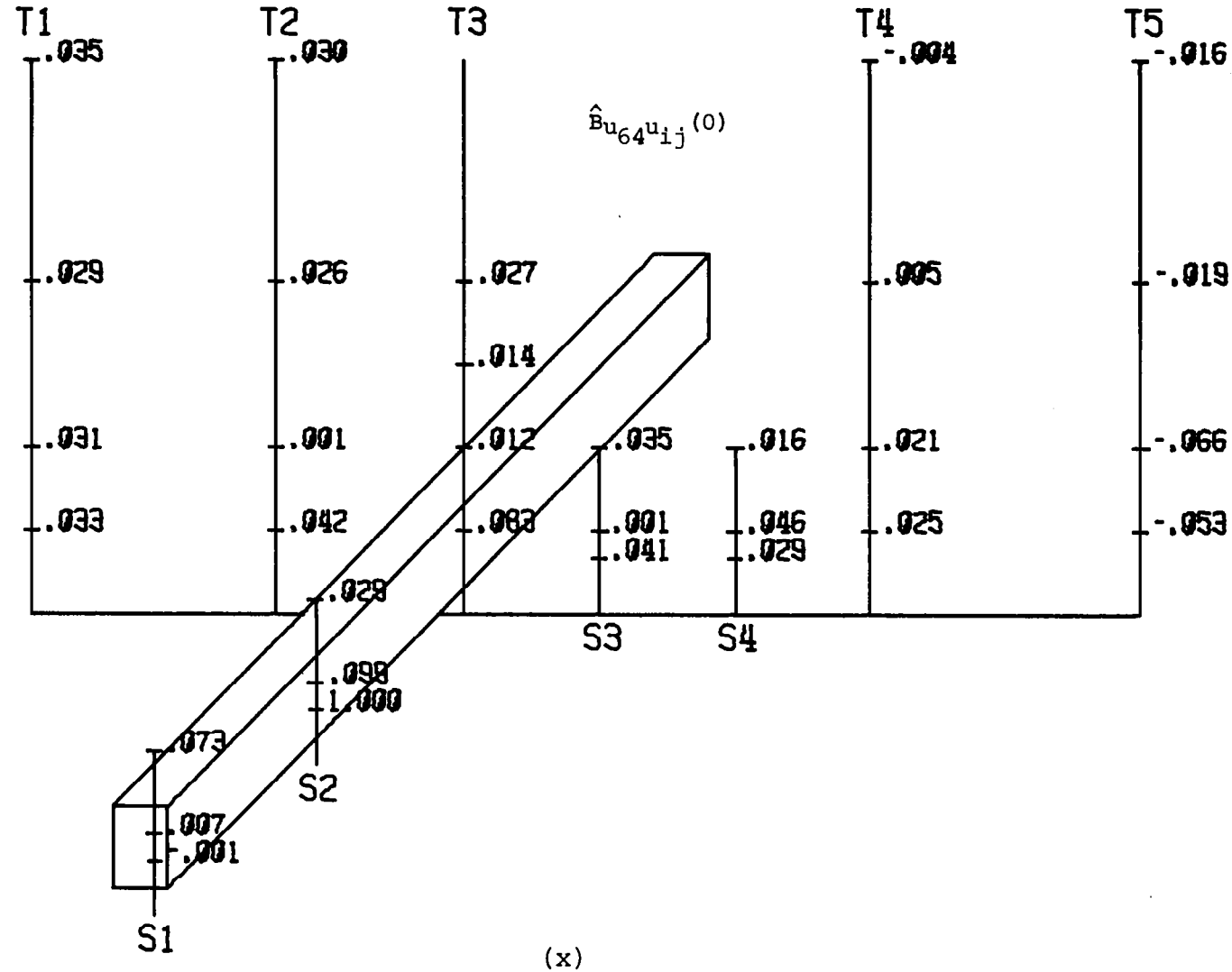

(x)

Figure 5-5 (continued)

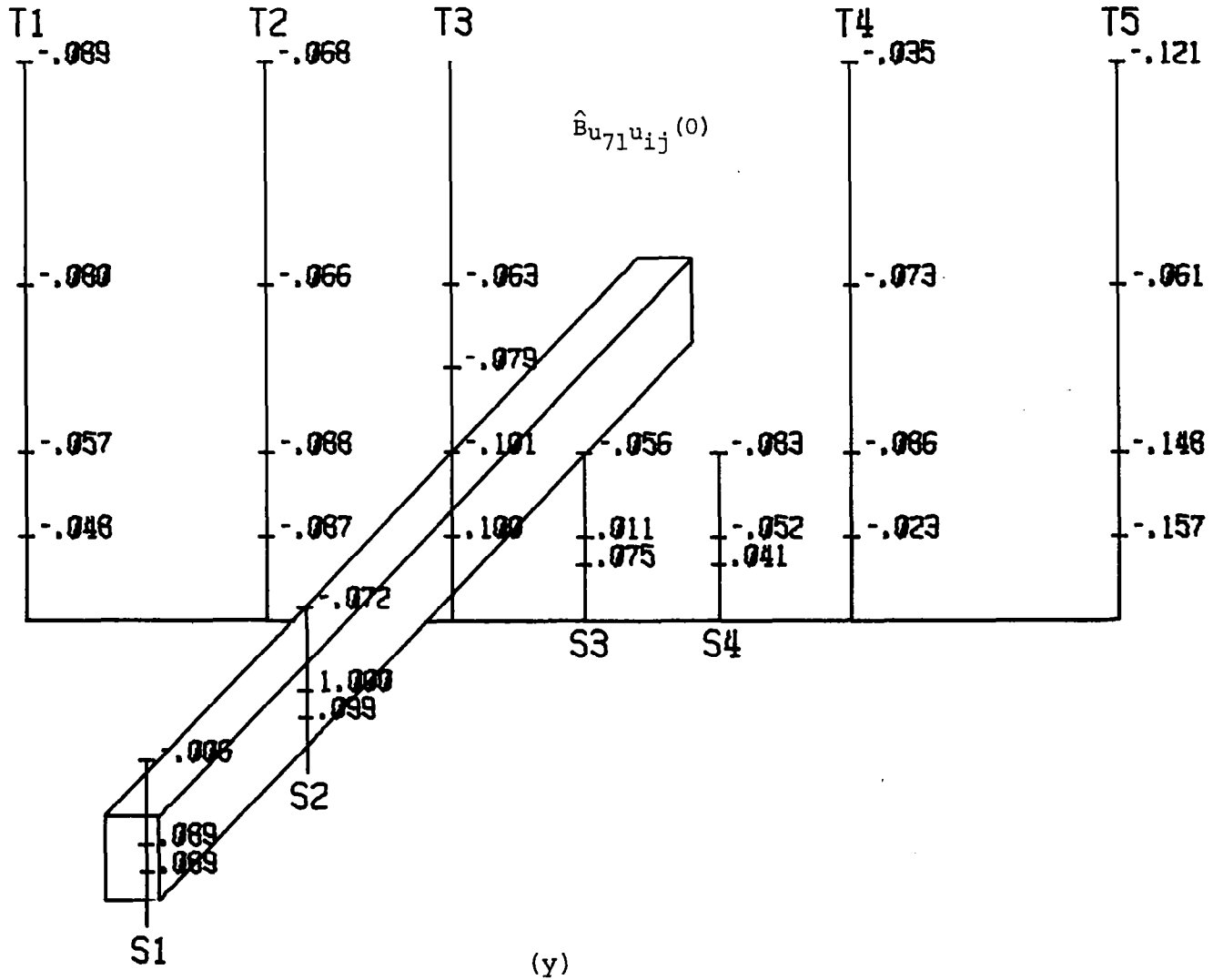

Figure 5-5 (continued)

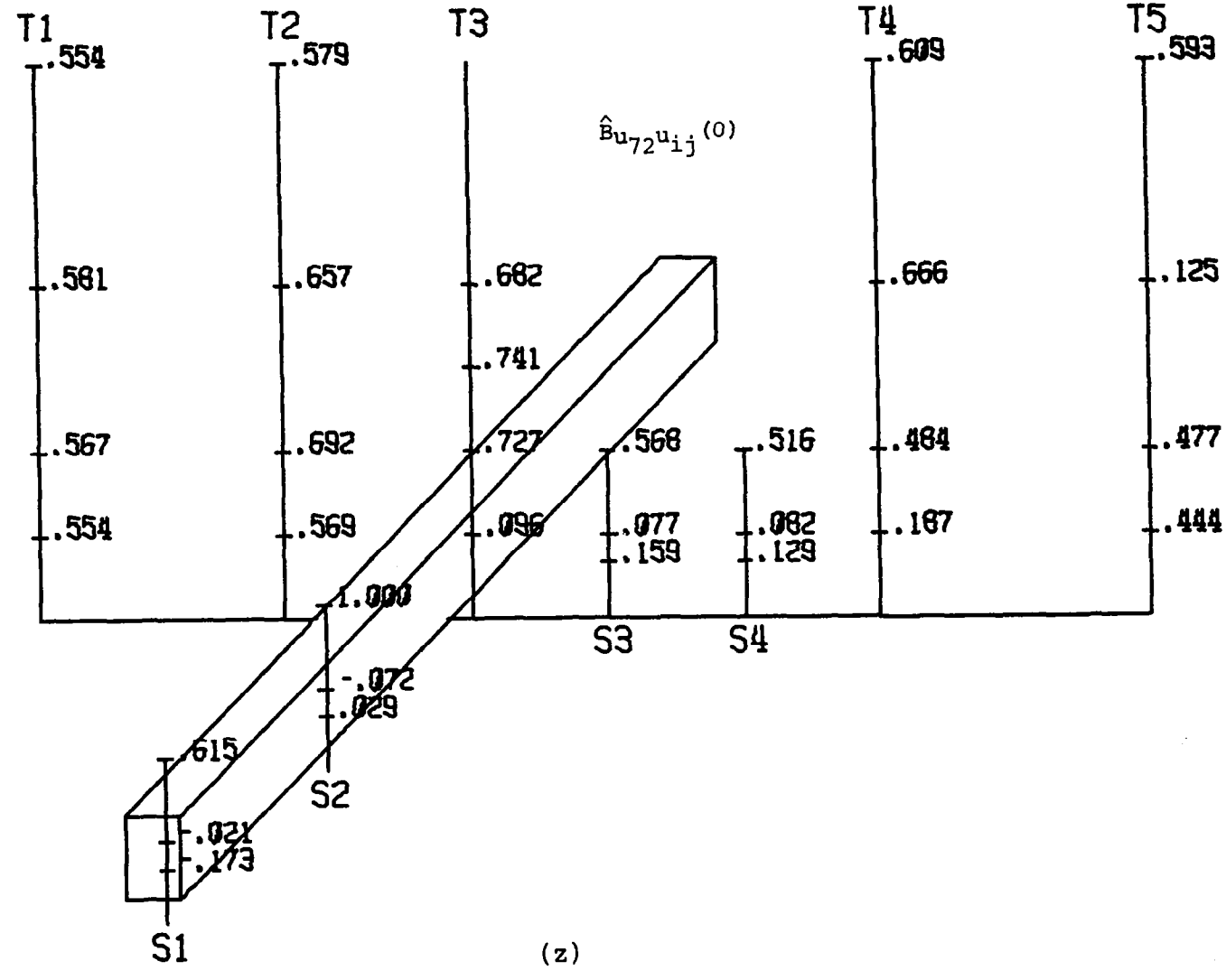

Figure 5-5 (continued)

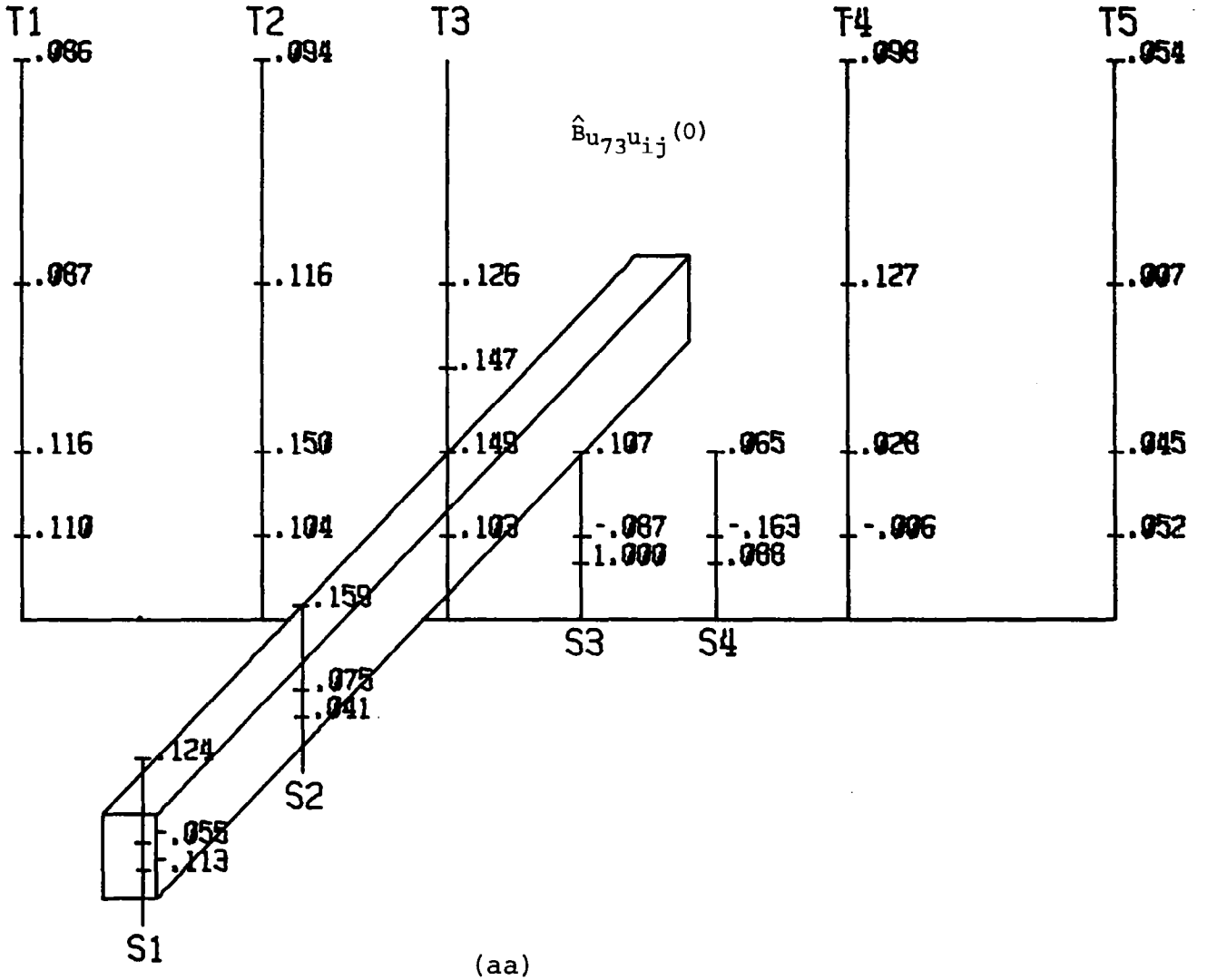

(aa)

Figure 5-5 (continued)

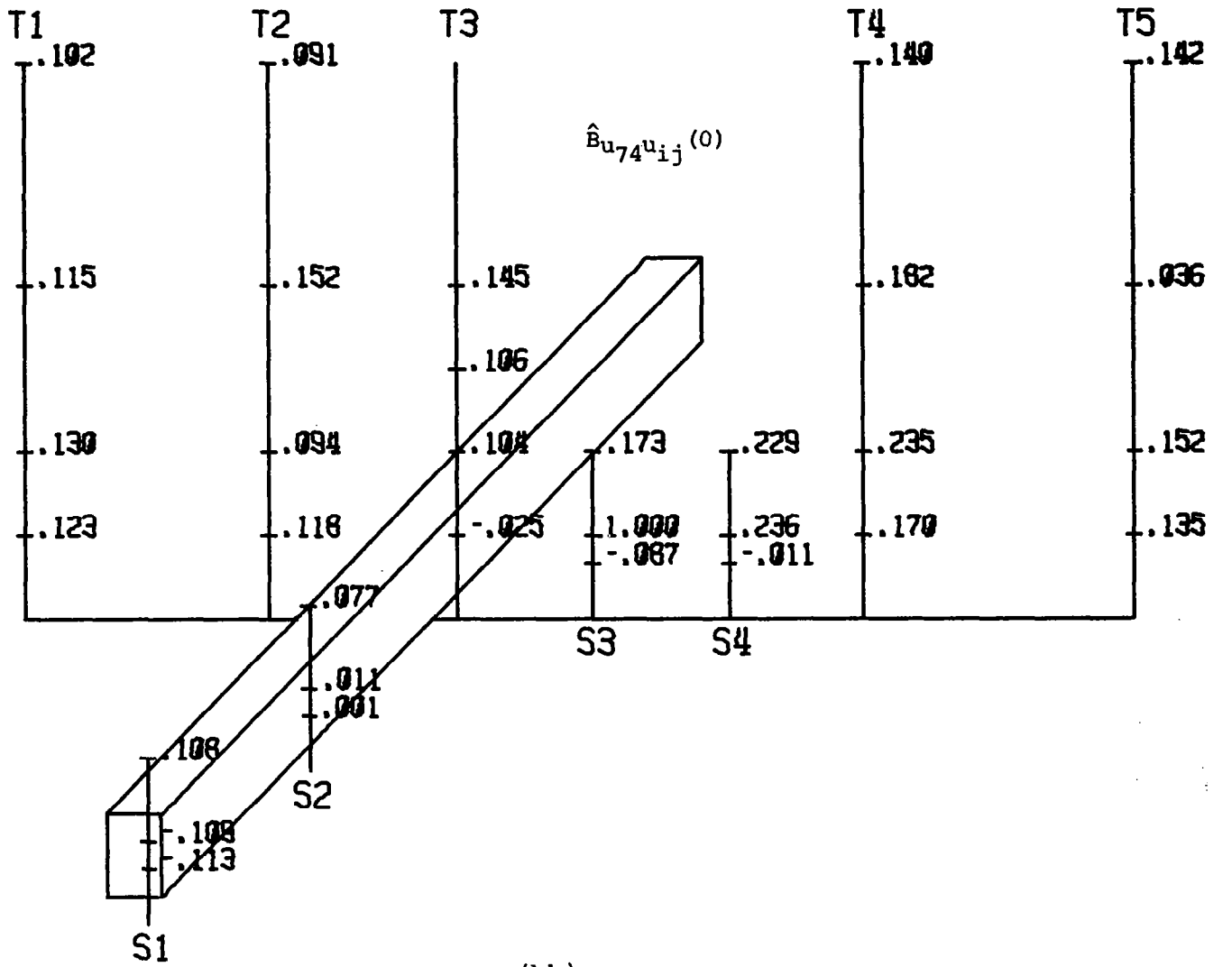

(bb)

Figure 5-5 (continued)

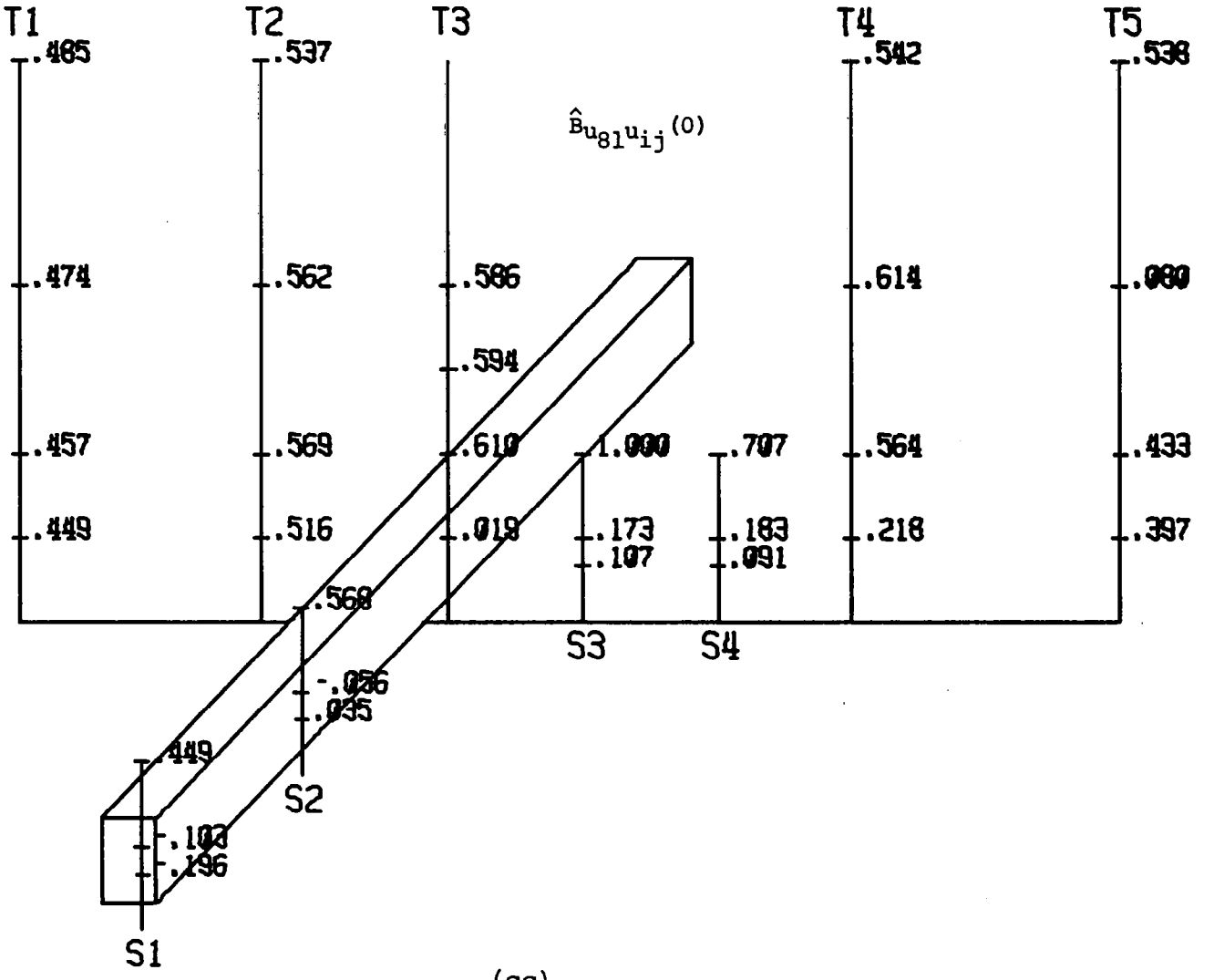

(cc)

Figure 5-5 (continued)

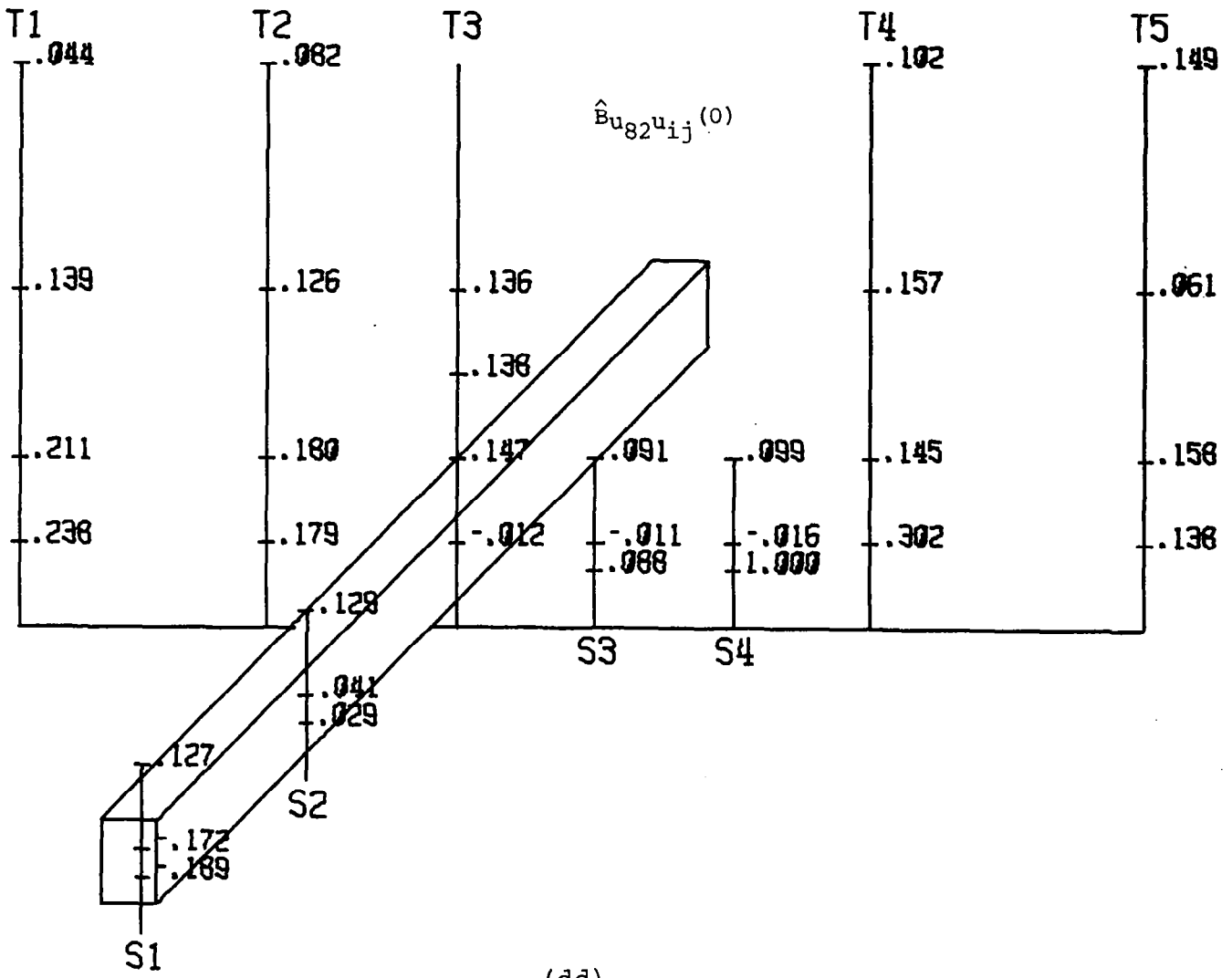

(dd)

Figure 5-5 (continued)

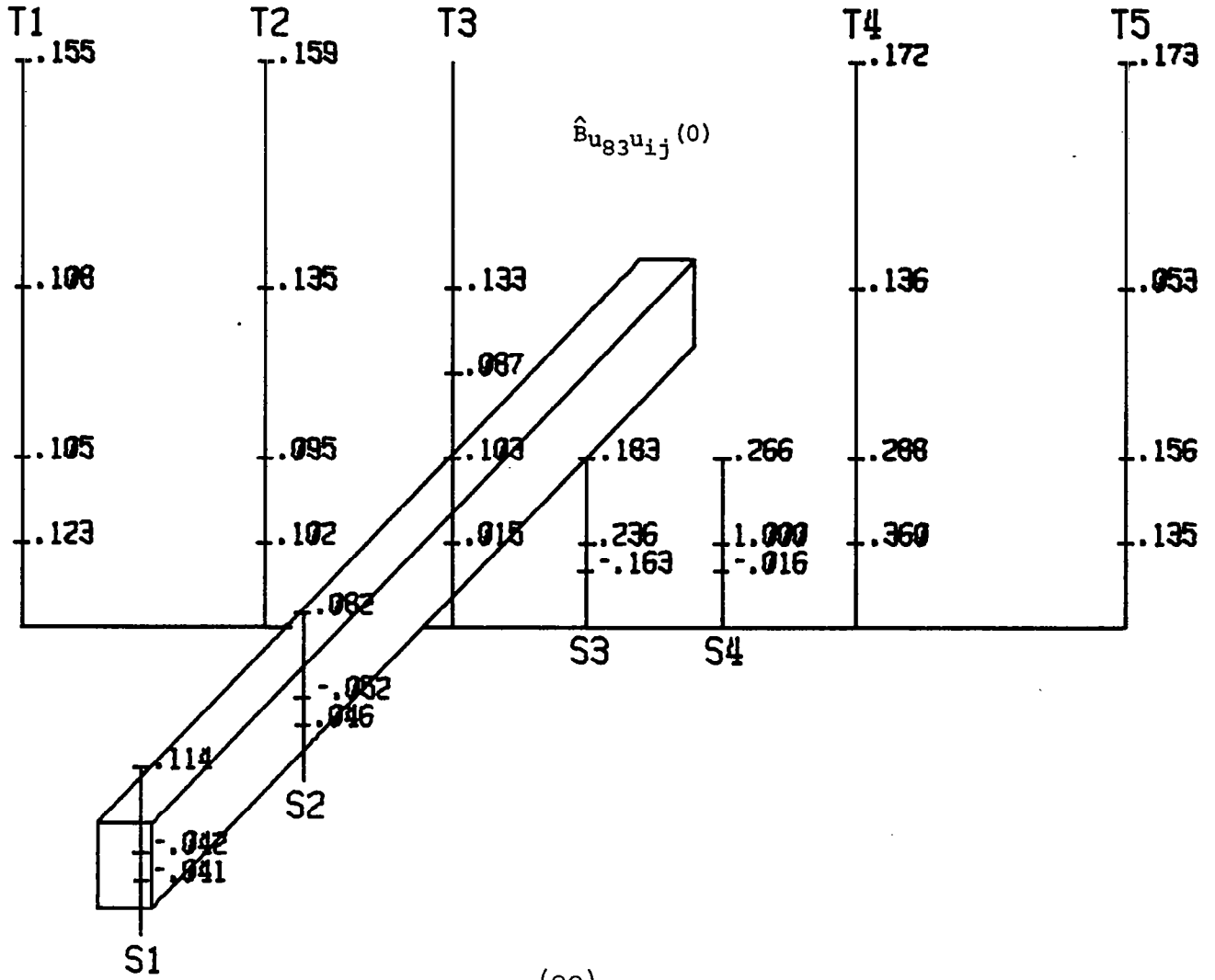

(ee)

Figure 5-5 (continued)

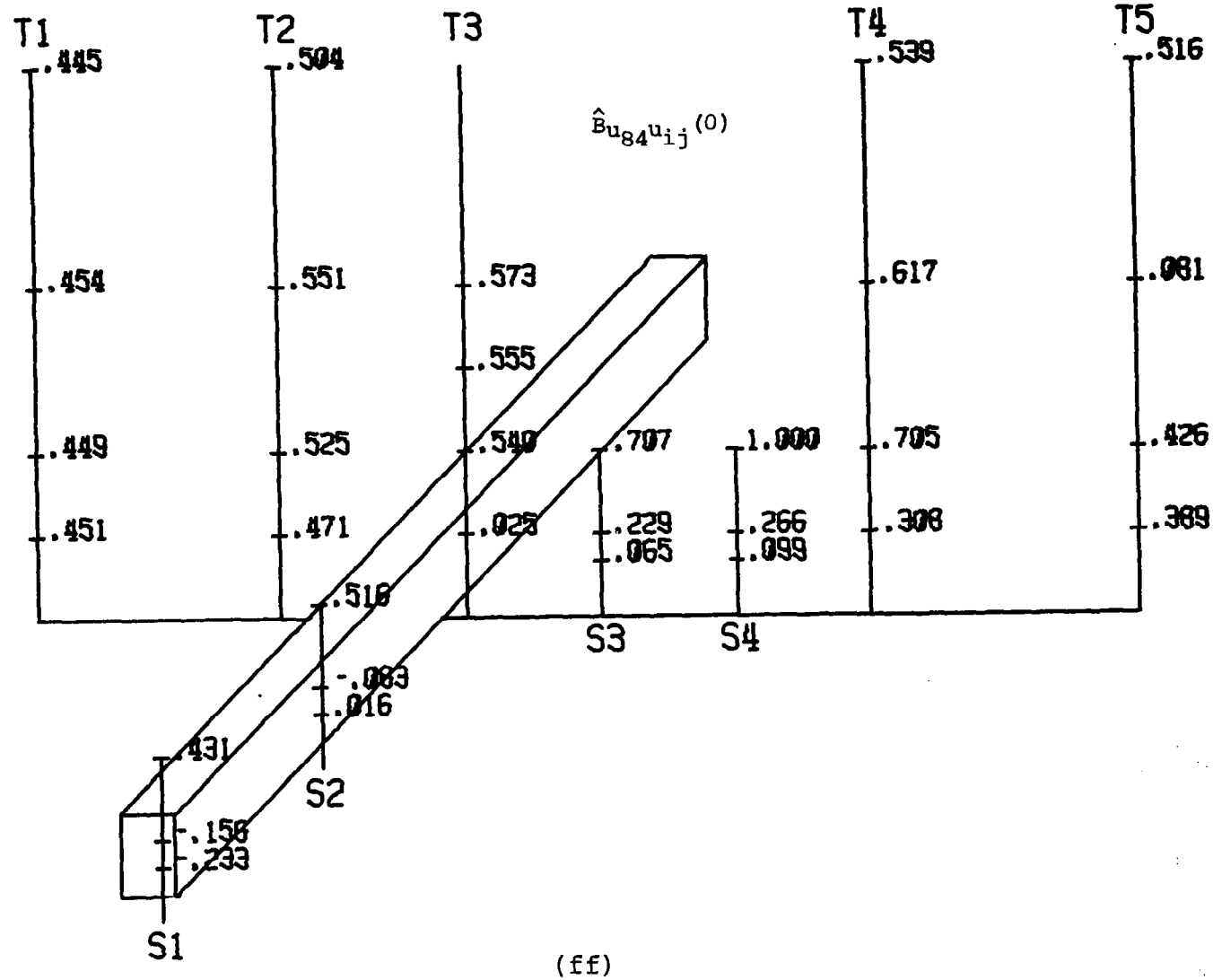

(ff)

Figure 5-5 (continued)

relative to T1L1, which is clearly evident from the fact that the correlation coefficient is unity at that position.

Some interesting properties of the correlation coefficient are observed in Figure 5-5. Again taking the plot in Figure 5-5(a) as an example, it can be seen that directly behind the block building there is very little correlation with the upstream position T1L1. This indicates a breakdown in the flow structure between the undisturbed flow upstream and the wake region behind the building. As the reference point for the correlation is raised to higher levels, the correlations (at the same level as the reference point) increase in the downstream direction. Also, as would be expected, the correlations in the free stream decrease with an increase in the distance separating the two points from which measurements were made. It should be noted that due to the definition of the two-point spatial correlation, $\hat{B}_{u_{ij}u_{k\ell}}(0) = \hat{B}_{u_{k\ell}u_{ij}}(0)$. (This is not true in general for all τ or the two-point space-time correlations.) A correlation of 1 indicates that the exact signal is felt instantaneously at the two points in question, and it is obvious that a point correlated with itself gives $\hat{B}_{u_{ij}u_{ij}}(0) = 1$ in all cases. (It should be noted that if $S = 0$, then $\hat{B}_{u_{ij}u_{ij}}(\tau)$ is not defined.) A negative correlation between two points suggests a structured reverse flow region where a longitudinal fluctuation in the positive direction at one point results in a negative fluctuation at

another point. If $B_{u_i j u_k \ell}(0) = -1$, then the velocities are equal in magnitude but opposite in sign.

The extent to which a signal is felt at two different points depends upon the time it takes the signal to travel from one point to the other, plus any changes which may have occurred during this time. A two-point space-time correlation, $B_{u_i j u_k \ell}(\tau)$, describes the general dependence of the longitudinal velocities at one tower and level to those at another position. Information relative to the time required for a signal to pass from one point to another in the wind field can be determined from the two-point space-time correlation. As the signal at one point is displaced in time relative to another point, the space-time correlation function will peak at the value of τ equal to the time required for the signal to propagate at the speed of the mean wind to the second point in space.

Figures 5-6 through 5-11 are plots of two-point space-time correlations. Figures 5-6 and 5-7 illustrate vertical correlations, whereas Figures 5-8 through 5-11 illustrate horizontal correlations. Figures 5-6 and 5-7 are plots of the space-time correlations of T1L4 with all other levels on T1 and of T5L4 with all other levels on T5, respectively. It can be seen from these two plots (Figures 5-6 and 5-7) that the correlation between levels on the downstream tower is relatively less in magnitude and that the peaks in the correlations occur with an increased lag

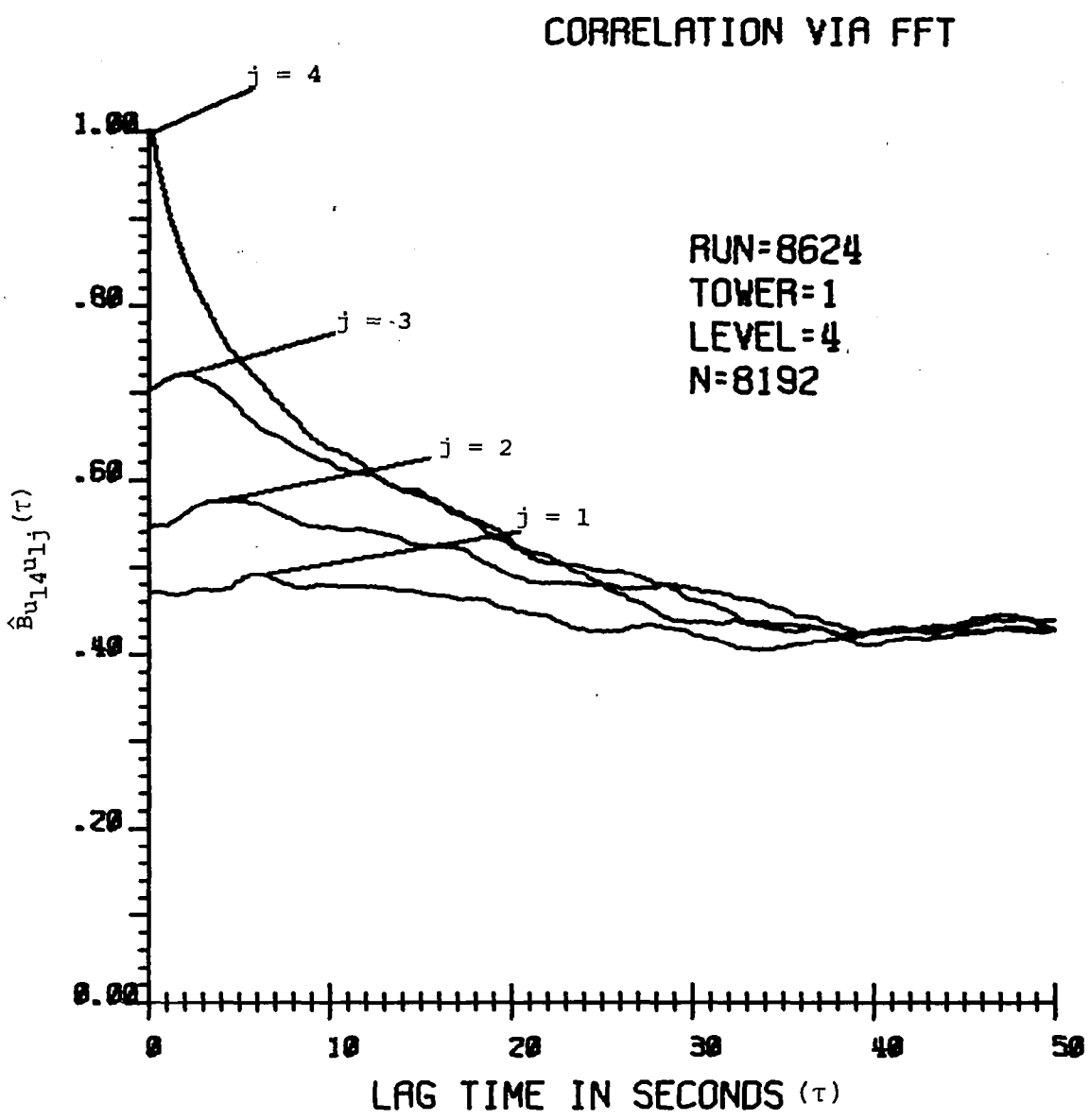

Figure 5-6 Vertical correlations relative to T1L4.

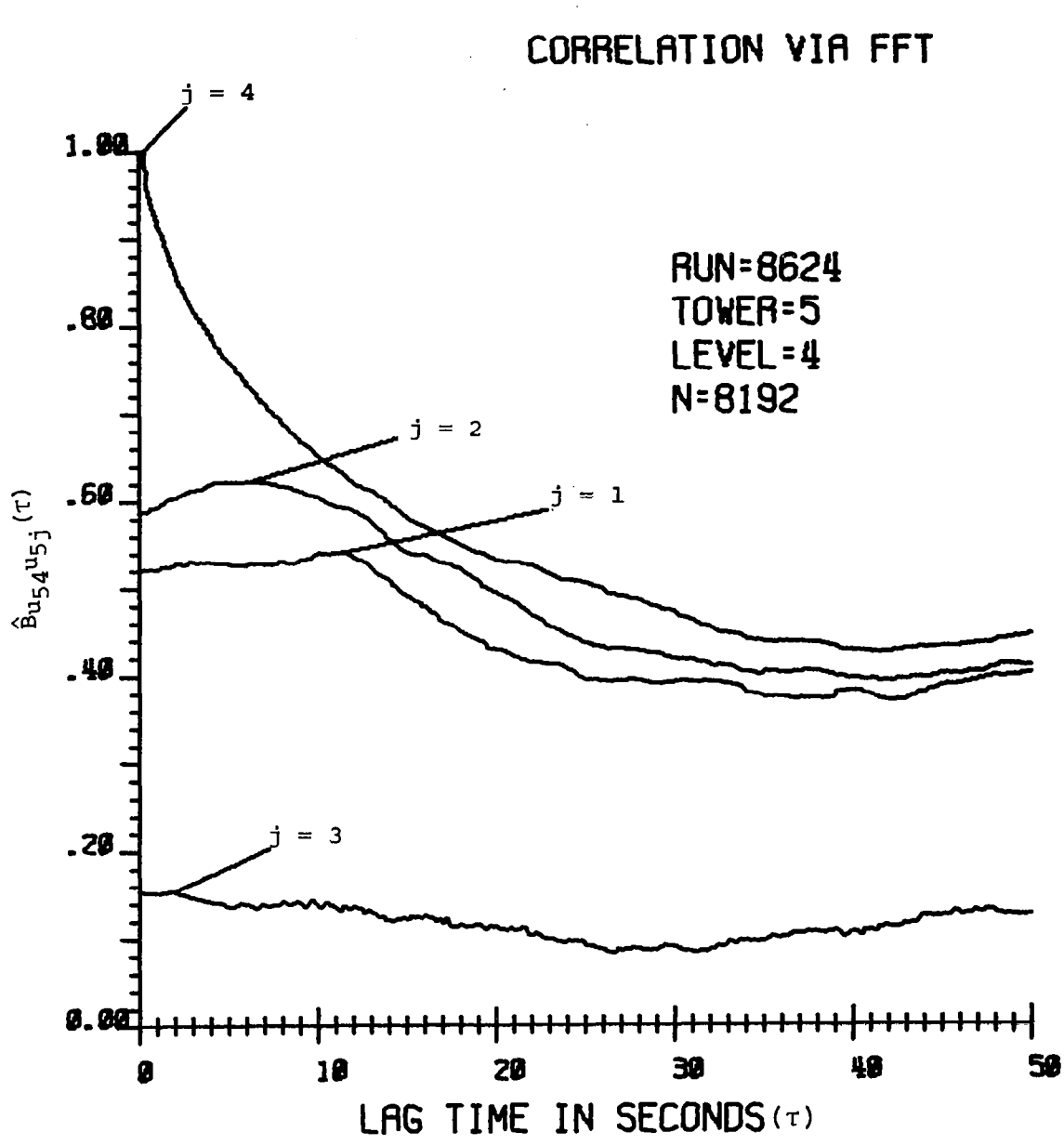

Figure 5-7 Vertical correlations relative to T5L4.

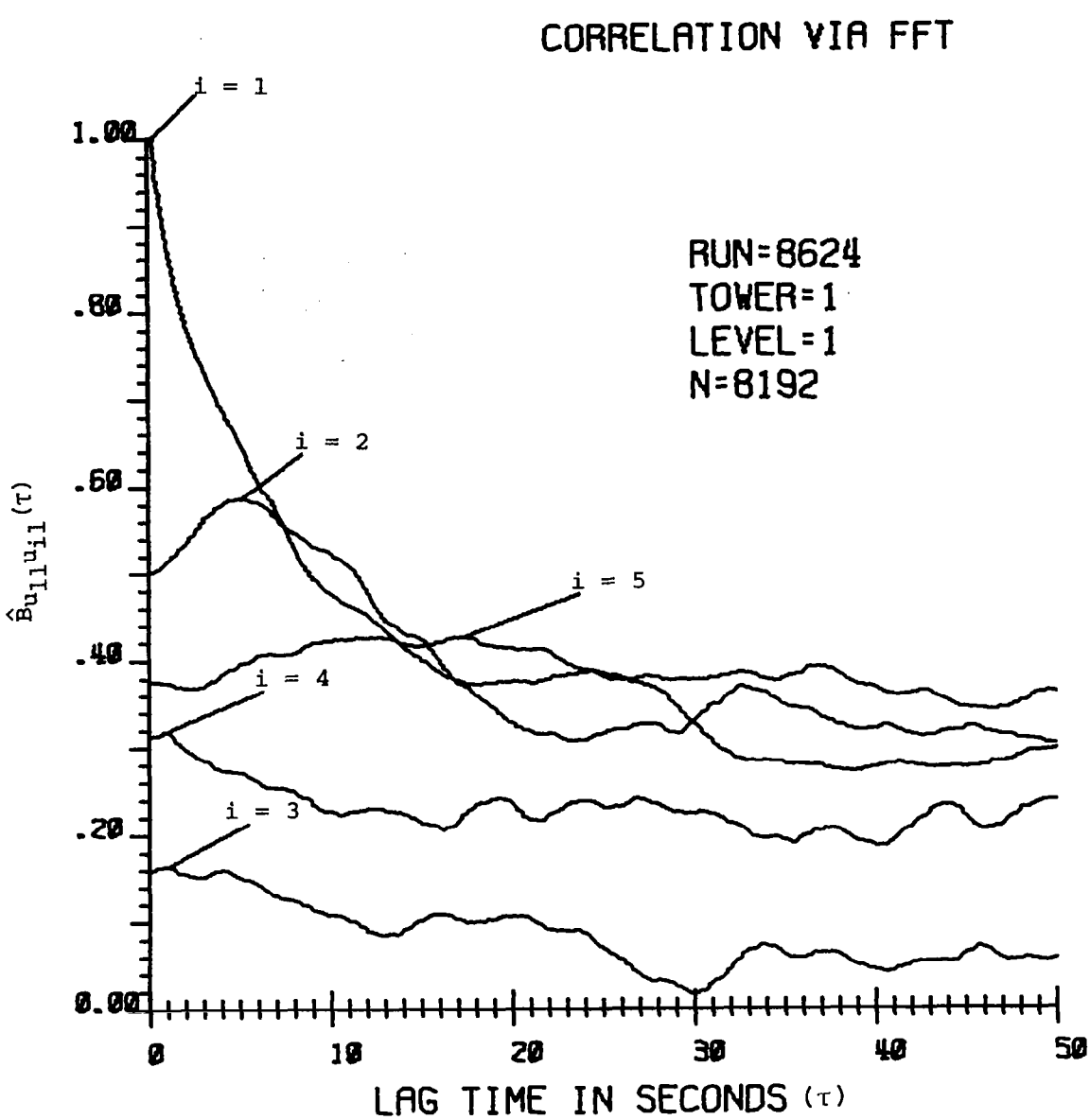

Figure 5-8 Horizontal correlations relative to T1L1.

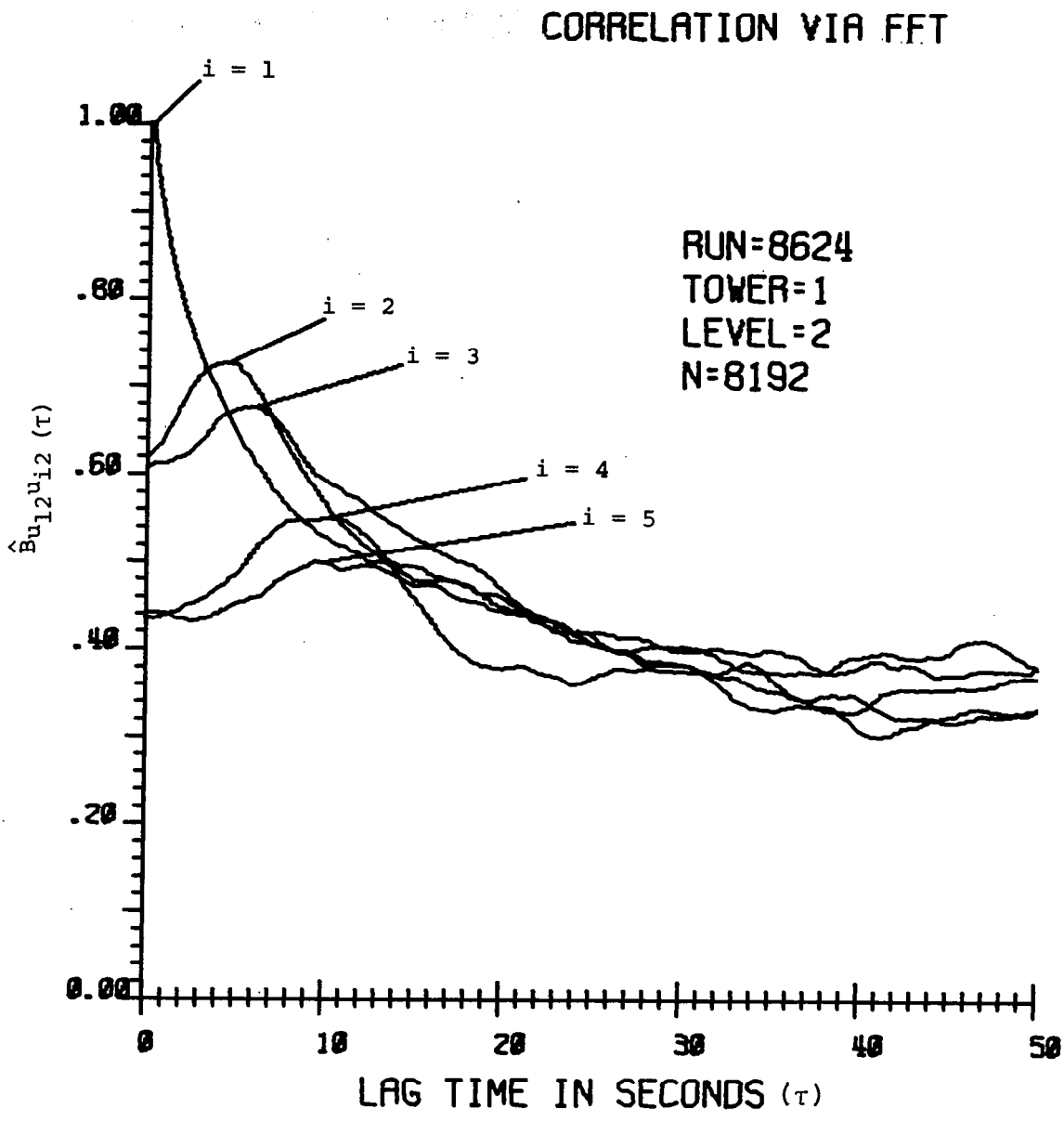

Figure 5-9 Horizontal correlations relative to T1L2.

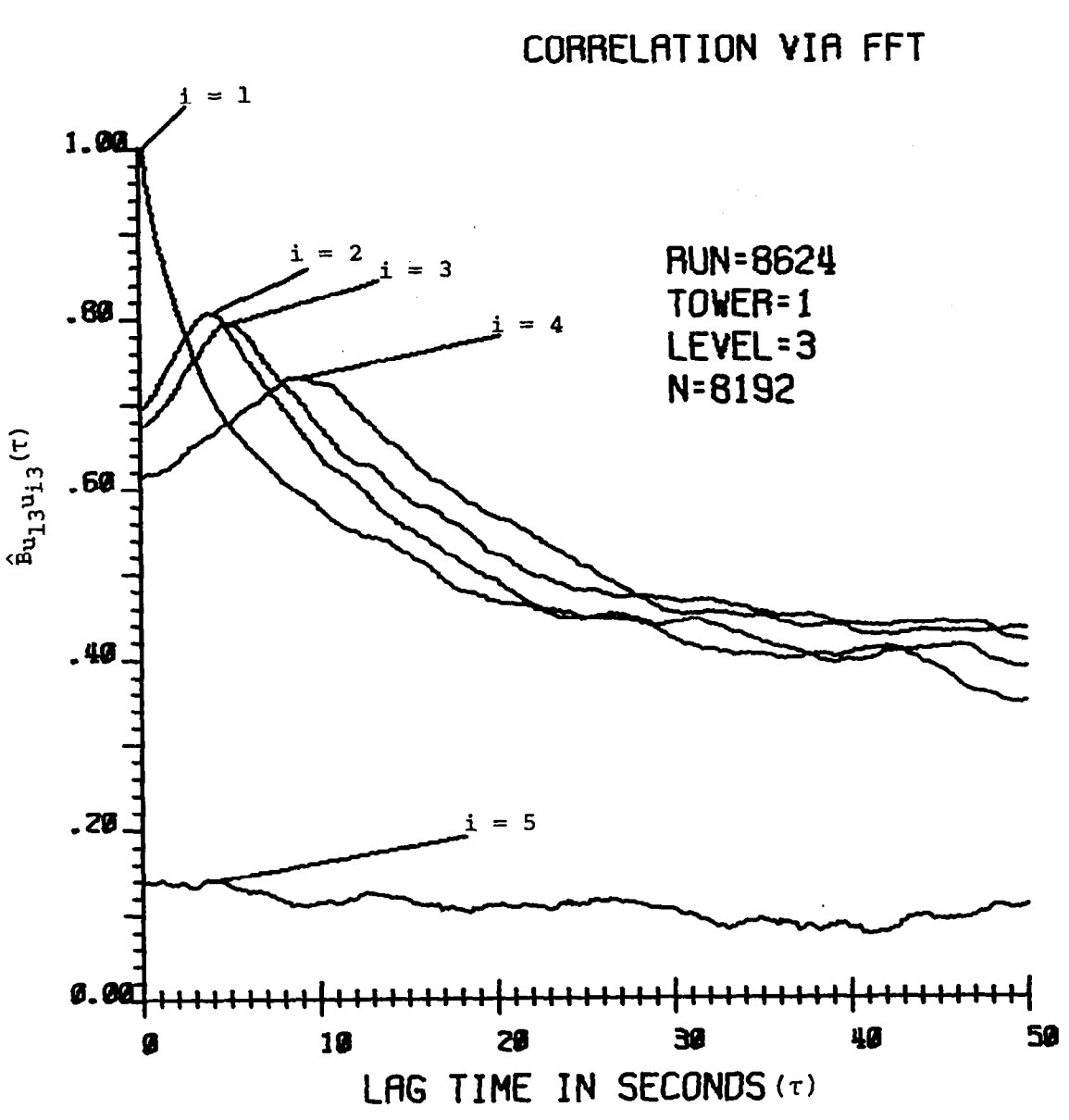

Figure 5-10 Horizontal correlations relative to T1L3.

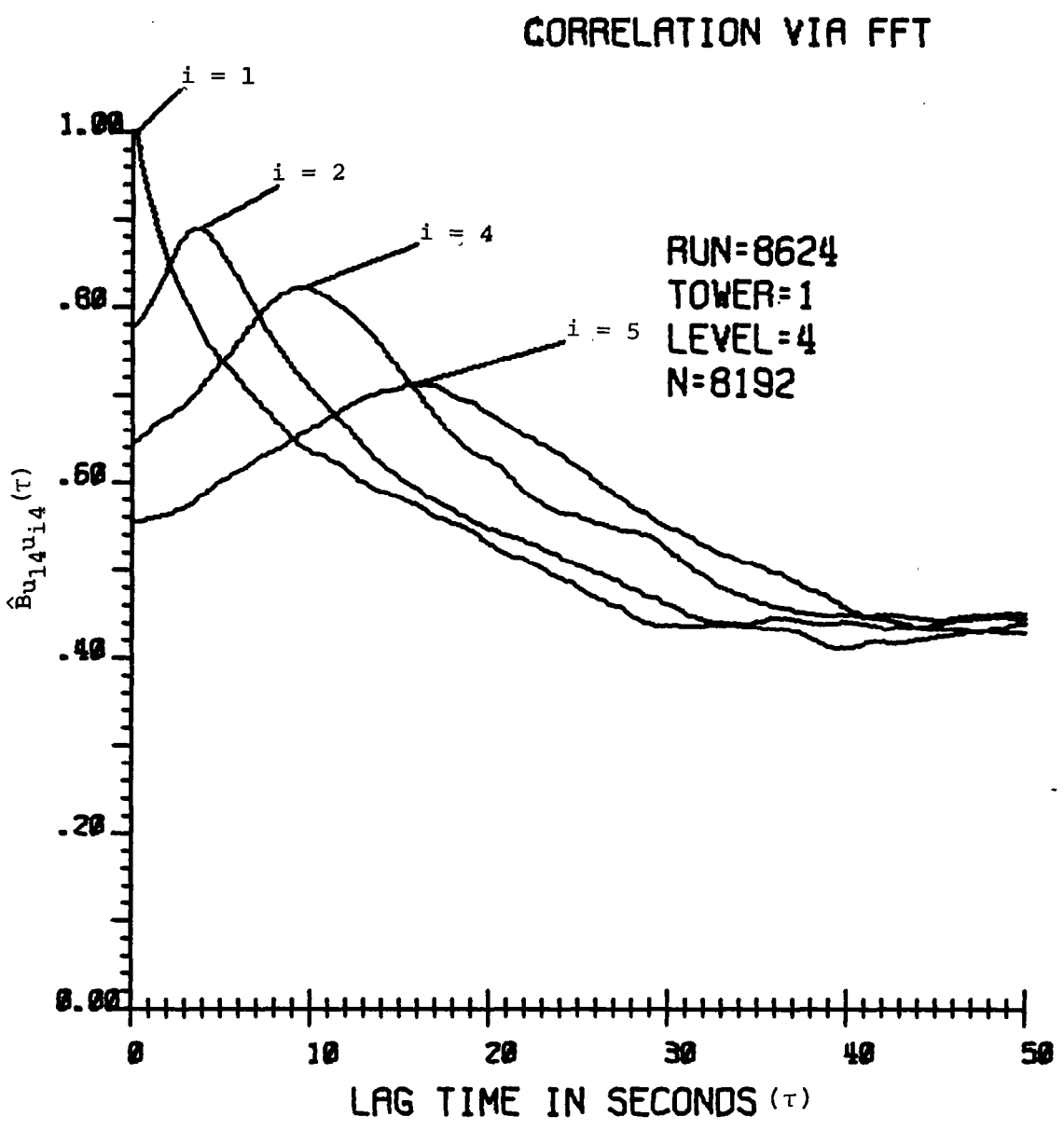

Figure 5-11 Horizontal correlations relative to T1L4.

time (τ). As mentioned earlier, it should be noted that the instrumentation on T5L3 was not operating correctly and is apparent from the erroneous plots of the correlation. The reduced relative magnitudes of the correlations relative to T5L4 are possible due to the higher levels of turbulence created by the shear layer emanating from the leading edge of the block. The increase in lag time at which the peak in the correlation occurs can be explained by the fact that the boundary layer has not fully recovered at T5. The lower mean velocities in the uncovered region result in the signal propagating at a slower speed and thus requiring a longer time to traverse a given distance.

In Figures 5-8 through 5-11 (horizontal two-point space-time correlations of the longitudinal velocity components) it can be seen that the correlations near the ground are greatly affected by the presence of the block building. As the reference point of the correlations is increased to higher levels, the effect of the building is less pronounced (higher correlations and shorter lag times at which the peak in the correlations occurs). It should again be noted that the instrumentation on T3L4 was moved to the 9 meter level, and for this reason it has not been included in Figure 5-11. The correlations in Figures 5-8 through 5-11 peak at a lag time which decreases with an increase in the reference point height and is due to increased mean velocities at the upper levels. This phenomenon also occurs with a decrease in the

distance separating the points from which the measurements were made and the correlations were computed. If a signal did not change as it propagated downstream, each peak would occur at a lag time equal to the ratio of the distance to the mean velocity at the time the measurements were made and the correlation function would have a peak value equal to 1, indicating the exact signal is felt downstream. However, this is not true, because the signal changes due to shearing, boundary and viscous effects and the peak in the correlations reduces as the distance between the two points of measurement increases.

It should be noted that $B_{u_i j u_k \ell}(\tau)$ is simply the autocorrelation function (coefficient) when $i = k$ and $j = \ell$. When this is the case, $B_{u_i j}(\tau)$ is a maximum at $\tau = 0$. This can be shown theoretically and is readily seen in Figures 5-6 through 5-11 for the different correlation coefficients $B_{u_i j u_k \ell}(\tau)$ when $i = k$, $j = \ell$, and the lag time (τ) equals zero.

Computational Techniques

Computation of the correlation coefficients was carried out originally to compare the FFT and the direct method computational techniques. In Figure 5-12 the accuracy of the two methods is exemplified. Only a selected number of points which were computed by the FFT method were plotted to illustrate the closeness of the two methods. The agreement is obviously very good. The numbers of datum points (N)

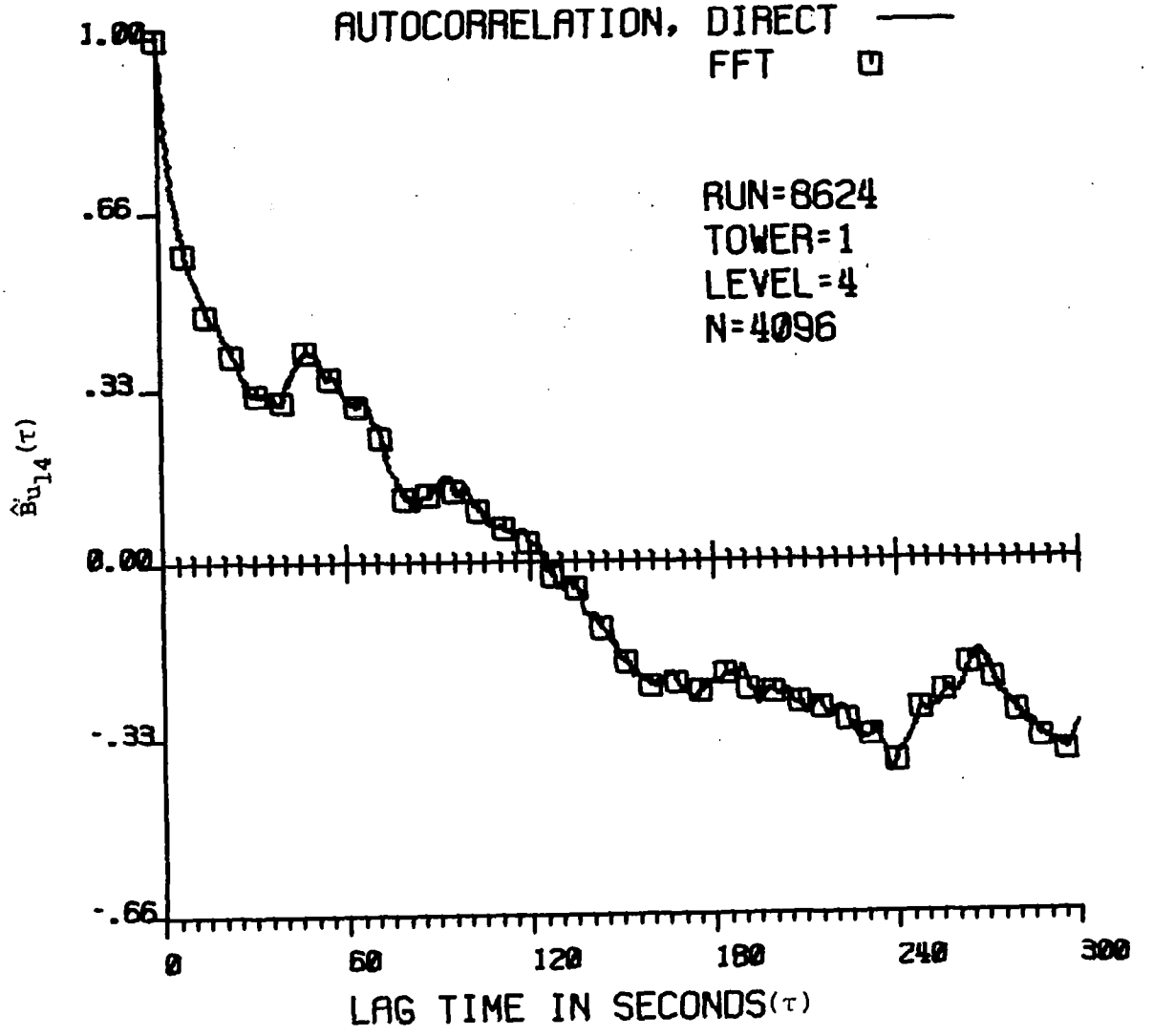

Figure 5-12 Comparison of direct and FFT methods for computing an autocorrelation function.

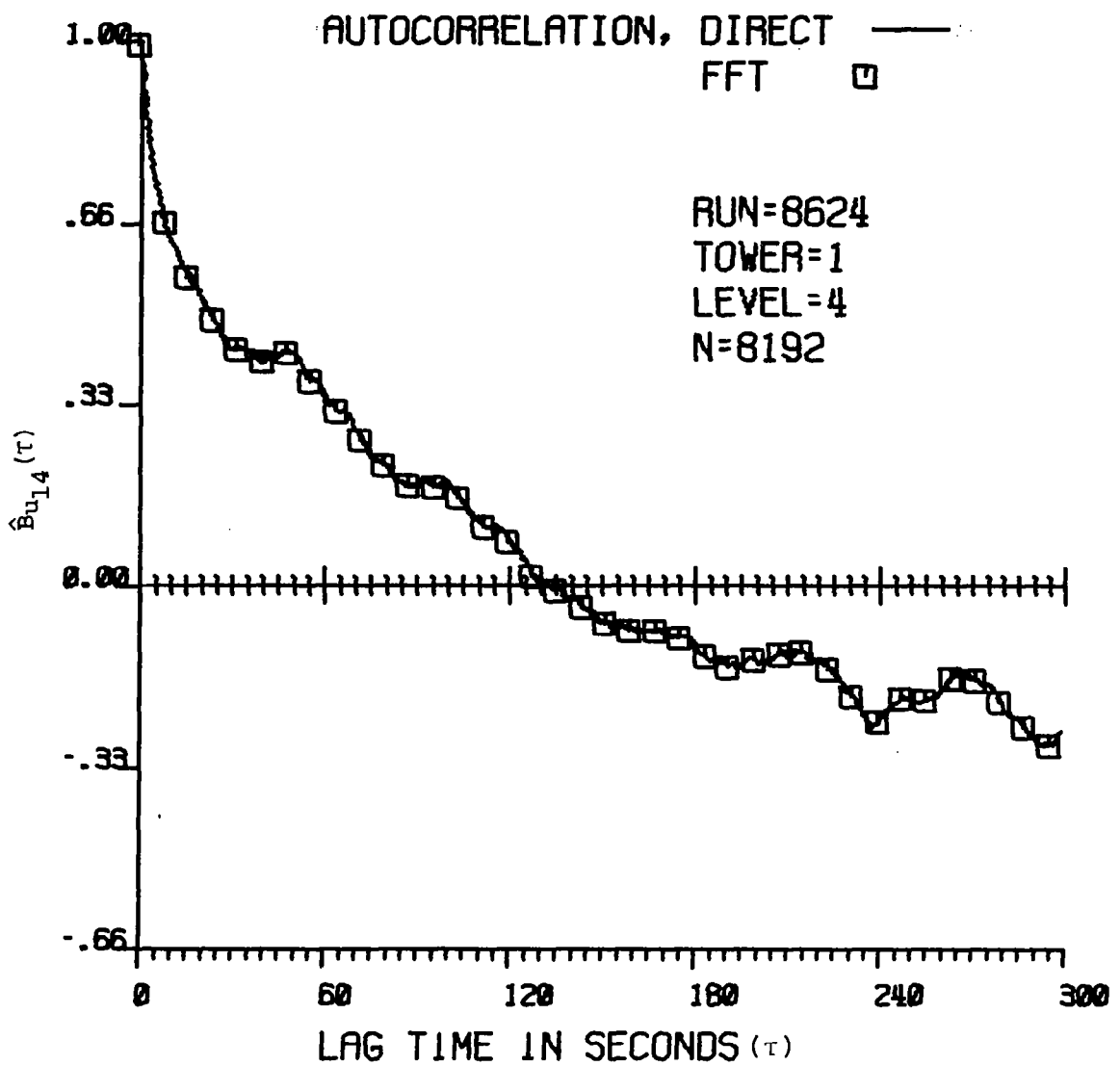

Figure 5-12 (continued)

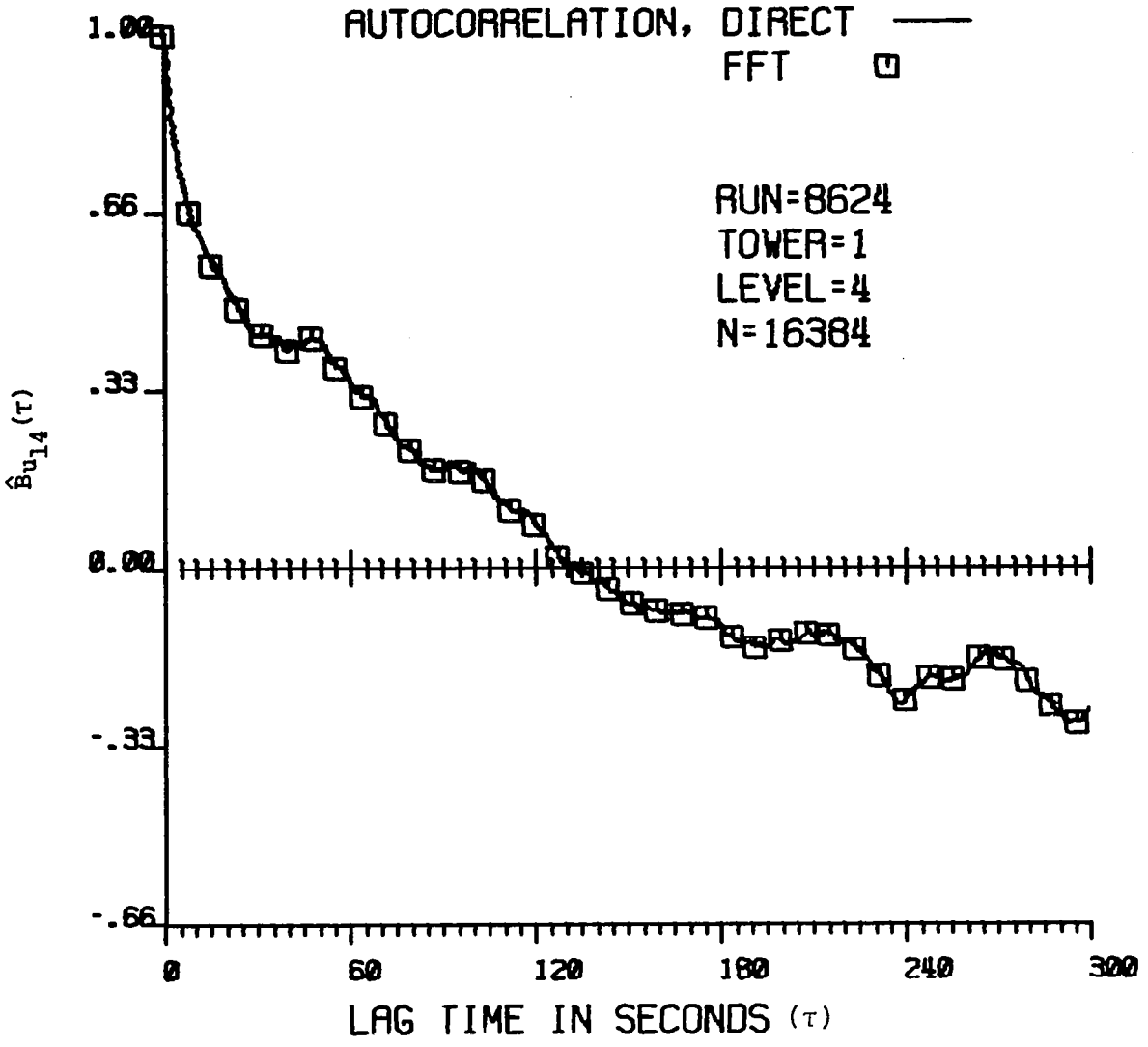

Figure 5-12 (continued)

used in the computational comparisons were 4096, 8192, and 16384. (Each is an integral power of two as required by the FFT procedure described in Section III.) The total cpu times for each computation are shown in Table 5-1. In all cases, the FFT method required less time, and as N increases, the ratio of the time for the direct method to the time of the FFT method increases very rapidly. (This, ultimately, will depend on the maximum lag time used in the computational procedure.) It should also be noted that the FFT procedure computes the correlation coefficient for a lag equal to the total length of the record being computed. Hence, the best comparison of the two methods would be to let the maximum lag time be equal to the record length.

Very little difference exists between the correlations using 8192 and 16384 datum points; therefore, all other plots are computed using 8192 datum points to minimize the total computer time. An autocorrelation function will generally decrease as τ increases and oscillate about zero

TABLE 5-1

COMPUTER EXECUTION TIME (MINUTES)

	Number of Data Points		
Method	4096	8192	16384
FFT	2.08	4.41	9.36
Direct	3.24	6.55	27.26

after a sufficiently long period of lag. Any sharp, predominant peak in the autocorrelation function is an indication of the presence of a periodic signal having a wavelength equal to the lag time at which the peak occurs. Thus, this method could be used to detect any periodic fluctuations in the flow field such as vortex shedding or low frequency directional fluctuations.

Testing Taylor's Hypothesis

It is interesting to test Taylor's hypothesis for the atmospheric flow over the simulated building. Mathematically, Taylor's hypothesis can be expressed as $x = \bar{u}t$ where x is the distance separating the two points in question, $\bar{u}$ is the mean velocity, and t is the time required for the signal to propagate from one point to the other. Sometimes this is stated as $u(t) = u(x/\bar{u})$ or $\partial/\partial t = -\bar{u}(\partial/\partial x)$.

The range over which Taylor's hypothesis can be applied is restricted. As the distance between the two points increases, the results become less valid; also, the mean velocity has to be relatively larger than the magnitudes of the turbulence fluctuations, $[(u(t) - \bar{u}) << \bar{u}]$. A detailed explanation of the restrictions to Taylor's hypothesis is given by Hinze [16].

Figure 5-13 shows a comparison between the spatial correlation computed from measurements separated in space to the correlation estimated by Taylor's hypothesis. In

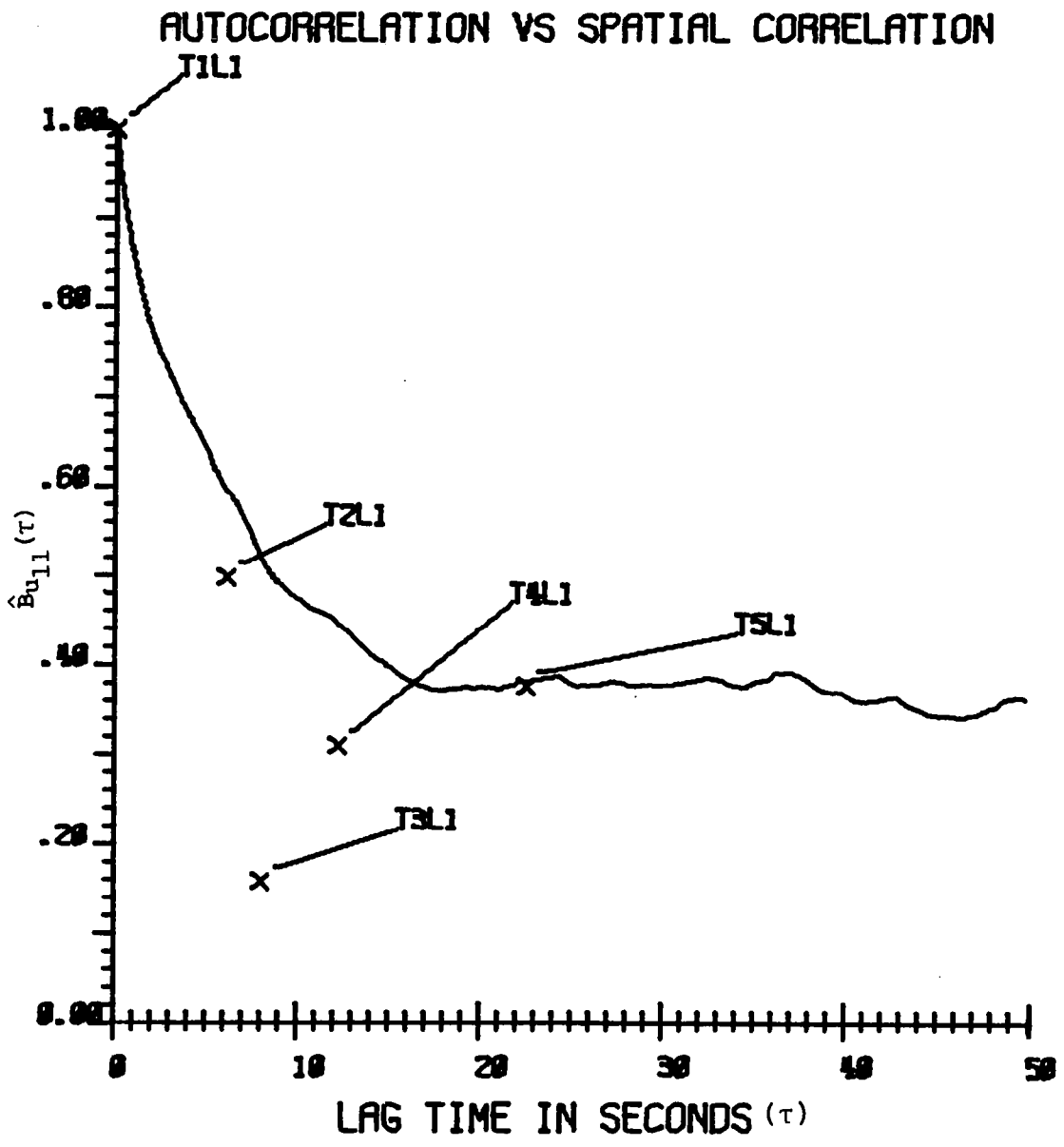

Figure 5-13 Comparison of autocorrelations computed by FFT procedures to autocorrelations computed by assuming Taylor's hypothesis.

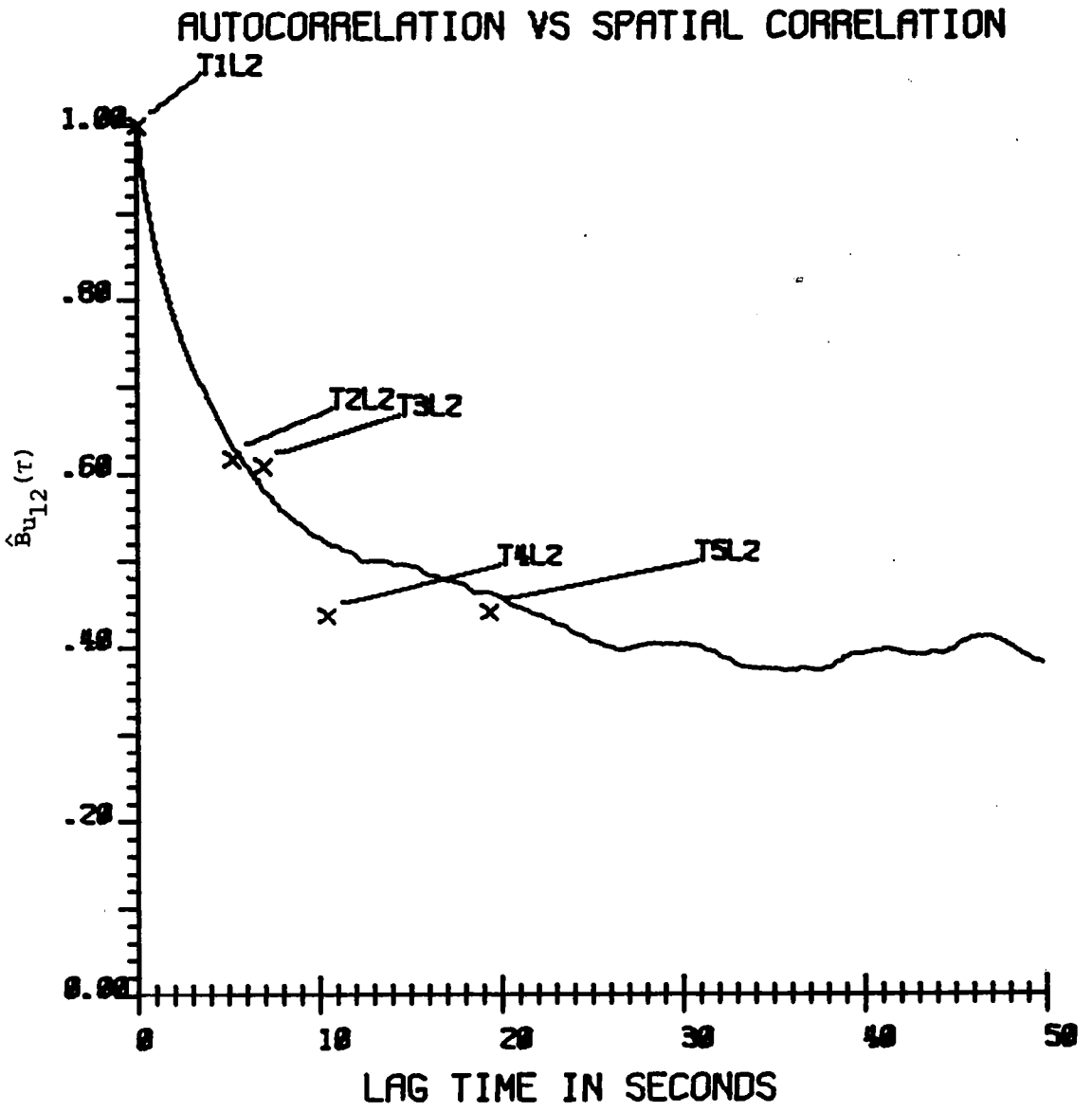

Figure 5-13 (continued)

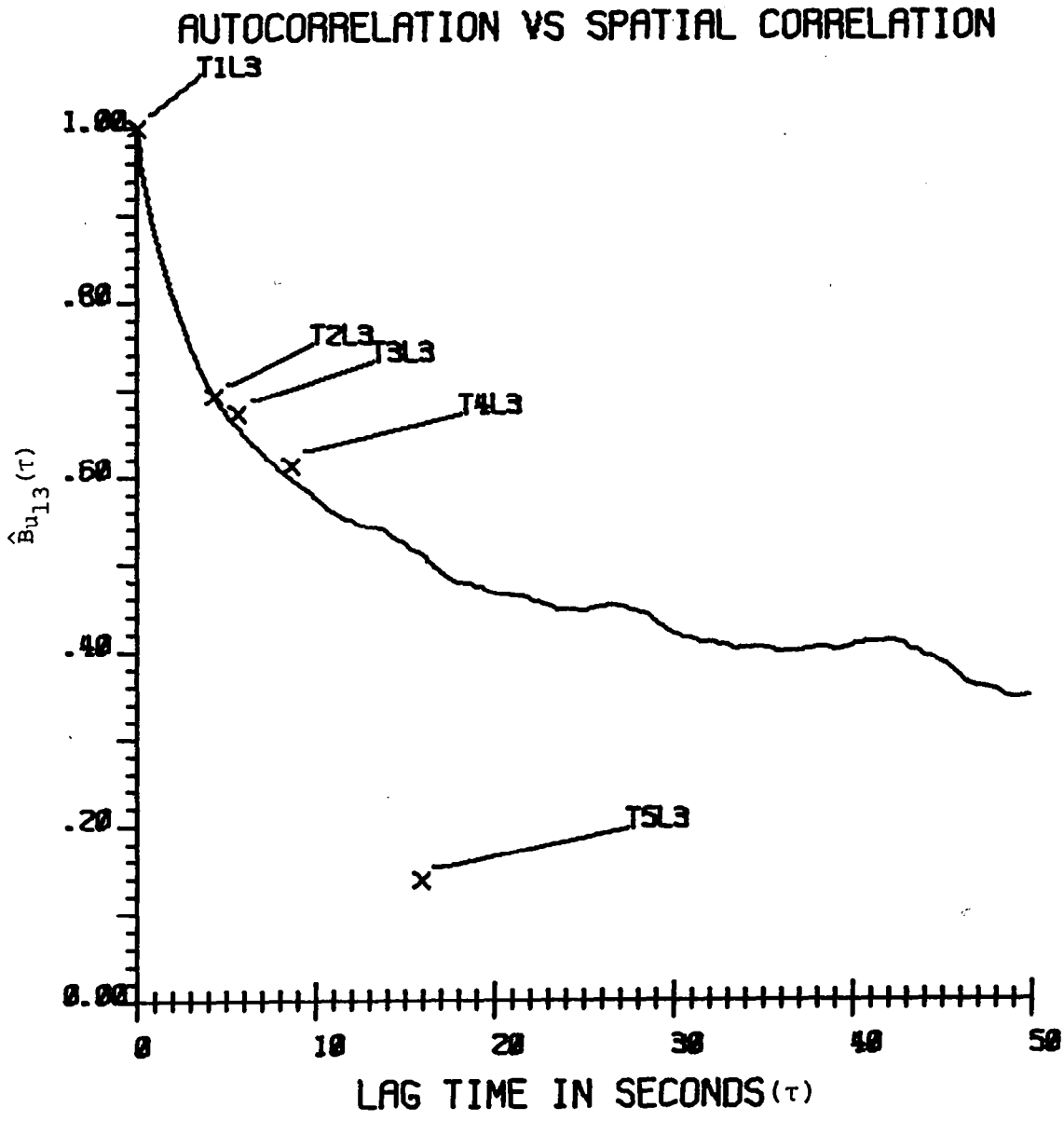

Figure 5-13 (continued)

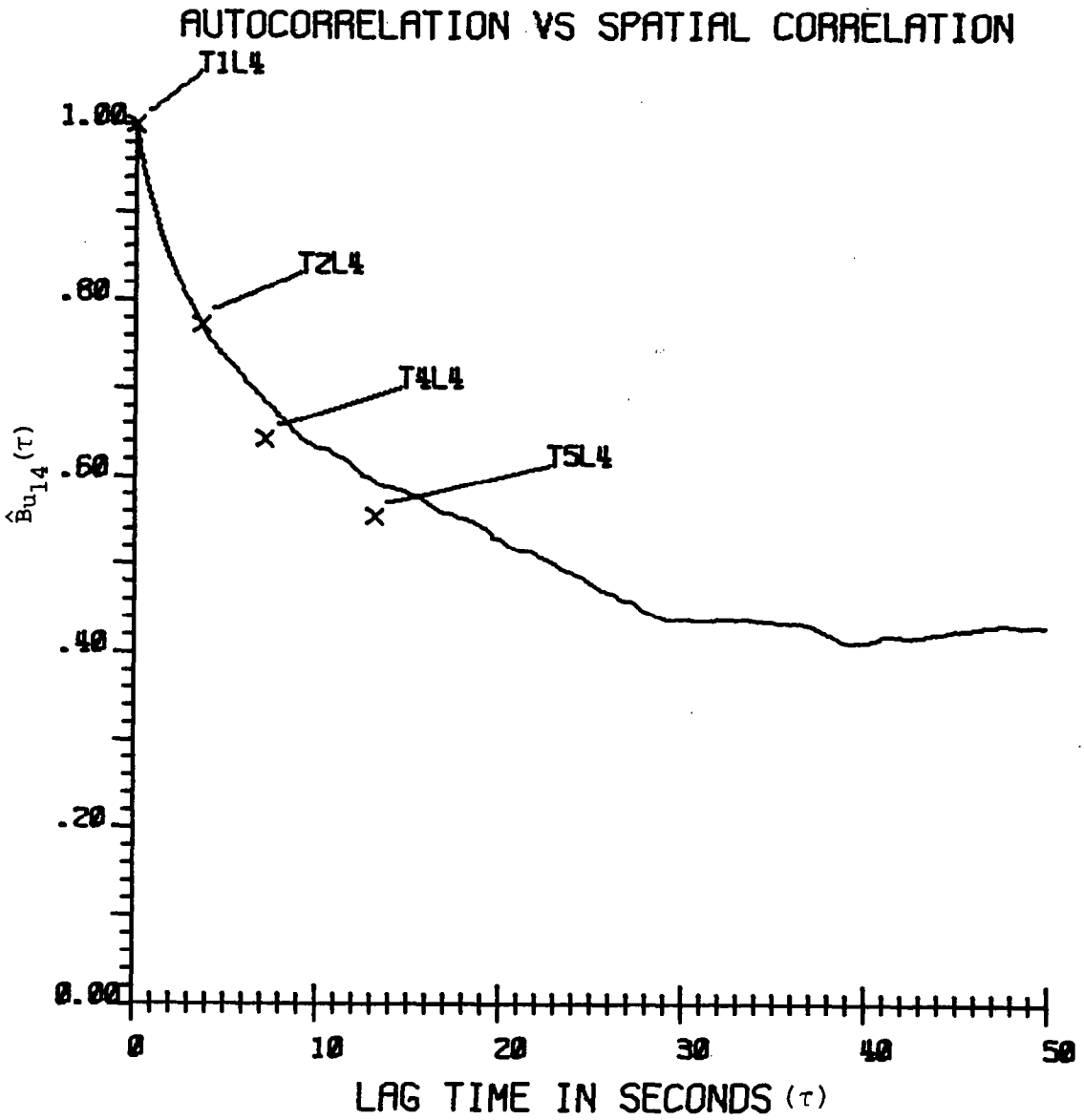

Figure 5-13 (continued)

producing these plots, the tower spacing was 0.0, 21.8, 43.3, and 80.3 meters between towers T1 and T1, T2, T4, and T5, respectively. The mean velocity $\bar{u}$ at levels L1, L2, L3, and L4 is 3.6, 4.2, 5.1, and 6.2 m/s, respectively. The two-point spatial correlations are indicated with an x in Figure 5-13. It is seen from this Figure (5-13) that in the undisturbed stream, very close predictions of the spatial is achieved by using Taylor's hypothesis. Less accurate results are obtained, however, at the lower levels where the influence of the building is more pronounced.

The more accurate results at the upper levels are expected, but some question exists as to the very close agreement obtained using Taylor's hypothesis at the lower levels for T5. Two explanations are proposed: (1) the signal felt upstream at T1 propagates over the building, remaining outside the wake region and therefore not being disrupted by the wake disturbance or (2) the direction of the mean wind is such that the upstream flow passes around the building without interacting with it. The latter of these two explanations is the most probable since the mean wind direction was 201 degrees for this particular study.

According to Lin [17], there is no justification, in general, for extending Taylor's hypothesis to shear flow, such as is found in the atmospheric boundary layer. However, it is felt by Lin that Taylor's hypothesis may still be a good approximation for those wavenumbers κ of the turbulence

such that

$$\frac{\kappa\bar{u}}{d\bar{u}/dz} >> 1$$

holds. The corresponding equation using frequency rather than wavenumber is

$$\frac{2\pi n}{d\bar{u}/dz} >> 1$$

where n is cyclic frequency.

Taylor's hypothesis, as used in this study, assumes correlation irrespective of frequency such that

$$\hat{R}(\tau) = \hat{R}(x = \bar{u}\tau)$$

where τ is the lag time of the autocorrelation and x is space lag with $x = \bar{u}\tau$, as described earlier.

It is desirable to ascertain in what manner this expression is supported by analysis of the field data taken in the surface boundary layer without the simulated block building being used (runs numbered 8700 and above). These data were not available due to errors encountered in tape conversions.

It would be of interest to measure the coherence in the horizontal plane and downwind direction at several levels to further test Taylor's hypothesis. The coherence function, when computed directly instead of the FFT method, would yield the correlation between two points as a function of frequency. The coherence function also provides the phase shift in the signals as a function of frequency from which the lag time can be obtained. It is believed that

higher frequencies (small eddies) are attenuated more than lower frequencies (large eddies) propagating downstream. Additionally, any protuberance will disrupt the signal propagating downstream and introduce new uncorrelated eddies. For this reason the analysis should be performed with data from the 8700 series tapes and compared with results obtained from the 8600 series tapes.

B. CONCLUSIONS

The experiment described herein is designed to obtain relevant measurements of the turbulent atmospheric boundary layer. In particular, the influence of a simulated block building is under investigation along with gust gradient analysis relative to flight characteristics and structural loading of wind turbine generators.

Hopefully, the experiment and data reduction procedures are described in sufficient detail to allow access to the available data. The preliminary analysis presented in this study has been performed to better understand the influence of surface obstructions on atmospheric flow. A much better understanding of the flow will be accomplished upon completion of the study which will investigate additional data sets and computation of power spectral density functions and coherence functions. This analysis is being completed and will be discussed at a later date.

LIST OF REFERENCES

1. Frost, W., G. Fichtl, J. R. Connell, and M. L. Hutto. "Mean Horizontal Wind Profiles Measured in the Atmospheric Boundary Layer About a Simulated Block Building," Proceedings of the Second U.S. National Conference On Wind Engineering Research. Fort Collins: Colorado State University, June 1975.

2. Frost, W., and A. M. Shahabi. "A Field Study of Wind Over a Simulated Block Building," National Aeronautics and Space Administration Contract Report No. NAS8-29584, George C. Marshall Space Flight Center, Huntsville, Alabama, March 1977.

3. Sacre, C. "Une Methode Numerique Pour Le Calcul Approche De La Surviteese du Vent Sur Une Colline," Centre Scientifique et Technique du Batiment, Establissement de Nantes, France.

4. Woo, H. G. C., J. A. Peterka, and J. E. Cermack. "Winds Tunnel Measurements in the Wakes of Structures," National Aeronautics and Space Administration Contract No. NASA CR-3806, prepared by Colorado State University, Fort Collins, March 1977.

5. Plate, E. J. Aerodynamic Characteristics of Atmospheric Boundry Layers. Oak Ridge, Tennessee: USAEC Technical Information Center, March 1972.

6. Logan, E., and J. Chang. "Wake Characteristics of Buildings in Disturbed Boundary Layers," National Aeronautics and Space Administration Contract Report No. NAS8-32357, George C. Marshall Space Flight Center, Huntsville, Alabama, May 1980.

7. Logan, E., and D. W. Camp. "Preliminary Comparison of Model and Prototype Wakes," AIAA Paper No. 78-254, 1978.

8. Instruction Manual for Model 011-1, Wind Speed Transmitter. Climet Instruments, Sunnyvale, California, February 1970.

9. Instruction Manual for Model 012-1, Wind Direction Transmitter. Climet Instruments, Sunnyvale, California, February 1970.

10. Instructions Gill Propeller Anemometer Model 27100, Model 27101. R. M. Young Company, Ann Arbor, Michigan, December 1969.

11. Sebestyen, L. G. Digital Magnetic Tape Recording for Computer Applications. London, England: Chapman and Hall, 1973.

12. Oppenheim, A. V., and R. W. Schafer. Digital Signal Processing. Englewood Cliffs, New Jersey: Prentice Hall, Inc., 1975

13. Frost, W., B. H. Long, and R. E. Turner. Engineering Handbook on the Atmospheric Environmental Guidelines for Use in Wind Turbine Generator Development. National Aeronautics and Space Administration TR-1359, George C. Marshall Space Flight Center, Huntsville, Alabama, December 1978.

14. Brigham, E. O. The Fast Fourier Transform. Englewood Cliffs, New Jersey: Prentice Hall, Inc., 1974.

15. Merzkirch, Wolfgang. Flow Visualization. New York: Academic Press, 1974.

16. Hinze, J. O. Turbulence. New York: McGraw-Hill Book Company, Inc., 1975.

17. Lin, C. C. Statistical Theories of Turbulence. Princeton, New Jersey: Princeton University Press, 1961.

*U.S. GOVERNMENT PRINTING OFFICE: 1980 735-006/10 1-3